Sara Alves de Melo Jerónimo

Licenciada em Ciências da Engenharia Civil

Hygrothermal Behaviour of Insulated Rammed Earth Walls

Dissertação para obtenção do Grau de Mestre em
Engenharia Civil – Perfil de Construção

Orientador: Fionn McGregor, Investigador,
École National des Travaux Publics de l'État, Lyon

Co-orientador: Paulina Faria, Professora Associada,
Faculdade de Ciências e Tecnologia da Universidade Nova de Lisboa

Júri:

Presidente: Prof. Doutor Mário Vicente da Silva
Arguente: Prof. Doutor Daniel Aelenei
Vogal: Doutor Fionn McGregor

FACULDADE DE CIÊNCIAS E TECNOLOGIA
UNIVERSIDADE NOVA DE LISBOA

Dezembro 2017

Acknowledgements

I would like to express my gratitude to Professor Paulina Faria that enabled this amazing experience to happen and for her concern shown during these six months.

I am deeply grateful to Dr. Fionn McGregor for all he taught me, for his availability, kindness and the invitation to continue this work in Lyon. In addition, I would like to thank Dr. Antonin Fabbri and Joachim Blanc-Gonnet and all the ENTPE team who always helped me. I would also like to thank ENTPE for the great welcome, financial support and availability to acquire all the material essential for my work.

This experience allowed me to grow up not only intellectually, but also as a person. I have dealt with so many challenges, a new language and customs. I met wonderful people from all over the world and learned so much with them. I loved to discover a new city with such rich culture and designed to benefit the citizens.

Therefore, I would like to thank my best friend Inês Costa that made part of this adventure and shared with me all these cheerful days (and not so good ones too). I am also thankful to my friends that have been part throughout the whole graduation and always kept me in touch and visited me.

I am grateful to my parents and sister, for always encouraging me to move out of my comfort zone and to enjoy meeting new places.

Finally, I would like to thank my boyfriend, Pedro Marreiro, who, even though being apart was so difficult, has always supported me in this adventure and visited me so many times.

Abstract

Rammed earth is an ancient construction technique for monolithic walls which consists in compacting raw earth in successive layers inside a formwork. The properties of the earth contribute to improve indoor comfort, acting as a buffer to relative humidity levels and internal temperature variations. Moreover, it has a low incorporated energy and it can be reused, contributing to a sustainable building industry.

However, earth walls have a low thermal resistance when compared with other solutions used nowadays, which in some regions makes it necessary to add further insulation. The sensitivity of earth wall to moisture content requires the added insulation material to be sufficiently vapour permeable to allow the necessary moisture regulation of the wall.

This dissertation aim is to measure in laboratory the behaviour of a rammed earth wall placed into a climatic chamber. In this regard, sensors measuring the temperature, relative humidity, heat flux and water content in different locations of the climatic chamber were introduced. The wall behaviour was monitored without any insulation and was then combined with two types of insulation materials: a synthetic and waterproof insulation board (polystyrene) and a bio-based plaster insulation (hemp-lime), both applied on the interior surface of the wall. The tests consisted in 8h cycles of defined temperature and relative humidity.

The obtained results confirmed that rammed earth walls present high thermal inertia properties. With the addition of a polystyrene insulation on the interior surface, the wall is no longer able to release heat when the interior temperature drops, as polystyrene acts as a barrier and the vapour exchange is blocked.

The hemp-lime plaster was added with the objective to include an insulation adequate to the vapour permeability requirements of the rammed earth wall. Due to the slow drying process of this particular insulation -with ~11% /month of relative humidity decrease- both the wall and insulation hygrothermal behaviours were not submitted to tests, being this left as future work.

Keywords: Monolithic wall; Rammed earth; Hygrothermal behaviour; Polystyrene insulation; Hemp-lime insulation; laboratory test

Resumo

A taipa é uma técnica de construção antiga que consiste na compactação de terra crua por camadas dentro de uma cofragem que se designa tradicionalmente por taipal, constituindo paredes monolíticas. As propriedades da terra contribuem para melhorar o conforto no interior das habitações, atuando como estabilizadora dos níveis de humidade relativa e proporcionando uma grande inércia térmica. Para além disso, ainda é ambientalmente sustentável pois é um material reutilizável que permite construir edifícios com baixa energia incorporada.

Em comparação com técnicas construtivas atualmente utilizadas, as paredes de taipa têm uma menor resistência térmica o que obriga a que, em certas regiões, funcionem em conjunto com isolamento térmico para obter resultados equiparáveis. A alta permeabilidade ao vapor de água de uma parede de taipa requer que o isolamento adicionado apresente características semelhantes, para o seu bom funcionamento.

O objetivo desta dissertação é estudar o comportamento de uma parede de taipa dentro de uma câmara climática, através de medições realizadas em laboratório. Para tal, foram inseridos sensores em ambos os lados da parede e ao longo da sua espessura, medindo grandezas como a temperatura, humidade relativa, fluxo de calor e teor de água. Inicialmente, o comportamento da parede foi monitorizado sem nenhum isolamento; posteriormente a parede foi estudada em conjunto com dois tipos de isolamento distintos colocados na sua face interior: um isolamento sintético e à prova de água (poliestireno), e um isolamento natural sob a forma de um reboco de cânhamo e cal. A parede foi sujeita a ciclos de 8h de temperatura e humidade relativa definidas.

Os resultados obtidos mostraram a capacidade da parede de taipa de reter calor e libertá-lo posteriormente. Com a colocação do isolamento de poliestireno, a parede deixou de ser capaz de reter energia calorífica e transferi-la na forma de calor para o ambiente interior, quando a temperatura deste baixou. Também as trocas de humidade entre a parede e o ambiente interior foram impedidas.

A fim de testar um isolamento com os requisitos de permeabilidade ao vapor de água semelhantes aos da taipa, foi adicionado um reboco de cânhamo e cal. Devido ao seu lento processo de secagem – decréscimo de humidade relativa de ~11%/mês - não foi possível estudar o seu comportamento higrotérmico, sendo apresentado para trabalho futuro.

Palavras-Chave: Parede monolítica, Taipa, Comportamento higrotérmico; Isolamento poliestireno, Isolamento de cânhamo e cal; Teste em laboratório

Notations and Symbols

A	Water absorption coefficient [kg/(m^2.s$^{1/2}$)]
A	Area [m^2]
a	Thermal diffusivity [m^2/s]
C	Specific heat [J/(kg·K)]
C	Mean curvature [m^{-1}]
C_P	Heat capacity at constant pressure [J/(kg.K)]
D	Diffusivity [m^2/s]
DF	Decrement factor [-]
E	Effusivity [J/(kg.m^2.$^{s-2}$)]
e	Thickness of the material or the layer [m]
h_c	Convective surface film coefficient [W/(m^2.K)]
HF_ext	Heat flux on external surface of rammed earth wall [W/m^2]
HF_ins	Heat flux on insulation surface [W/m^2]
HF_int	Heat flux on internal surface of rammed earth wall [W/m^2]
HF_int_s	Heat flux on internal surface of rammed earth wall measured with a small heat flux meter [W/m^2]
J	Diffusion flux [mol/(m^2.s)]
K	Intrinsic permeability of the porous medium [m^2]
L	Latent heat [J/kg]
p	Equilibrium pressure [Pa]
M_{H2O}	Molar mass of water molecules [g/mol]
p_{atm}	Atmospheric pressure [Pa]
p_L	Liquid pressure [Pa]
p_v	Water vapour partial pressure [Pa]
p_v^{sat}	Saturated vapour pressure [Pa]
Q	Amount of heat energy [W]
q’	Internal heat generation [W/m^3]
R	Perfect molar gas constant [J/(mol.K)]
RH	Relative humidity [%]
RH_bonduary	Relative humidity measured on the exterior edge of insulation [%]
RH_control_int	Relative humidity which controls the heater and humidifier devices [%]
RH_ext	Relative humidity measured on external side ambient of the chamber [%]
RH_int	Relative humidity measured on internal side ambient of the chamber [%]

RH_ref_air	Relative humidity outside the chamber [%]
RH_wall	Relative humidity measured in the middle of rammed earth wall [%]
RH_wall_10cm	Relative humidity measured 10 cm from the interior surface of rammed earth wall [%]
RH_wall_ins	Relative humidity measured between rammed earth wall and insulation [%]
R_{si}	Internal surface thermal resistance [(m².ºC)/W]
R_{se}	External surface thermal resistance [(m².ºC)/W]
R_{value}	Thermal resistance [(m².ºC)/W]
r	Capillary radius [m]
S	Sensitivity [V/(W/m) ^{2}]
S_r	Water saturation ratio [-]
t	Time [s]
T	Temperature [K]
T_0	Reference temperature [K]
T_bonduary	Temperature measured on the exterior edge of insulation [ºC]
T_control_int	Temperature which controls the heater and humidifier devices [ºC]
T_ref_air	Temperature outside the chamber [ºC]
T_wall	Temperature measured in the middle of rammed earth wall [ºC]
T_wall_10cm	Temperature measured 10 cm from the interior surface of rammed earth wall [ºC]
T_wall_ins	Temperature measured between rammed earth wall and insulation [ºC]
Ta_ext	Ambient temperature measured on external side of the chamber [ºC]
Ta_int	Ambient temperature measured on internal side of the chamber [ºC]
Ts_ext	Surface temperature of the wall measured on external side of the chamber [ºC]
Ts_int	Surface temperature of the wall measured on internal side of the chamber [ºC]
TL	Time lag [h]
U	Voltage [V]
U_{value}	Thermal conductance [W/(m^2.ºC)]
V	Volume [m^3]
Vw_wall	Water content in the middle of rammed earth wall [%]
w	Water content [kg/m^3]
W_L	Liquid mass of water content [kg/kg]

$\propto$	Heat transfer coefficient [W/(m^2.K)]
β	Water vapour transfer coefficient [kg/(m^2.s.Pa)]
δ_a	Permeability of the air into water vapour [kg/m.s.Pa]
ε	Emissivity of the material [-]
ηL	Dynamic viscosity of water [Pa/s]
ϕ	Porosity [-]
ϕ_L	Porosity filled by the liquid phase [-]
θ	Contact angle formed by the liquid/vapour interface [º]
k	Intrinsic permeability of the porous medium [m^2]
k_r^L	Relative liquid permeability [-]
λ	Thermal conductivity [W/(m.°C)]
μ	Water vapour diffusion coefficient
ρ	Dry density [kg/m^3]
ρ_d	Density of the dried earth material [kg.m^{-3}]
ρ_L	Liquid water density [kg.m^{-3}]
σ	Surface tension [N/m]
σ_0	Stefan-Boltzmann constant [W/(m^2.K^4)]
Φ	Heat flux [W/m^2]
∇	Gradient operator

Contents

List of Figures

List of Tables

1. Introduction

1.1. Context

Low environmental impact is an increasing concern in building design. For this reason, the use of raw earth materials available on the construction site that need low energy for preparation have been continuously tested.

The main benefit of earth lies with the fact that this material can be easily sourced locally and does not require industrial processing (Morel, J. et al., 2001). If no stabiliser is added to the raw earth, it can be infinitely reused, thus it has very low impact in terms of embodied energy when used as building material in construction (Habert, G. et al., 2012).

Rammed earth is an ancient earth construction technique that can be currently found spread all over the world. It is one of the most recent earth techniques, compared to others (adobe, cob, …). It was identified for the first time in Carthage, Tunisia, founded around 814 BC (Jaquin, 2012). In the 8th century, rammed earth reached Europe and it is very commonly used in the region of Rhône-Alpes, France, and in Alentejo, Portugal, until nowadays. This technique consists in compacting local raw earth with a rammer in successive layers, one after another, inside a removable formwork. The earth is composed of aggregates such as clay, silt, sand and gravel, with the clay matrix as the binder of larger aggregates.

Stabilized rammed earth consists in introducing a binder component as additive that enhances the cohesion of earth (Hall, 2007). Air lime was used for stabilization. In Portugal, the so called military rammed earth (taipa militar) can be found in several fortresses from the period of Muslim occupation of Iberian Peninsula. In modern times, Portland cement or lime are used as a stabiliser with proportions that do not exceed 10% of total dry mass (Hall & Allinson, 2009).

Besides being environmental friendly in terms of materials, the rammed earth walls have a performance that contributes to improve hygrothermal and acoustic indoor comfort. The porous material acts as a buffer to relative humidity (RH) levels and internal temperature (T) variations (Taylor & Luther, 2004). The material behaves adsorbing the moisture in excess and releasing during low moisture phases (McGregor et al., 2016).

It was proved that the control of the indoor humidity environment benefits the inhabitants health (Soudani et al., 2017), can help to improve the durability of the building envelope and the design of building ventilation, provides thermal comfort and therefore reduces the energy consumption (Zhang & Yoshino, 2010), (Ramos, 2007).

In terms of health, high values of RH (> 75%) lead to the development of unwanted moulds causing respiratory discomfort and allergies (Bornehag et al., 2001). On the other hand, exposure to low values of RH (< 30%) for an extended period of time, may affect the mucous membrane and it is related to dryness of skin and throats, sensory irritation of eyes and may even lead to viral infections (Mizoue et al., 2004).

By reducing the frequency of high humidity periods at the wall surface, the rammed earth walls were judged to be highly beneficial in reducing mould growth in buildings (Allinson & Hall, 2010).

The affinity of raw earth for water molecules confers cohesion to the material, through suction effects. This affinity allows buffering RH variations and increases the thermal inertia of the wall, bringing quality to interior comfort in terms of acoustic, hygric and thermic aspects (Chabriac et al., 2014).

Liquid water content of a rammed earth wall is an essential parameter to understand the behaviour and the strength of this material (Chabriac et al., 2014). With the water content increasing, the strength of unstabilised earth materials decreases (Champiré et al., 2016; Morel et al., 2007).

Rammed earth walls have a lower thermal resistance (R-value) than common solutions with insulations such as polystyrene and polyurethane, even when insulated with natural wood fibres (Serrano et al., 2016), which induce them to provide inferior performance in terms of insulation, although, with the best dynamic performance and the longest thermal lags.

Rammed earth walls usually present a large thickness, between 30 and 50 cm, since the reduction of their thickness heavily penalizes its thermal behaviour (Taylor, et al., 2008). In addition, thinner samples are more affected by the surface film resistance (McGregor et al. 2017). Their thermal conductivity (~0.6 W/m.K) makes it necessary to add further insulation in most rehabilitation cases. The sensitivity of earth wall to moisture content requires the added insulation material to be sufficiently vapour permeable to allow the necessary moisture regulation of the wall.

1.2. Objective and Methodology

The aim of this work is to study the performance of a construction material with low embodied energy such as rammed earth, and compare its efficiency when an insulation is applied on its internal surface. In this regard, one of the most industrial materials used nowadays (polystyrene) is submitted to several tests. Afterwards, the same tests are made and therefore, compared with a bio-based insulation material (hemp-lime plaster). For this purpose, the thermal and hygroscopic performance of an earth-based wall inside a test chamber is monitored.

The objectives are to understand the heat and mass transfer within the rammed earth wall and the impact of the addition of insulating material on the behaviour of the wall. Specifically, the behaviour at the interface between the insulation and the rammed earth will be monitored.

A numerical simulation based on the material properties and classical hygrothermal model is made using COMSOL Multiphysics, giving valuable information about the heat and vapour penetration in rammed earth. To test the efficiency of the chamber an infrared thermography study is performed.

1.3. Dissertation Structure

The present dissertation begins with a literature review given in chapter 2. Earth materials have a special behaviour due to its hygroscopic characteristics and to make a proper study, a preliminary knowledge is required. The relation between the rammed earth and the environment was studied: the mechanisms of heat transfer, the moisture behaviour, the thermal behaviour and therefore the hygrothermal behaviour of constructions made with rammed earth.

The chapter 3 defines the earth composition of the studied rammed earth wall and also the composition of the two insulations applied on its internal surface. The type of sensors used in this work are defined as well as its location along the wall. In the same chapter it is also presented the procedure that submitted the wall to several tests where T and RH were the variables. An analysis of the climatic chamber efficiency was made appealing to an infrared thermography.

Afterwards, in chapter 4, an analysis on the experimental procedures results was made. Primarily, each constructive solution results were studied separately, and then, all solutions were compared in terms of its heat storage capacity, time lag, moisture buffering and thermal inertia.

Finally, the conclusion of this dissertation and proposals for future works were presented in chapter 5.

2. Heat Transfer and Hygrothermal Behaviour

This second chapter intends to explain the heat and moisture phenomena that occur in or across the walls of hygroscopic materials such as rammed earth. It starts with heat transfer, moisture behaviour, thermal behaviour and finally, it makes the link between these aspects and the hygrothermal behaviour.

2.1. Heat Transfer

In buildings physics, there is an interest for the heat flux in systems that are not in equilibrium. The basic condition for heat transfer to happen in a wall is the existence of a gradient of T between two surfaces of the wall. This heat flux goes from the high temperatures to low temperatures and it ends when the equilibrium between the two temperatures is reached.

The amount of heat transfer, Q, through a given surface, per unit time, Δt, is called heat flux, Φ. The heat flux density, q, presented in (1), is the heat rate per unit area, A, measured in W/m^2.

$$q = \frac{Q}{A} \tag{1}$$

There are three mechanisms of heat transfer: conduction, convection and radiation, further explained below in the next section.

2.1.1. Conduction

The heat transfer in a material is stated by the general equation of heat diffusion, equation (2).

$$\frac{\partial}{\partial x}\left(\lambda\frac{\partial T}{\partial x}\right)+\frac{\partial}{\partial y}\left(\lambda\frac{\partial T}{\partial y}\right)+\frac{\partial}{\partial z}\left(\lambda\frac{\partial T}{\partial z}\right)+q'=\rho c_p\frac{\partial T}{\partial t} \tag{2}$$

This equation describes real conditions, which means that it is in function of time, t. It also depends on ρ, which is the dry density [kg/m^3] and C_p, that is the heat capacity at constant pressure [J/(kg.K)]. In addition, q' is the internal heat generation and λ is the thermal conductivity of the material.

Specific heat capacity, $C_{P,}$ is the amount of energy required to raise 1ºC the T of 1 kg of a material, and is usually expressed in J/(kg.K). *In situ* measurements made by Chabriac (2014) provide the heat capacity value of the used rammed earth as C_P = 647 J/(kg·K).

The conduction of heat energy happens by physical contact between solids at different temperatures and between points at different temperatures in the same solid. The mode also works for liquids, gases and between phases. The energy is spread when vibrating atoms collide and free electrons move collectively. Conduction occurs from higher to lower temperatures.

For steady-state unidirectional heat conduction, the Fourier law is:

$$q_x = -\lambda \frac{dT}{dx} \tag{3}$$

Equation (3) states that the heat flux in the x direction, q_x, is directly proportional to the temperature gradient dt/dx. It is expressed in [W/m^2]. λ in [W/m.ºC] represents the thermal conductivity of the material.

The heat flux is the quantity of heat that passes through the thickness of the material, per unit area. The negative sign means that heat flux is positive in the direction of decreasing temperature. This equation shows that the energy kept in one construction element, like a wall, depends on the density of that element, the specific heat, the volume of the element and the thermal conductivity (Henriques, 2011).

Thermal conductivity, λ, is a material property to conduct heat. It can be defined as the quantity of heat transmitted through a unit thickness of a material per unit area due to T gradient and it is measured in W/(m.ºC). Lower values of thermal conductivity lead to better thermal insulation. For simplicity reasons, this property is assumed constant and scalar. Thermal conductivity is a function of T, moisture content, thickness and sometimes age.

2.1.2. Convection

Convection is the principal form of heat transfer in liquids and gases. The T variation in fluids leads to position change of the mass and variation in density. This results in convection currents, where the hotter fluid comes up and the cold one goes down. It only happens in fluids given that there is no possible variation of volume in solids.

Newton's law of cooling gives the relation of the heat flux by convection between the surface at temperature T_1 and the environment with the temperature T_2, presented in equation (4).

$$q_{conv} = h_c(T_1 - T_2) \tag{4}$$

q_{conv} is the heat quantity and h_c is the convective surface film coefficient [W/(m^2.K)]. The latter depends of the geometry of the surface, the fluid nature and the type of movement (natural or forced convection). The natural convection means that the movements of the fluid are done due to the T gradient, whereas the forced convection happens when there is another source creating fluid movement, like a fan, for example.

2.1.3. Radiation

Radiation is the transfer of energy that results from the emission and absorption of electromagnetic waves without any medium to transport the heat. Above 0 K, each surface emits electromagnetic energy. Between surfaces at different temperatures, the emission results in heat exchanges.

Although the impact of solar radiation is an important element in building materials experiences, it is not going to be mentioned in this work because, during the experience that will be presented, the climatic

chamber was placed inside a laboratory building. So, the only radiation considered is between the surfaces of the rammed earth wall and cork used to insulate the chamber at different T.

The value of the radiated energy for a body, Q [W], with a certain absolute temperature, T [K], of a material, follows the Stefan-Boltzmann equation, presented in equation (5).

$$Q = \sigma_0 . \varepsilon . A . T^4 \tag{5}$$

In this equation the σ_0 is known as Stefan-Boltzmann constant, equal to $5{,}67 \times 10^{-8}$ W/(m^2.K^4), ε is the emissivity of the material, dimensionless, and A is the area [m^2].

The emissivity is the capability of a surface to retransmit the heat that was already absorbed by radiation. It is also the coefficient that links the energy emitted by one surface and the maximum amount that a perfect black body can emit at the same T. The maximum value of the emissivity is 1.

2.2. Moisture Behaviour of Building Materials

2.2.1. Moisture Sorption and Storage

Rammed earth is considered a hygroscopic material which means that its water content changes with the variation of the RH in the surrounding environment, along with interstitial condensation and rain absorption.

Water content, w, is understood as the sum of the water occupation of pores either of three phases (vapour, liquid and gas) due to the complexity to determine each physical state separately by measuring, and due to the fact that individual states constantly change under natural conditions.

The hygroscopic porous medium of rammed earth is constituted by solid material, liquid water, water vapour and dry air as presented in a representative scheme in Figure 2.1. The components interactions between these three phases are responsible for the complex behaviour of earth materials. Under unsaturated conditions, which is the case for rammed earth materials, dry air and water vapour are always present (Fabbri, 2017).

The interaction between the phases results in liquid and vapour mass transfer equations is clarified below, in the next section.

Defined before as a solid material, rammed earth contains in their composition aggregates such as sand, clay, silt and gravel. The specific particle size distribution of these aggregates, allied with an optimized moisture content for a given energy of compaction, allow a high compaction of the soil inside the formwork.

The optimal moisture content for filling the material depends on the clay and silt content which is usually around 10% mass (Miccoli et al., 2014). In addition to the natural binding effect of clay, capillary cohesion contributes to higher stiffness and shear strength of the material.

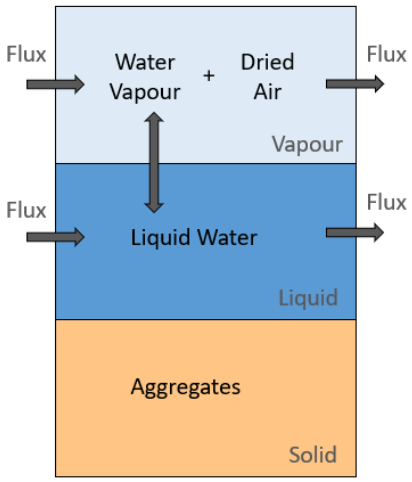

Figure 2.1 - Representation of the porous medium and their interactions (based on Fabbri, 2017)

Capillarity originates from the adhesion between water and air molecules and the pore-wall. This adhesion, named as suction forces, induces movements that usually go against gravity.

When moisture access a dry or unsaturated material, it may be classified into one of three domains, presented in Figure 2.2: sorption or hygroscopic, when moisture is absorbed in the vapour phase; capillary, when moisture is absorbed in the liquid phase; and finally, supersaturated, when liquid moisture cannot be reached by normal suction. It might occur through diffusion in temperature gradient or through suction under pressure. In moisture range C, there are no state of equilibrium and all cavities are filled (Künzel, 1995), (Hall & Allinson, 2009).

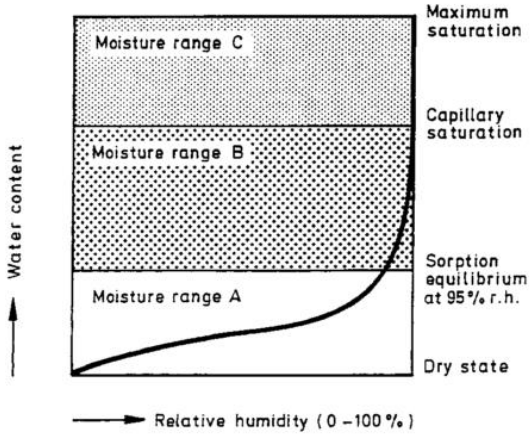

Figure 2.2 – Diagram of moisture storage (Künzel, 1995)

The interface between the liquid phase and the vapour phase in equilibrium is called meniscus. The shape of this meniscus enables the determination of the pressure based on the Young-Laplace equation (6).

$$\Delta p = 2\sigma C \tag{6}$$

Where Δp is the capillary pressure, σ is the surface tension and C is the mean curvature.

The saturation pressure of the porous is lower in concave meniscus than in plane surfaces. This causes the condensation limit to occur for RH lower than 100%.

The Kelvin equation relates the vapour pressure variation between liquid and vapour interfacial curvature. This allows us to understand that the vapour pressure and the RH decrease with bigger pore radius (Hill, 1952).

Kelvin's Law may be written in the form of equation (7).

$$\ln p/p_v^{sat} = \frac{-2\sigma V cos\theta}{r.R.T} \tag{7}$$

In this equation p is the equilibrium pressure, p_v^{sat} is the saturated vapour pressure having a plane surface, σ is the surface tension of the adsorbate, V is the volume of one mole of the liquid adsorbate, θ is the contact angle formed by the liquid/vapour interface, r is the capillary radius, R is the gas constant and T is the absolute temperature.

The Kelvin Law was used to express the water content in function of suction (Soudani et al., 2016) and, in function of RH, the variables that are going to be studied. It may be written in the form of equation (8).

$$p_{L-}p_{atm} = \frac{\rho_L.R.T}{M_{H2O}}\ ln\varphi \tag{8}$$

In this equation pL is the liquid pressure [Pa], p_{atm} is the gas pressure known as the atmospheric pressure [Pa], R is the perfect gas constant [J/(mol.K)], T is the absolute temperature [K] and M_{H2O} is the molar mass of water molecules [g/mol].

2.2.2. Vapour Transfer

Air contains water vapour. Moist air is considered a mixture of dry air and water vapour.

The RH is the rate between the pressure of water vapour that exists in the air and the maximal value of partial vapour pressure that the air can hold at a given T. Consequently, the water vapour condensates above this value (Soudani, 2016) (equation 9).

$$RH = \frac{p_v}{p_v^{sat}\ (T)} \times 100 \tag{9}$$

In equation (9), RH[%] is related to p_v [Pa], the water vapour partial pressure and to p_v^{sat} (T) [Pa], the saturated vapour pressure at a given T.

If p_v increases until the maximum value is reached, it will be equal to p_v^{sat}. Thus, the relative humidity will be 100% and consequently, dew point is reached when p_v increases to a maximum value equal to p_v^{sat}. So, the water vapour then starts to condensate.

Moreover, the p_v^{sat} still is a function of T. Therefore, the relations between the water vapour concentration [g/m^3], the air temperature [ºC] and the RH [%] can be represented by a psychrometric chart shown in Figure 2.3.

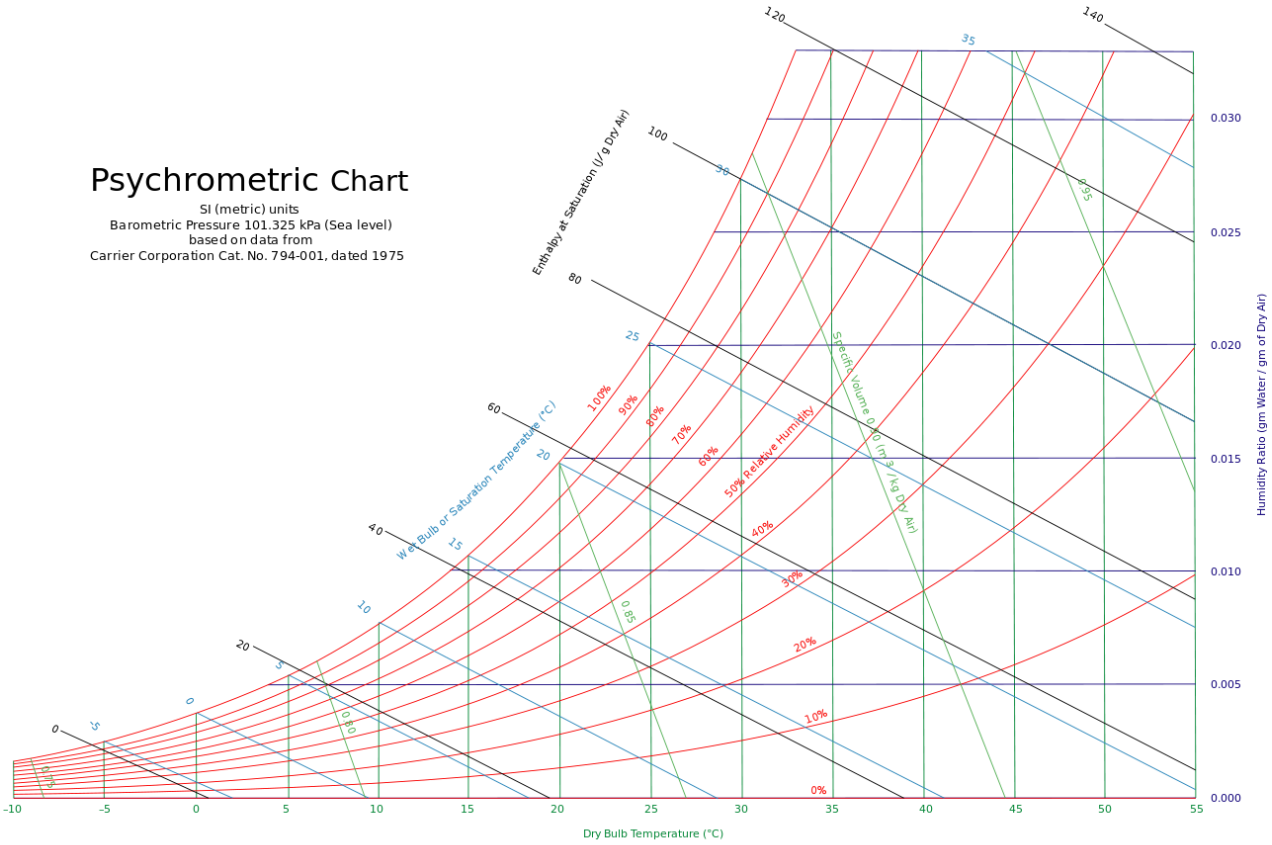

Figure 2.3 - Psychrometric chart (Willis Carrier, 1975)

Through the analysis of the psychrometric chart it is evident that if the water vapour concentration is kept constant and the T rises, the RH will consequently decrease. On the other hand, keeping the T as a constant and rising the water vapour concentration will increase the RH. Furthermore, if both of them vary in opposite sides, increasing the water vapour concentration and decreasing T leads to upper values of RH and vice versa.

Under moist air circumstances, water fills open pores in a dry porous material, regardless of RH. This phenomenon is called adsorption.

The reverse phenomenon, in other words, the water loss due to lower RH values, is called desorption. Ideally, these values should match to adsorption values. However, the desorption is a slower process than adsorption. The gap between the two phases is called hysteresis, presented in Figure 2.4.

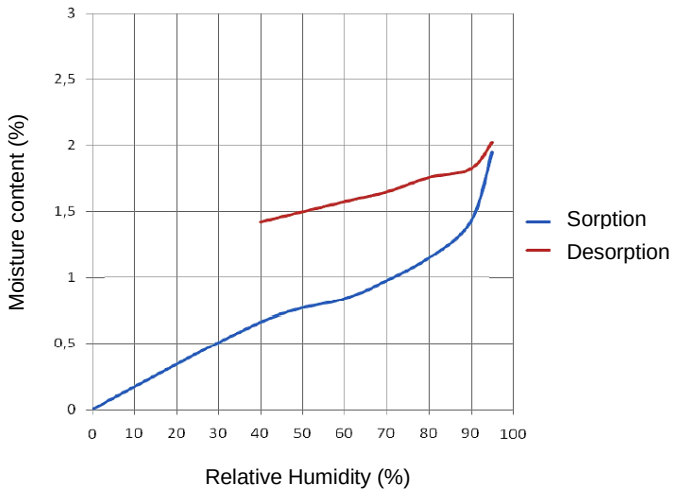

Figure 2.4 - Hysteresis in mineral materials (adapted from Henriques, 2011)

As a function of relative humidity, the sorption isotherm allows the equilibrium of moister contents with a hysteresis between humidification and dehumidification. Each material has his own S-curve which characterizes it (Hens, 2012) (Figure 2.5).

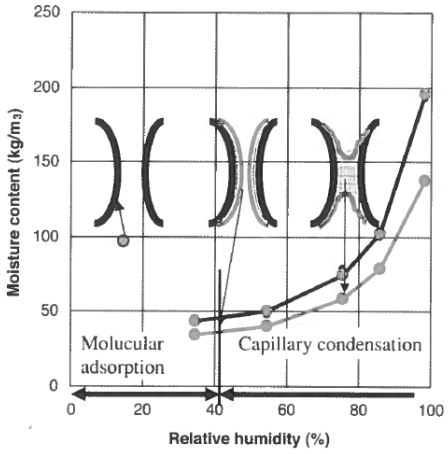

Figure 2.5 - Sorption isotherm (Hens, 2012)

The mechanisms that bind water molecules depend on the value of relative humidity. For lower values (less than 40%), the adsorption of water molecules at the pore walls occurs, whereas, for higher values, capillary condensation on the water menisci formed by the adsorbed layers happens. The saturation zone is achieved when the maximum hygroscopic moisture content at equilibrium is 98%.

Kelvin's Law links the porous radius and the relative humidity value where saturation occurs (Henriques, 2011). For 20ºC the saturation graphic presented in Figure 2.6 shows that, the wider the pores, the higher must be the relative humidity for capillary condensation.

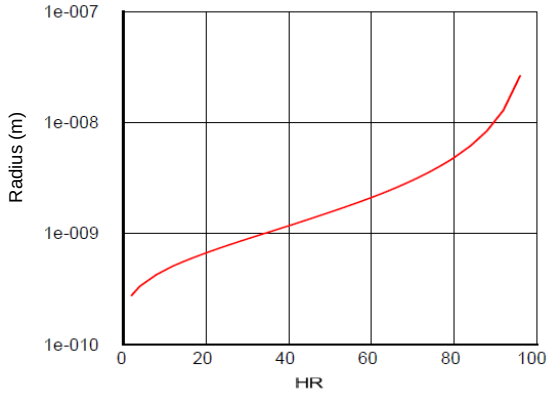

Figure 2.6 - Saturation from Kelvin law at 20ºC (adapted from Henriques, 2011)

Water saturation ratio, designated by $S_{R,}$ is the actual volume of liquid water per unit of actual porous volume and is represented in equation (10).

$$S_R = W_L \frac{\rho_d}{\emptyset . \rho_L} \tag{10}$$

In this equation W_L is the liquid mass of water content [kg/kg], ρ_d is the density of the dried earth material [kg.m^{-3}], $\emptyset$ is the porosity [-] and ρ_L is the liquid water density [kg.m^{-3}].

The water content can be defined as the total mass of water, liquid plus vapour phase.

2.2.3. Moisture Transport

Moisture transport inside the porosity of a material is the result of different phenomena that lead to the movement of the contained water in both liquid and vapour phases.

The passage of dry air increases the drying potential of an assembly and discharges water vapour before it may condense. On the other hand, it may increase heat loss and heat gain substantially if placed close to insulation.

As said before, water vapour and liquid water can be found in the porous network of a hygroscopic material. Depending on the different phase the water is found, the transport will be different and follows a different equation.

The first phenomena of heat flux described above - conduction - corresponds to one mass transfer: diffusion. The water vapour diffusion process is a response to a gas concentration gradient where a natural redistribution of that concentration will occur until equilibrium is reached (Henriques, 2011).

Fick's Law is represented in the equation (11) and describes the water vapour diffusion.

$$J = -\delta_a \nabla p_v \tag{11}$$

In this equation J is the diffusion flux (in mol.m^{-2}.s^{-1}) and δ_a is the permeability of the air into water vapour (kg/m.s.Pa) that depends on the water vapour diffusion, the ideal gas constant and the absolute T.

The ∇p_v is the gradient of the pressure. Fick's Law was given in another form by Soudani (2016), presented in the equation (12), which was used in Comsol Multiphysics simulation.

$$J = \frac{M_{H20}}{RT} D_e^v . \nabla p_v \tag{12}$$

In another way, Fick's Law may also be written using the M_{H20} which is the molar mass of the water molecules [g/mol], R is the ideal gas constant and is equal to 8,314 J/(K.mol), T is the absolute temperature [K], D_e^v is the effective diffusion coefficient [m^2/s] and ∇p_v is the gradient of water vapour partial pressure [Pa].

Based on the equation of mass conservation of water vapour, equation (13) was obtained by Soudani et al. (2016). The vapour mass conservation is equal to the transport of the vapour – explained before as the Fick's Law - plus the phase change (capillary condensation and adsorption) within the material.

$$\frac{\partial m_v}{\partial t} = \nabla \left(\frac{M_{H20}}{RT} D_e^v . \nabla p_v \right) + \dot{m}_{\to v} \tag{13}$$

On the other hand, to study the liquid water transport there is the Darcy's Law presented in equation (14).

$$\phi_L V_L = -\frac{k . k_r^L}{\eta_L} \nabla p_L \tag{14}$$

In this equation $\phi_L = S_r \phi$ [-] is the porosity filled by the liquid phase, k [m^2] is the intrinsic permeability of the porous medium, k_r^L [-] is the relative liquid permeability, ηL [$Pa.s^{-1}$] is the dynamic viscosity of water, equals to 10^{-3}.

If the relative velocity of the liquid in the pores follows Darcy's Law, neglecting the term of gravity, the conservation of the liquid water mass can be deduced (Soudani, 2016) and it is presented in equation (15).

$$\frac{\partial m_L}{\partial t} = \rho_L . \nabla \left(\frac{k . k_r^L}{\eta L} \nabla p_L \right) - \dot{m}_{\to v} \tag{15}$$

2.3. Thermal Behaviour of Building Materials

2.3.1. Thermal Transmittance

The thermal resistance is a performance indicator of the insulation of a certain wall. The behaviour depends on the thermal conductivity, λ [(W/(m.ºC)] and the thickness, e [m], of the material. The thermal resistance [(m².ºC)/W], also known as R_{value} is given by equation (16).

$$R_{value} = \frac{e}{\lambda} \tag{16}$$

The R_{value} is a measure of how well an insulation material will resist to the flow of heat or cold. With higher values of thermal resistance, the insulation effectiveness is greater.

There is another indicator well-known as thermal transmittance, U_{value} [W/m².ºC] that is presented in equation (17).

$$U_{value} = \frac{1}{R_{value} + R_{si} + R_{se}} \tag{17}$$

For a horizontal heat flux, such as the case of a wall, the external and internal superficial thermal resistances used was the European norms, from ITE50 (Santos and Matias, 2006). The internal thermal resistance, R_{si}, is 0.13 (m².ºC)/W and for external thermal resistance, R_{se}, the value is 0.04 (m².ºC)/W.

The lower the U_{value}, the better will be the performance of the wall.

2.3.2. Thermal Inertia

Thermal inertia is the ability that prevents the flux from immediately passing through the wall. Instead, the wall will be warmed up gradually and the accumulated heat will be stored inside the wall and released gradually hours after. Stored heat inside a wall depends on many factors such as time, density, specific heat, volume of the wall and finally, thermal conductivity. The delaying of the T transmission is called time lag. It also depends on how fast the heat is absorbed and dispersed.

In conditions that the T in one side (for example, external temperature, T_e) is lower than on the other side (internal temperature, T_i), the heat flux (q) can be calculated by equation (18). In the case the T_e and T_i have the same value, the flux that crosses the wall will be null.

$$q = U_{value}(T_e - T_i) \tag{18}$$

When a disturbance happens in a system, the thermal mass has a tendency to bring the material to a new equilibrium T. The time lag represents how long it will take to reach this new equilibrium. The higher the thermal mass is, the greater is the time lag.

A material that induces high time lags and low decrement factors provides almost constant inside temperatures which results in a good comfort level. This was underlined by (Sun et al., 2013)

The decrement factor (DF) is defined in equation (19)

$$DF = \frac{T_i^{max} - T_i^{min}}{T_e^{max} - T_e^{min}} \tag{19}$$

In this equation, T_i^{max}, T_i^{min}, T_e^{max} and T_e^{min} represent the maximum and minimum temperatures of the interior and exterior surfaces, respectively.

The time lag (TL) is defined in equation (20)

$$TL = t_{Ti}^{max} - t_{Te}^{max} \tag{20}$$

In this equation, t_{Ti}^{max} and t_{Te}^{max} represents the time when the interior and exterior surface temperatures are on their maximum. Analogously, it can also be calculated for the minimum peak.

2.3.3. Diffusivity and Effusivity

Diffusivity and effusivity are parameters used to quantify thermal mass of a construction material. They enable the measurement of heat exchanges for different materials.

The thermal diffusivity, D [m^2/s], expressed in equation (21), is the ability of the material to transfer T variations. It shows how fast heat is spread inside a material. Thermal diffusivity is directly proportional to the heat transfer rate, thus, heat transfer is inversely proportional to the heat capacity. Low values of diffusivity will be able to buffer T variations.

$$D = \frac{\lambda}{\rho C_p} \tag{21}$$

In equation (21), λ is the thermal conductivity of the layer between the sensor and the surface [W/(m.K)], ρ is the dry density [kg/m^3] and C_p is the heat capacity at constant pressure [J/(kg.K)]. The lower the diffusivity is, the higher are the buffering effects of the material.

On the other hand, thermal effusivity, E [$J/(kg.m^2.s^{1/2})$] is a measure of the ability of the material to exchange energy with its surroundings and it is defined with the same variables that were used in diffusivity. It is presented in equation (22).

$$E = \sqrt{\lambda \rho C_p} \tag{22}$$

The higher the effusivity is, the more quickly the material absorbs heat without T rise at its surface which means that the wall is not going to store heat efficiently.

Recent studies evidence that earth materials, whether are dry or wet, seem to have a good compromise between a low diffusivity and a high effusivity, which means that the outside temperature variations will be lowered by the material. However, it is not capable of storing heat (Soudani et al., 2017).

2.4. Hygrothermal Behaviour

Walls are exposed to thermal and hygric gradients. External walls surfaces interact with external environment through the exchange of heat (convection and radiation), moisture (wind driven rain and vapour diffusion) and finally, liquid water (sorption, desorption and capillarity). They also interact with the indoor environment through the exchange of heat and water, both in liquid and vapour phases (Figure 2.7).

Since the experimental work that will be presented in this dissertation is performed inside a laboratory, the variables related to solar radiation, wind driven rain and capillarity are not considered. The heat transfer will be further discussed through T.

Interior T and RH can be significantly influenced by the interactions previously described (Janssen & Roels, 2009). The transport and storage of heat and water inside the wall depends on construction materials properties.

Rammed earth has a great thermal mass since it can absorb, store and release substantial amounts of heat, keeping stable interior air T. On the other hand, it has a high hygric mass since it can absorb, store and release significant amounts of water, keeping stable the RH on the interior (Allinson & Hall, 2010).

Nevertheless, the impact of evaporation and condensation is a non-negligible phenomenon on the surfaces.

The use of surface film coefficients for heat transfer and thermal conductance does not reflect exactly the reality. These coefficients are used to obtain simplified results in steady state, but then the moisture buffering has no impact. The mass transfer causes energy displacement. This movement includes kinetic energy and potential energy as a result of gravity, suction forces and pressure, which in turn induces heat transfer (Fabbri, 2017). Each solid, liquid or gas at a certain T contains a quantity of heat per mass-unit, given by equation (23).

$$Q = c\,(T - T_0) \tag{23}$$

In this equation, c is the specific heat [J/(kg·K)], T is temperature and t_0 is the reference temperature.

The hygrothermal behaviour is the coupling between mass transfer (liquid and water vapour) and heat transfer in the same porous material. It happens in a transient regime, where T and heat flux change with time. The hygrothermal coupling is represented in Figure 2.7.

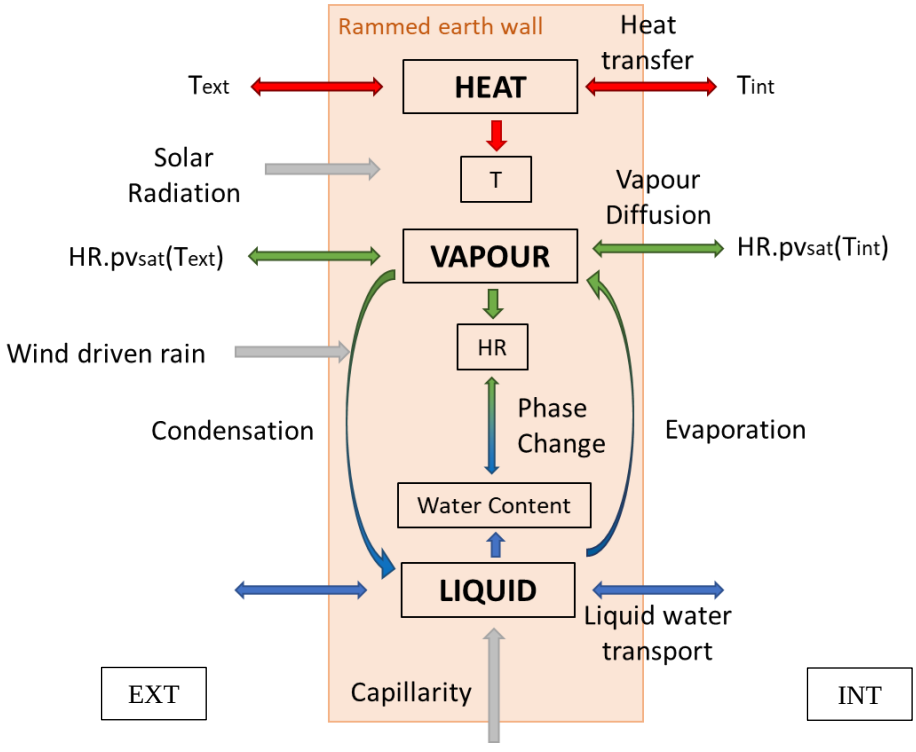

Figure 2.7 - Hygrothermal coupling (based on Soudani, 2016)

The hygrothermal coupling is going to be measured experimentally, and more precisely the T progress due to evaporation and condensation of the water vapour is measured during moisture ingress.

When energy is provided to a material, its T changes. However, during phase changes, the T of the material stays constant. This happens because energy is required to change the phase of the material. Once heat is added to a liquid, the molecules start to vibrate faster, and this allows the liquid to transform into vapour.

The latent heat, L [J/kg] is obtained by the amount the heat energy, Q, per mass unit, m, required for phase change to occur (equation (24)).

$$L = \frac{Q}{m} \tag{24}$$

Rammed earth seems to be able to store latent heat because of liquid to vapour phase changes occurring within the pores. This provides the high thermal mass of the material to avoid elevated temperatures in summer and low temperatures in winter (Soudani, 2016).

The hygrothermal behaviour of rammed earth wall has been studied *in situ* by several researchers (Soudani, 2016), (Taylor & Luther, 2004), (Taylor et al., 2008) and in laboratory by Chabriac et al. (2014, 2016). Most of them also made the laboratory characterization of the material. The hygrothermal properties were also studied in laboratory by McGregor et al. (2016) providing the moisture buffering performance of rammed earth and in comparison with compressed earth block and earth plaster samples. Penetration depth below 2 cm were obtained for calcareous-clay materials formulations (McGregor et al., 2017).

The calibration procedure to monitor the hygrothermal behaviour of a rammed earth wall was defined by Chabriac et al. (2014).

Allinson & Hall, (2010) created a model to study the hygrothermal behaviour of a cement stabilised rammed earth building with vapour resistance renders and then validated the model with *in situ* measurements.

Several research studies have been conducted to study other characteristics of rammed earth, such as: impact of moisture in mechanical behaviour (Champiré et al., 2016); mechanical characteristics in compression (Miccoli et al., 2014); thermal comfort and energy reduction (Taylor & Luther, 2004), (Taylor et al., 2008); and finally, durability to external conditions (Bui et al., 2009).

The hygrothermal behaviour between other bio-based materials and the environment has been studied by many authors for straw concrete walls (Rahim et al., 2017), wooden insulation panels (Serrano et al. 2016) and for hemp-lime (Holcroft & Shea, 2013), (Collet et al., 2013). The latter was also tested with different coatings applied on the surface (Tran Le et al., 2016). These researchers measured the effect of latent heat during moisture buffering tests where cycles of sorption/desorption with different ranges of RH and different hour periods were simulated. The results underline that hemp fibre did influence the moisture buffering and storage capacities of hemp concrete.

3. Materials and Methods

3.1. General Remarks

A rammed earth wall is monitored without and with two different types of thermal insulation applied on its internal surface. This chapter describes the tested materials and the experimental tests performed.

This study was made using specific equipment such as heat flow meters, hygrometers and thermometers. After an exhaustive set up and calibration of all sensors, the wall was submitted to several tests where T and RH were the variables.

Throughout the tests, insulation improvements were made firstly in the chamber and then in the rammed earth wall. The wall was insulated with a synthetic and waterproof insulation and compared to an earth based insulation. The chamber improvements were verified by infrared thermography.

3.2. Materials

A rammed earth wall was placed into a climatic chamber made with waterproofed cork with 10 cm thickness. The rammed earth wall has 1.00 m in width, 1.50 m in height and 0.30 m in depth, as presented in Figure 3.1 (a) below. The dimensions of the chamber are 1.20 m in width, 1.70 m in height and 1.90m depth. The access to the interior of the chamber is made by two entrance doors, which allow both sides of the rammed earth wall to be seen. The real chamber is presented in Figure 3.1 (b). A heater and a humidifier are placed inside the chamber. On the other hand, outside the chamber is visible in Figure 3.1 (b) the wiring which connects the devices and sensors to the computer that collects the data.

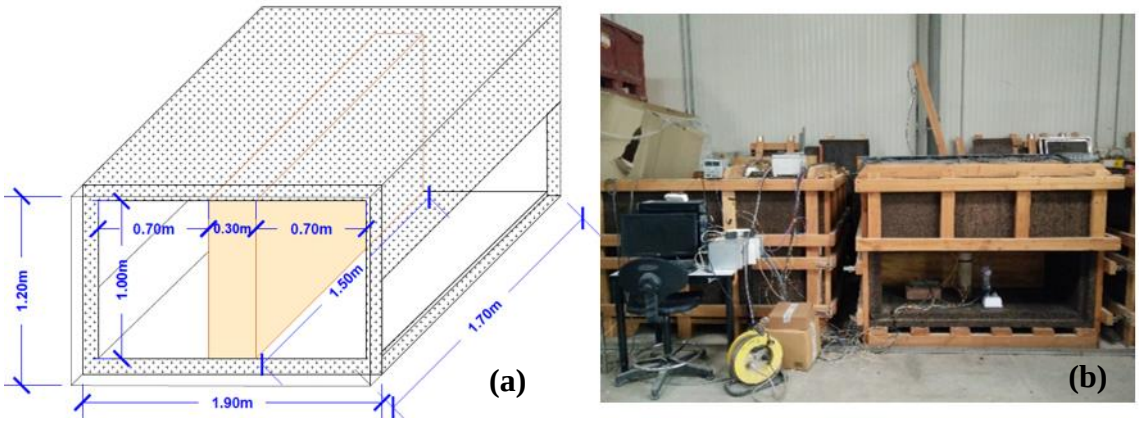

Figure 3.1 - Design of the climatic chamber (a) and the real climatic chamber (b)

The climatic chamber is situated inside a laboratory made of metallic walls, and between two similar chambers. One of the entrance doors are side turned to the edge of the laboratory, and the other entrance, on the opposite side, turned to the centre of the laboratory. Parallel to both entrance doors, the rammed earth wall is inserted in the middle of the chamber. Near to the chamber there are two big garage doors, frequently

opened in Summer time. Above the garage doors are windows and early in the morning, the sun irradiates in the direction of the chamber. For a better understanding, see Figure 3.2.

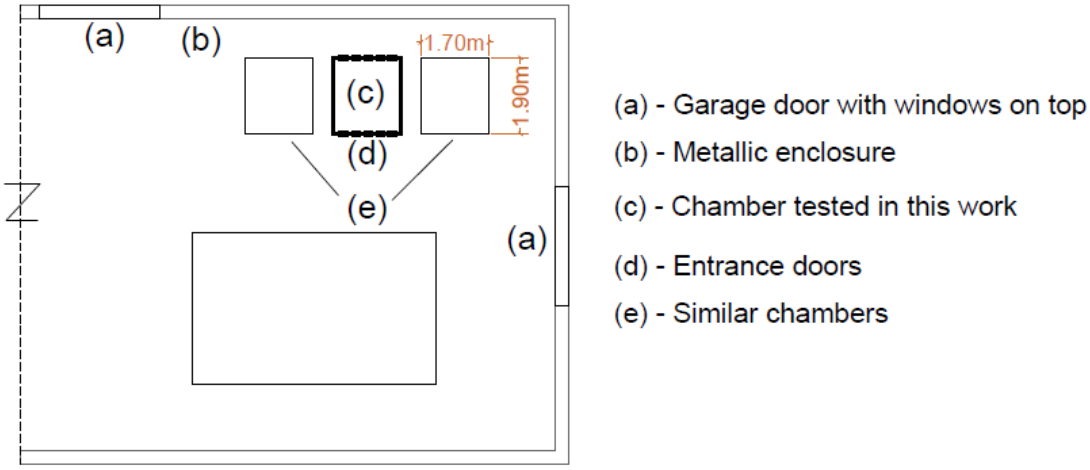

Figure 3.2 – Chamber location in the laboratory

The rammed earth wall was already manufactured by Nicolas Meunier Company, specialist in rammed earth. The earth used for the construction of the wall was taken from St. Antoin l'Abbaye region, in Rhône-Alpes, France.

The earth composition is silt, sand and gravel which contains nearly 10% mass of aggregates with the diameter greater than 40 mm. Moreover, the earth always contains clay that acts as binder between the grains, in this case with approximately 16% mass. The grading curve of this earth may be found in Chabriac (2014). The soil was stabilized with 2.5% mass of natural hydraulic lime NHL5 with the purpose of increasing the durability and mechanical performance of the wall.

The rammed earth wall has been pre-fabricated, composed by several layers of earth with 10-15 cm thick placed inside a removable metallic formwork. Each layer has been compacted with a pneumatic rammer obtaining a final layer with 6-10 cm. The procedure was repeated until the experimental wall was accomplished.

The mechanical properties of rammed earth walls depend on a few factors: granulometry of the earth, moisture contents, compaction type and power, and finally, type and content of additions. These previous factors define the rammed earth apparent density and porosity (Miccoli et al., 2014).

Some properties of this rammed earth wall were already studied elsewhere (Chabriac, 2014): heat capacity $C_p = 647$ J/(kg.K), thermal conductivity $\lambda = 0.64$ W/(m.°K), porosity $\emptyset = 0.345$, water vapour diffusion coefficient μ = 9 and, at last, water absorption coefficient A= 0.37 kg/(m^2.s$^{1/2}$).

Considering that some properties of the rammed earth wall has already been studied by Chabriac (2014), the aim is to continue his work, going further and applying two different insulations on the rammed earth wall earlier presented.

An expanded polystyrene board (EPS), a common synthetic insulation used nowadays, was applied. This material is one of the most versatile insulations available: it has a low thermal conductivity λ=0.04 W/(m.°K), a light weight, it is easily shaped, as well as it is cheap. Nevertheless, its permeability to water vapour is low. The aim was to see the hygrothermal behaviour of rammed earth when in contact with a synthetic and waterproof barrier.

On the other hand, a hemp-lime plaster was applied to the same rammed earth wall. Besides being a recyclable resource, the characteristics of this insulation is consistent with the behaviour of the rammed earth wall since it allows the moisture to be released, avoiding condensation issues. The pore structure of hemp-lime allows it to dampen variations in environmental heat and humidity (Shea et al., 2012), as well as rammed earth. It also has a good thermal performance with a relatively low thermal conductivity λ=0.304 W/(m.°K) obtained from one tested sample. Other fibres have been studied and it was concluded that hemp fibres are more resistant to biological decay when compared to other bio-based building materials, such as straw (Shea et al., 2012). Due to their low mechanical resistance (Arnaud & Gourlay, 2012), hemp-lime is mainly applied as wall insulation or even as roof and floor insulation.

Table 3.1 – Materials properties

Material	Thermal Conductivity (λ) [$W/(m.K)$]	Dry density (ρ) [kg/m^3]	Heat Capacity (C_p) [J/(kg.K)]
Rammed Earth (RE)	0.640 (1)	1800 (5)	647 (1)
Polystyrene (EPS)	0.037 (2)	20 (6)	1500 (6)
Hemp-Lime (HL)	0.304 (3)	478 (4)	1100 (4)

Reference sources: (1) Chabriac, 2014; (2) Santos and Matias, 2006; (3) Sample tested by the author; (4) Rahim et al., 2017; (5) Hall & Djerbib, 2004; (6) Technical report GmbH.

With the lower density of the three materials, polystyrene requires more energy to raise the T 1ºC, based on Table 3.1. In addition, it has the lower thermal conductivity which makes it the best insulation for the rammed earth wall in terms of thermal performance.

Thermal resistance (R-value) for rammed earth wall is 0.47 (m^2.ºC)/W according to its thickness (30 cm) divided by its thermal conductivity, presented in Table 3.1. Therefore, using Rsi and Rse provided by Santos and Matias (2006), a U-value of 2.1 W/(m^2.ºC) is achieved. When combined with 10 cm of EPS, rammed earth reaches an R-value of 3.17 (m^2.ºC)/W and a U-value of 0.3 W/(m^2.ºC). Finally, for rammed earth wall combined with 8 cm of hemp-lime plaster, it reaches R-values of 0.73(m^2.ºC)/W and a U-value of 1.1 W/(m^2.ºC). In terms of thermal resistance, the best solution is the one with lower U-value, therefore the rammed earth combined with EPS.

3.3. Tests Procedure

To study the behaviour of the rammed earth wall, four constructive solutions were conducted. Firstly, the cork worked as the insulation of the test chamber and the rammed earth wall had no insulation. This

combination corresponds to constructive solution 1; the chamber is presented in Figure 3.3 (a) and the rammed earth wall placed inside the chamber is presented in Figure 3.4 (a), both without any insulation. Every test counts with the installation of three fans inside the chamber and the reason is explained below, in chapter 3.5.

It was realized that the cork was not a proper insulation, because the outside conditions variation was influencing the chamber variation. For this reason, polystyrene boards were added outside the chamber with 4 cm on the lateral sides of the chamber and with 10 cm on the top side of the chamber (where heat losses were bigger as will be seen further on in chapter 4.2.2). In addition, in the interior side of the cork chamber, was added a thermal insulation coating made by Granomural®. This thin insulation (3 mm) is an ecologic solution based on wood fibre and cellulose, used both for thermal and acoustic insulation.

The improvements made outside the chamber are shown in Figure 3.3 (b) and inside the chamber in Figure 3.4 (b), corresponding to constructive solution 2. As it can be noticed, one side of the chamber was not insulated because it worked as the external side and, for this reason, it was determined that it would stay always open to the outside environment. The described chamber insulation remained until the end of the experiments.

Figure 3.3 - Improvements in chamber: constructive solution 1 (a) and constructive solution 2, 3 and 4 (b)

Afterwards, corresponding to constructive solution 3, the behaviour of rammed earth was combined with 10 cm expanded polystyrene board (EPS) with a thermal conductivity λ=0,055 W/(m.°C). As said before, the aim was to see the behaviour of rammed earth with a synthetic and waterproof insulation. The board was placed on the interior side and was 2 cm distant from the wall, assured with spacers. This gap is simulating that EPS was applied fixed to an intermediate structure for a false interior surface wall. Sensors

between the wall and the waterproof insulation were added, further explained in the next section. The improvements on the rammed earth wall are shown in Figure 3.4 (c).

The purpose of the 4th and last constructive solution was to study the behaviour of the rammed earth when combined with a hemp-lime insulating plaster, presented in Figure 3.4 (d).

Figure 3.4 - Improvements in rammed earth wall: constructive solution 1 (a), constructive solution 2 (b), constructive solution 3 (c) and constructive solution 4 (d)

The hemp-lime mortar is a bio-composite material which consists in a mixture of hemp shives, natural hydraulic lime NHL 3.5 and water. This mortar was prepared inside a concrete mixer (see Figure 3.5 (a)) with a ratio of 10% mass of hemp, 46% of binder and 44% of water for the first layer and a ratio of 9% mass of hemp, 40% of binder 51% of water for the second and third layers. The layers were applied with an interval of 7 days, in order to allow the first layer to dry and gain resistance before the application of the second. Before the application of the mortar layers, the surface was moistened with a sponge to improve the adhesion. The hemp-lime mortar was applied by manual projection technique, visible in Figure 3.5 (b).

Besides, to obtain the real thermal conductivity value of the insulation, a small sample was gathered in one mould with 12 cm of diameter and 8 cm of thickness (see Figure 3.6 (a)). The size of the sample is representative of the insulation thickness. The thermal conductivity was tested in laboratory conditions at 24 ºC and 65% RH, in Faculdade de Ciências e Tecnologia da Universidade Nova de Lisboa, with a ISOMET Heat Transfer 2104 equipment, with a 6 cm diameter contact probe API 210412, one month after the preparation, when sample was already dried (see Figure 3.6 (b)).

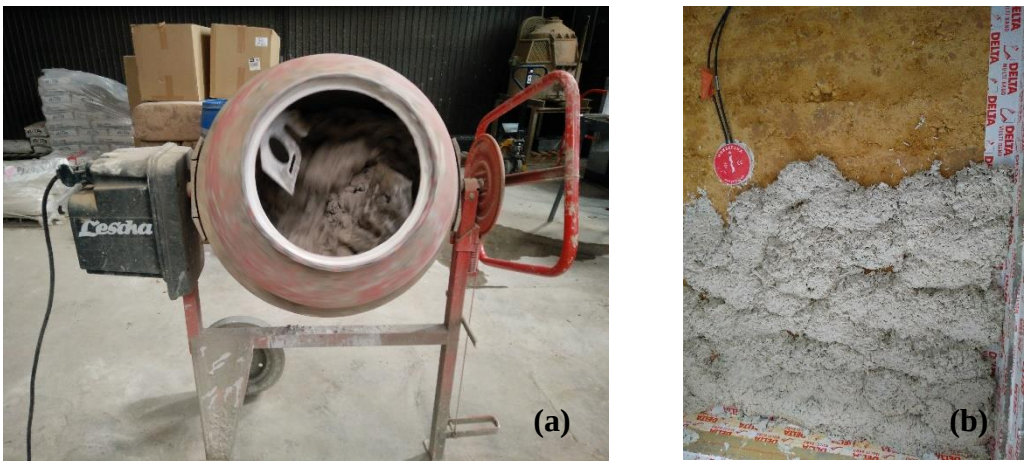

Figure 3.5 – Preparation (a) and aplication (b) of hemp-lime plaster

Figure 3.6 – Hemp-lime sample (a) and thermal conductivity determination (b)

The expected drying time of the hemp plaster applied on the wall was one to two months; however, after four months, the moisture content between the rammed earth and the insulation was 70%, while the daily peak of ambient RH was 60%. Since the plaster has not dried completely in the available time for this work, the tests that follow were not achieved. Nevertheless, the drying curve was analysed and reasons that might have affected the drying period were discussed.

For each constructive solution (apart from the last one), the influence of T and RH combined was studied, and then each one separately in order to highlight the heat flux due to adsorption of moisture in the wall. Only the internal side was submitted to these T and RH 8h cycles, while the external side was permanently open where the variations was due to the outside environment. The 8h cycle has the aim to characterize an office building or a bedroom (8h occupancy versus 16h free of occupants).

The devices used to control T and RH inside the chamber enable only to increase its values; so, when the cycle ends (e.g. T=30ºC for 8 hours), it slowly returns to equilibrium state. Due to this limitation, the T chosen to the cycles was 30ºC in order to keep the T on the interior side always higher than on exterior side. Thus, it was guaranteed that during the entire experience (from Winter to Summer) the heat flux was

permanent from the interior to the exterior (since interior side T will always be higher than outside T, guided by the external T of the lab). Moreover, it was chosen 80% for RH cycles, regarded as an uncomfortably high RH value, which might cause adverse building and health effects, in accordance with conducted studies about house occupancy (Arundel et al., 1986).

For each constructive solution, the procedure conducted for each test is detailed below and exemplified in Figure 3.7.

Constructive Solution 1 – Chamber without insulation / Rammed Earth (R.E.) wall without insulation

→ T and HR with outside variation;

→ T=30ºC constant;

→ Cycle T=30ºC during 8h and switched off the rest of time.

Constructive Solution 2 – Chamber with polystyrene insulation / R.E. wall without insulation

→ Cycle T=30ºC and RH=80% during 8h and switched off the rest of time;

→ Cycle T=30ºC during 8h and switched off the rest of time and RH=60% remains constant;

→ Cycle RH=80% during 8h and switched off the rest of time and T=30ºC remains constant.

Constructive Solution 3 – Chamber with polystyrene insulation / R.E. wall with polystyrene insulation

→ T=30ºC constant;

→ Cycle T=30ºC and RH=80% during 8h and switched off the rest of time;

→ Cycle T=30ºC during 8h and switched off the rest of time and RH=60% remains constant;

→ Cycle RH=80% during 8h and switched off the rest of time and T=30ºC remains constant.

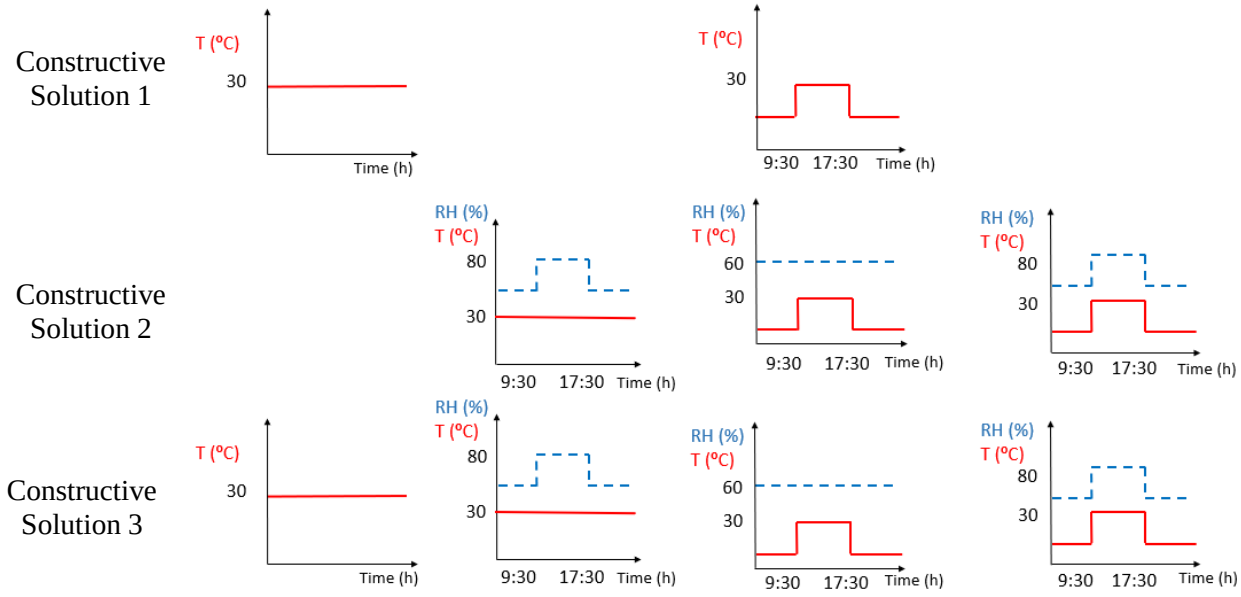

Figure 3.7 - Representation of T and RH cycles for each constructive solution

3.4. Sensors and Data Acquisitions

3.4.1. Constructive Solution 1 – Without Insulation

Ten sensors were initially used to monitor the rammed earth wall. They are represented in a side view in Figure 3.8 and in an upper view in Figure 3.9. One side will perform like external environment (cold side) and the other side will perform like the internal environment (warm side).

For acquiring ambient T and RH, four CS215 sensors were installed. They are represented in pink in Figure 3.8 side view and Figure 3.9 for an upper view. The real sensor is showed in Figure 3.10 (a). According to the manufacturer, the CS616 probe accuracy is ± 0.4ºC for T measurements and ± 2% for RH measurements (Campbell Scientific, 2016a).

One of the four CS215 sensors was placed inside the earth wall and it measures both the T and RH in the middle of the wall. Their designations are ***T_wall*** for the T and ***RH_wall*** for RH.

Two other CS215 sensors measure the ambient T and RH inside the chamber, in both internal and external environments. Their designations are ***Ta_ext*** and ***RH_ext*** for the external side and ***Ta_int*** and ***RH_int*** for internal side.

The fourth CS215 sensor was used to monitor the environment outside the cork chamber and it was placed far away from the influence of the heating which might pass through the chamber walls. Their designations are ***T_Ref_Air*** for the T and ***RH_Ref_Air*** for the RH.

Represented in red in Figure 3.8 and Figure 3.9, two 107 Temperature Probe sensors were installed to measure the surface T of the rammed earth wall. Their designations are ***Ts_ext*** for the external environment and ***Ts_int*** for the internal. The real sensor is showed in Figure 3.10 (b). This probe accuracy is ± 0.4ºC for T measurements, according to the manufacturer (Campbell Scientific, 2016b).

Another sensor was also used, of type CS616 Water Content Reflectometer, to measure the water content inside the wall, designated by ***VW_wall*.** It is represented in blue colour in the same figures (Figure 3.8 and Figure 3.9). According to the manufacturer, the CS616 probe accuracy is ± 0.4ºC for T measurements and ± 2% for RH measurements (Campbell Scientific, 2016c).

At last, two thermal HFP03 sensors by Hukseflux® were installed with the propose of measuring the heat flux. As in previous, the designation ***HF_ext*** was used for the external environment and ***HF_int*** for the internal environment. They are represented in purple. The sensor is shown in Figure 3.10 (c).

The HFP03 sensor is known as a thermopile which consists of a certain quantity of thermocouples, which are two metals electrically connected in series. Every thermocouple will generate an output voltage that is a linear function of the T difference between its hot and cold joints. Putting thermocouples in series amplifies the signal. The uncertainty of calibration for this sensor is ± 6%. (Hukseflux - HFP01 & HFP03, 2016).

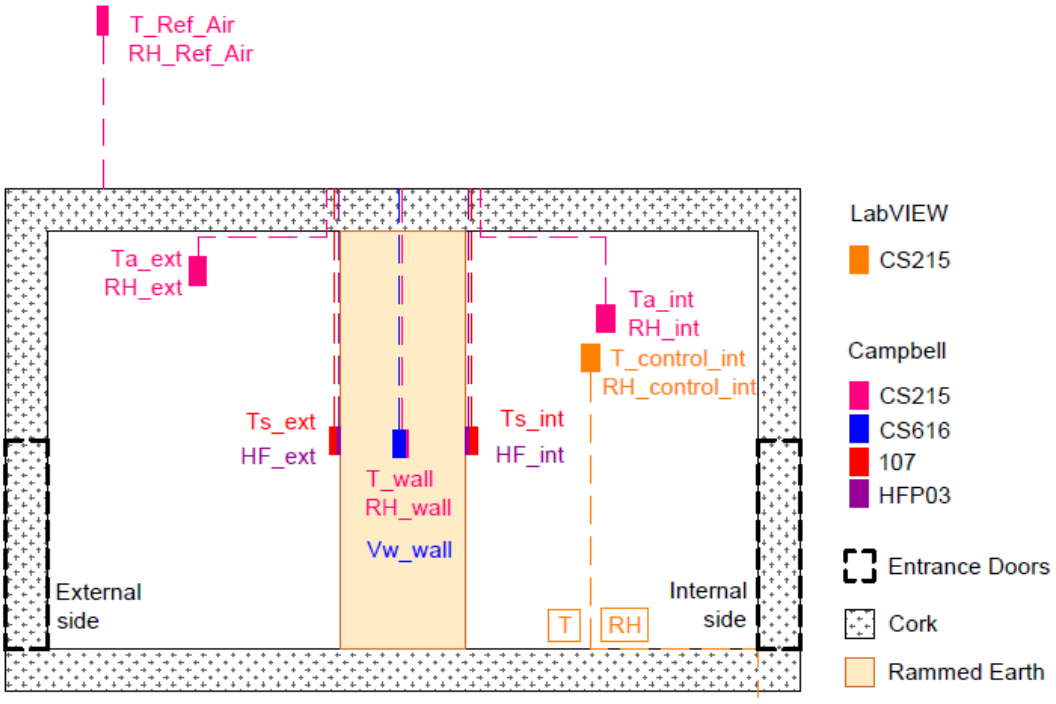

Figure 3.8 - Sensors location in constructive solution 1 - side view

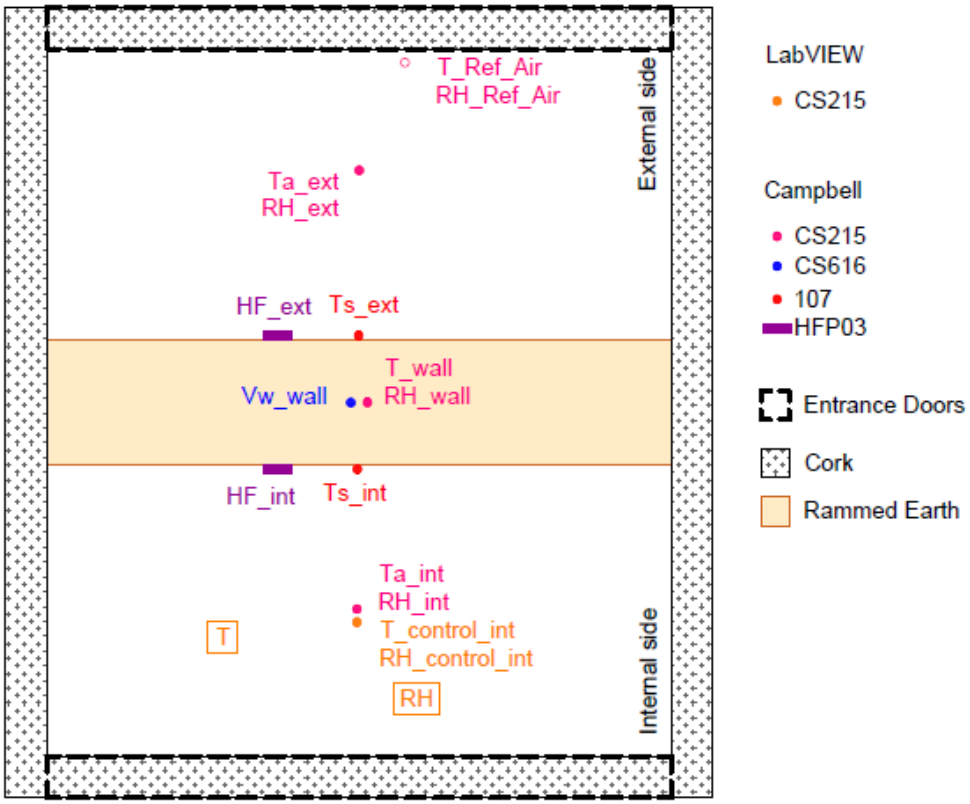

Figure 3.9 - Sensors location in constructive solution 1 - Upper view

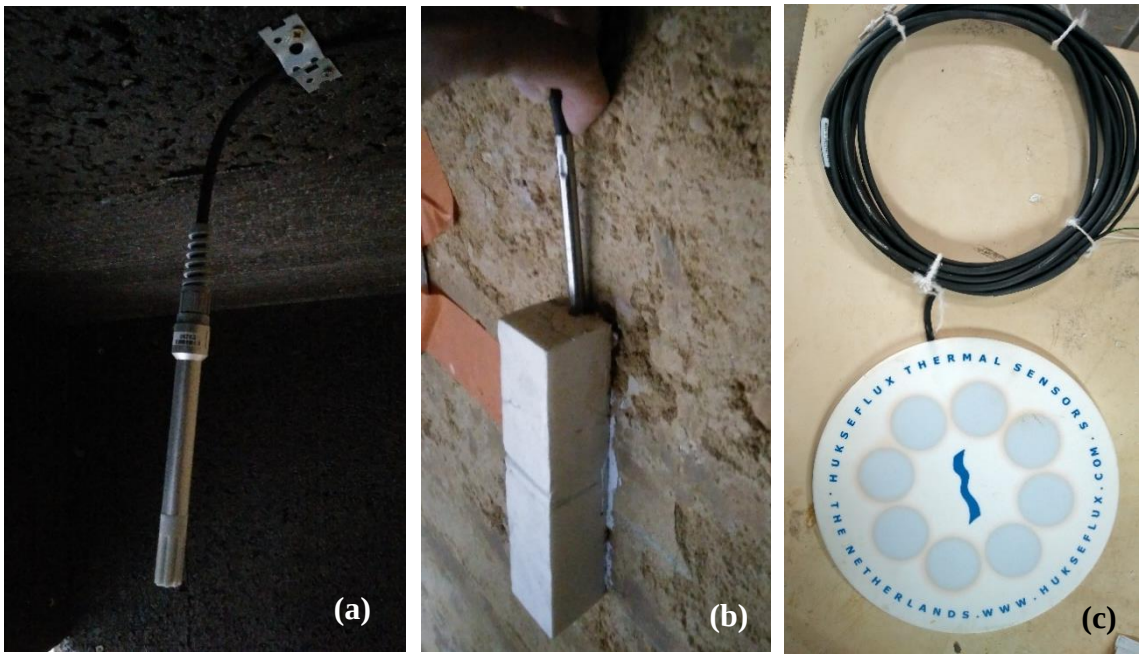

Figure 3.10 - CS215 sensor (a), 107 Temperature Probe sensor (b) and HFP03 sensor (c)

The heat flux, $\emptyset$ [W/m^2] is proportional to the same T difference divided by the effective thermal conductivity of the heat flux sensor body.

$$\emptyset = U/S \tag{25}$$

In this equation, U is the voltage [V] and S is the sensivity of the thermocouples which is equal to $514{,}5 \times 10^{-6} \pm 31 \times 10^{-6}$ V/(W/m^2) for this sensor.

Due to experimental limitations of heat flux meters, it is recommended that sensors should not be exposed to direct solar irradiance or only night time date may be included in the analysis. (Naveros et al., 2017). The laboratory measurements have the advantage of creating a steady-state conditions that is not influenced by solar irradiance.

The heat flux plate is set up in order to provide a positive flux if the heat transfer (from higher to low temperatures) goes from interior to exterior and in turn, negative flux if it goes from exterior to interior (see Figure 3.11). For example, if the T of the wall is higher than both sides of the wall, it loses heat for both sides, and HF_ext have a positive value and HF_int have a negative value.

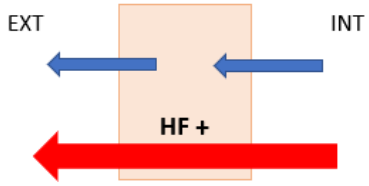

Figure 3.11 – Heat flux positive direction

The heat flux plate was attached to the rammed earth wall with silicone heat transfer compound plus (HTSP) by Eletrolube®. This thermally conductive heat transfer paste allows making a thermal connection

between two interfaces, with a dissipation of heat homogeneous and also has a wide operating temperature range, thus offering highly accurate results.

The sensors mentioned above were connected to an acquisition centre produced by Campbell Scientific Dataloggers® CR1000 (Campbell Scientific, 2013). This technology allows to collect all the information that the sensors are reading. The data acquisition is done by LoggerNet that recognises the sensors and creates a database of the measured values. A measurement is taken every 10 minutes and it shows the average of the value recorded in that period.

In addition, another data acquisition was used, by NI LabVIEW® 2013 connected to one T and RH probe. They are designated as ***T_control_int*** and ***RH_control_int*** for the internal T and RH, and it is coloured in orange, in Figure 3.8 and Figure 3.9.

The LabVIEW is a program that allows to control the conditions inside the chamber. The probe measures the conditions in the chamber and is linked to one heater and to one humidifier, by Medisana, which enable the program to control the values of T and RH respectively. They can only be used to increase T or RH.

Before they started to be used, all of them were properly calibrated.

3.4.2. Constructive Solution 2 – Chamber with Insulation

In addition to the improvements made in the cork chamber mentioned before in section 3.2, two extra sensors were installed: one heat flux sensor and another T and RH probe inside the wall.

A HFP01SC self-calibrating heat flux sensor of Campbell Scientific, designated as ***HF_int_s***, was added, with a sensing area of 8 cm instead of 17 cm, of the one installed in constructive solution 1. Its sensitivity is 60×10^{-6} V/(W/m^2). The self-calibrating property allows the sensor to adjust measurement errors caused by lack of stability of the sensor, thermal conductivity of the surrounding area (which varies with the moisture content) and for T dependence. This heat flux has a film heater coating that is activated to perform a self-test every 6 hours (Hukseflux - HFP01SC, 2016).

This new sensor was placed inside the internal boundary of the rammed earth wall, close to ***HF_int***, as shown in the upper view in Figure 3.13, and a side cross-section in Figure A. 1, in Appendix I, with the purpose of conducting a future analysis on the influence of the size of the flux meters. The difference between the sizes is showed in Figure 3.12.

A new data acquisition linked to HW4® Rotronic was connected to one more CS215 probe that measures T and RH. This probe was placed inside the rammed earth wall, 10 cm far from its boundary. Their designation is ***T_wall_10cm*** for T and ***HR_wall_10cm*** for RH marked in green in Figure 3.13, with an upper view, and Figure A. 2, in appendix I, with a side cross-section. This records the data every 10 minutes.

Figure 3.12 - Heat flux plates: HFP01SC (left) and HFP03 (right)

A 1D simulation using the mass conservation equation with the RH as the variable was made to evaluate the penetration depth in the rammed earth wall of the RH variation, see chapter 4.6.6. This simulation gave indications on the position to place the sensor, 2 cm would have been the ideal situation. Some tests were made in a similar rammed earth wall and it was concluded that is impossible to insert a sensor so close to the surface without destroying it. Therefore, the option was to insert it with 10 cm.

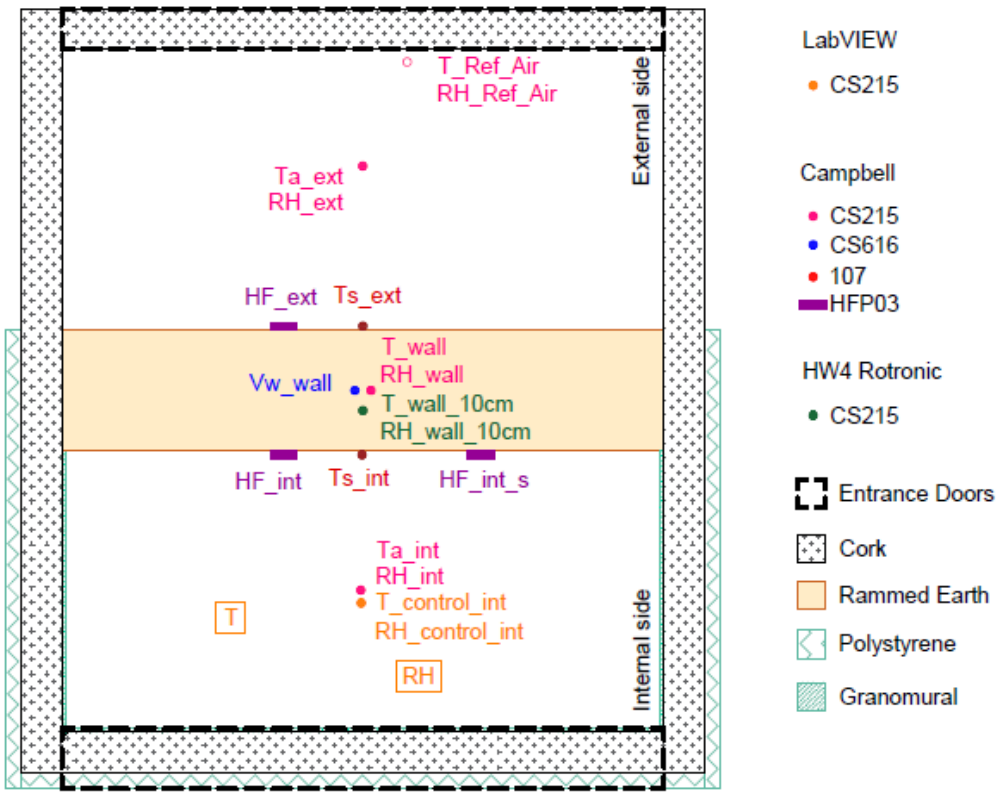

Figure 3.13 - Sensors location in constructive solution 2 - Upper view

3.4.3. Constructive Solution 3 – Rammed Earth with Polystyrene Insulation

In the third test, a 10 cm board of expanded polystyrene insulation was added to the rammed earth wall. For that reason, it was necessary to install one more heat flux HFP03 sensor on the outside surface of the insulation to measure the heat flux that passes through it. The designation of this sensor is ***HF_ins*** and it is represented in purple, with an upper view in Figure 3.14 and with a side cross-section in Figure A. 3, in Appendix I.

Two new T and RH probes were connected to HW4® Rotronic sensor. One of them was introduced between the rammed earth wall and the insulation to measure the conditions between the two elements. Their designation is ***T_wall_ins*** for T and ***RH_wall_ins*** for RH.

The other one was placed close to the insulation and measures the boundary conditions between the insulation surface and the ambient air. Their designation is ***T_boundary*** for T and ***RH_boundary*** for RH.

Both sensors are represented in green in Figure 3.14.

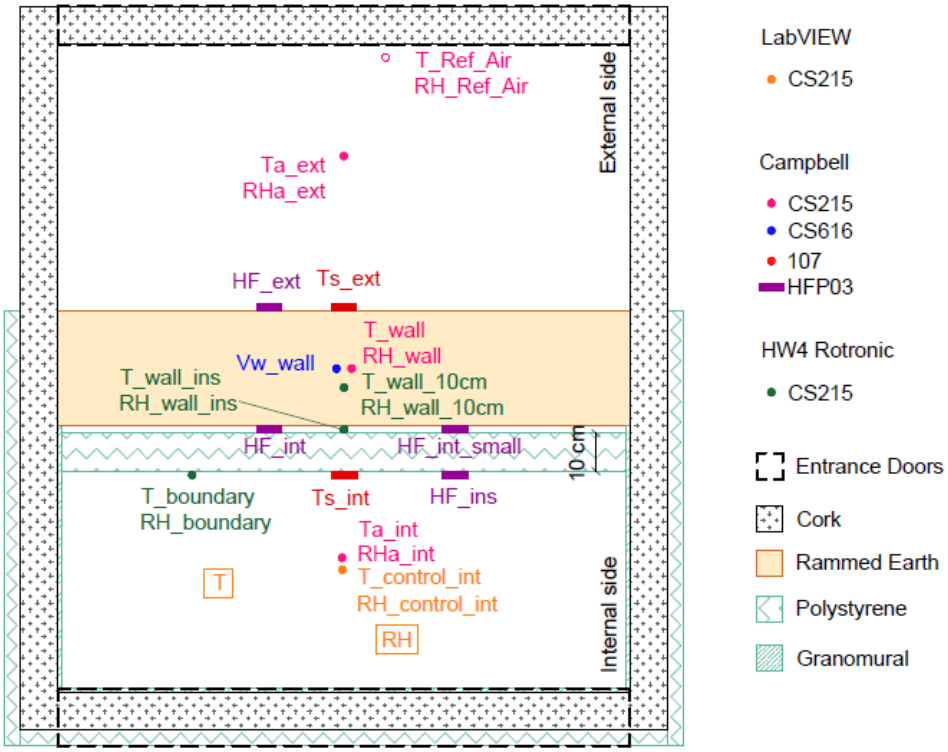

Figure 3.14 - Sensors location in constructive solution 3 - Upper view

3.4.4. Constructive Solution 4 – Rammed Earth with Hemp Insulation

The last test had, the polystyrene replaced by the hemp-lime plaster insulation. The sensors are the same as those used previously in constructive solution 3 and have the same designations, presented in Figure 3.15. Considering that the plaster was applied directly to the rammed earth wall, it was applied also upon the sensors ***HF_int***, ***HF_int_s*** and ***T_wall_ins/RH_wall_ins***.

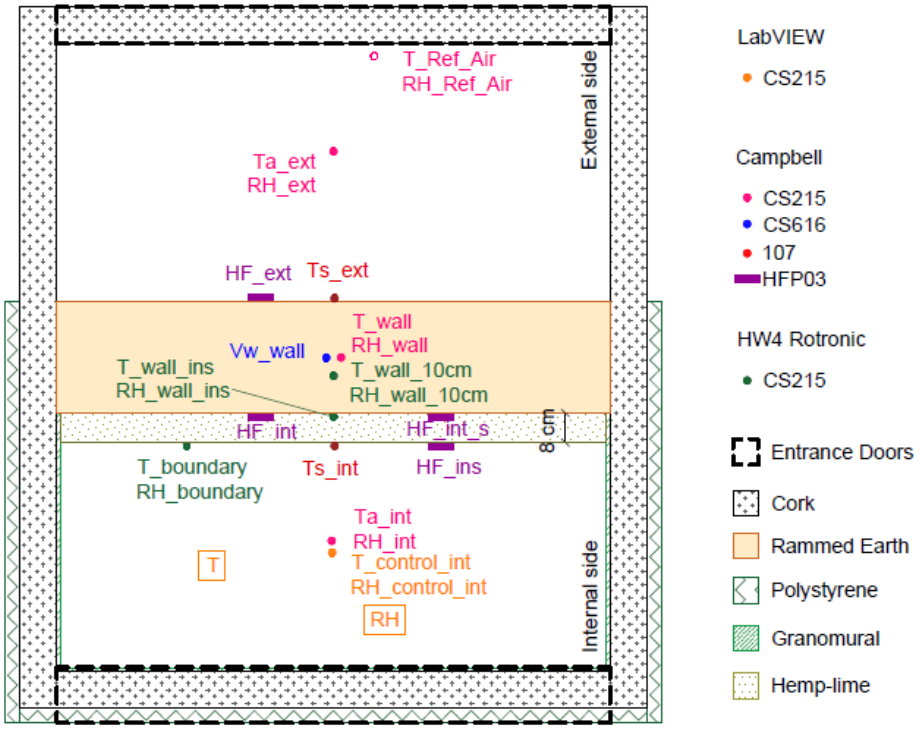

Figure 3.15 - Sensors location in constructive solution 4 - Upper view

3.5. Infrared Thermography

Infrared thermography is a fast and non-intrusively method able to give qualitative results about thermal losses, thermal bridges, sources of moisture through the building envelope and detachments of tiles (Lourenço et al.,2017). The method is particularly useful because it provides spatially resolved surface T (Fokaides, 2011).

The accomplishment of the infrared thermography was made with the infrared camera, produced by CEDIP® Infrared Systems, as shown in Figure 3.16. It was used to analyse the chamber efficiency.

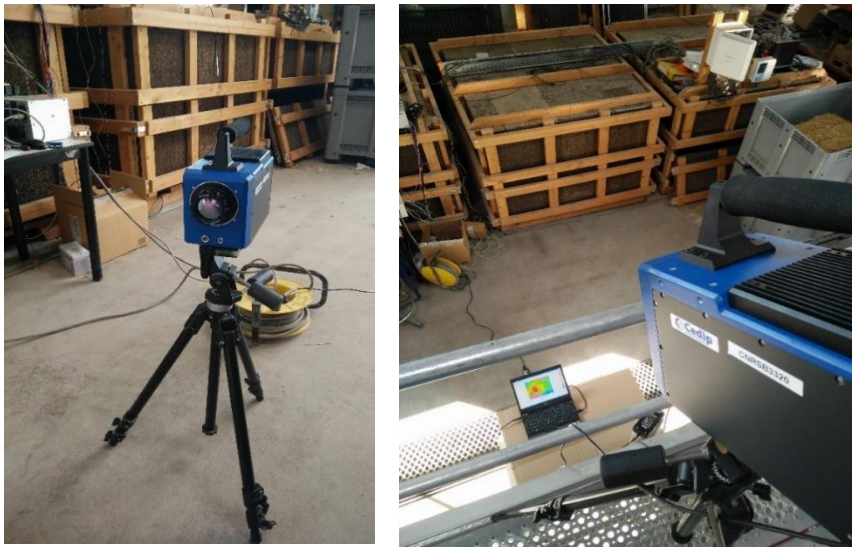

Figure 3.16 - Infrared camera analysing the chamber

4. Results and Discussion

4.1. Preliminary Remarks

In this chapter the results obtained from the tests described in the previous chapter are presented and discussed.

Firstly, each constructive solution is analysed separately and then, all solutions are compared. Throughout the analysis of these results, it is important to consider that the sensors are only measuring a single point on the whole surface. Due to rammed earth heterogeneity, there may be some variation across the surface, which is not detected by this method.

4.2. Constructive Solution 1 – Without Insulation

4.2.1. Outside Variation

Initially the chamber is set with both the entrance doors permanently open, so that the variation inside the chamber is only due to the T_ref_air.

In Figure 4.1(a) the measured T variations along a period of six days are presented. The major T range is of T_ref_air, in yellow. The most stable variation belongs to T_wall, as is the T in the middle of rammed earth wall. The ambient temperatures in both sides of the chamber have approximately the same variation. However, a T offset from the exterior to the interior side is observed (green and red lines). This offset is thought to be due to the position of the chamber inside the laboratory (see Figure 3.2). Since the external side is near to the laboratory edge, this T is expected to be close to the outdoor T (T outside the laboratory), while the internal side is affected for open doors ventilation and sun radiation, being closer to the T_ref_air.

Comparing the T curve shape with the corresponding RH and heat flux curves, it is highlighted that at every cycle the peak of higher values of T matches with the peak of lower values of RH and with the peak of higher values of heat flux. As explained before in chapter 2.2.3, considering the psychometric chart in Figure 2.3, when T rises, while water vapour concentration is kept constant, RH decreases. With the increase of T and decrease of RH, the rammed earth wall seeks for being in thermal equilibrium with the environment. As equilibrium is reached, the rammed earth wall temperatures approach the same value and the heat flux through the surfaces, a measure of the heat exchange, decreases.

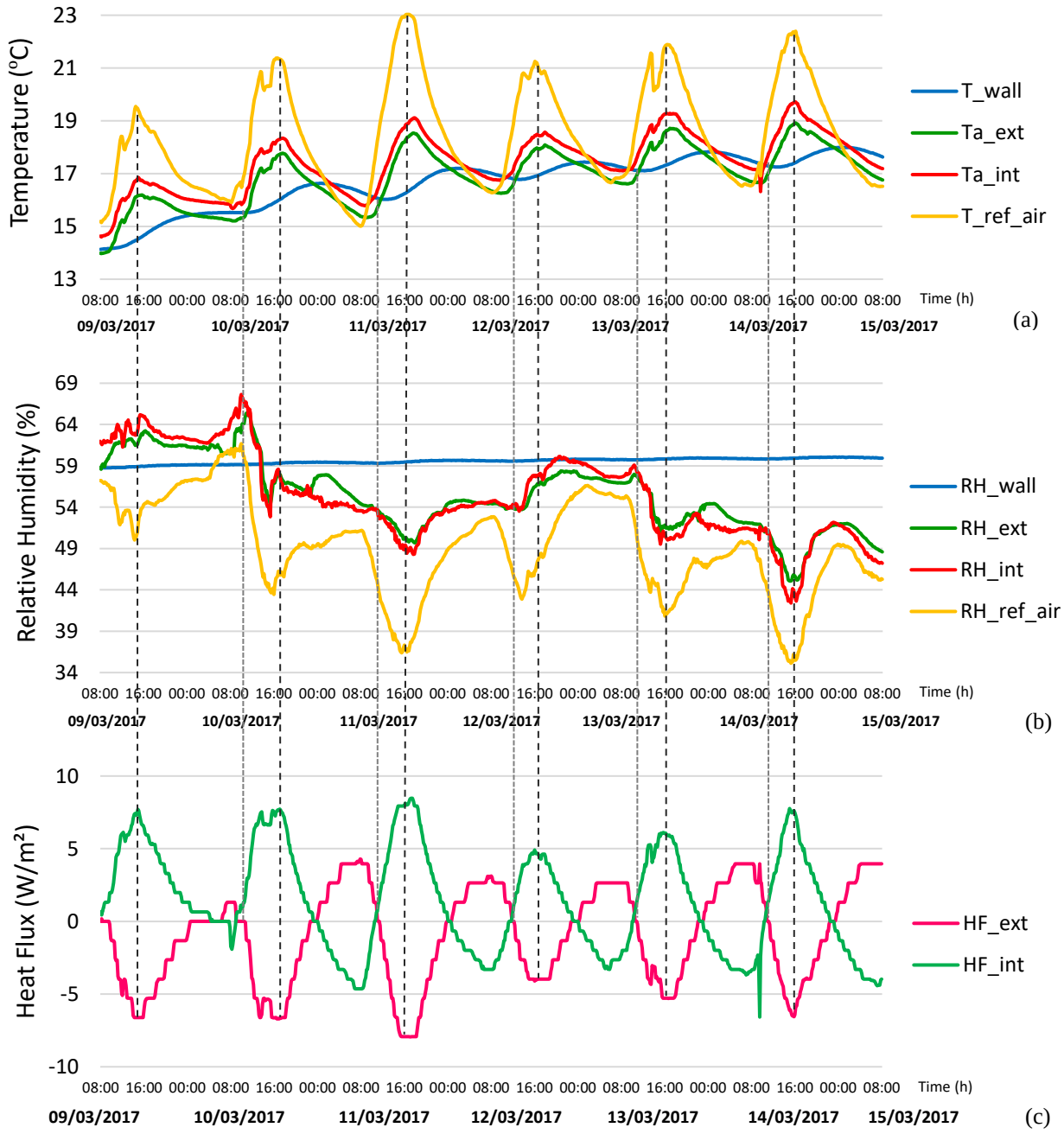

Figure 4.1 – Comparison between T (a), RH (b) and heat flux (c) variations during constructive solution 1.

4.2.2. Analysis of the Chamber Efficiency

In order to analyse the chamber heat loses, infrared thermography is applied to the studied system.

The first infrared capture was performed with heating turned on and T_int stabilized at 30ºC. The outside T (T_ref_air) was 22ºC. Due to space constraints, it was not possible to collect only a single image capture. The compilation of collected images are presented below in Figure 4.2.

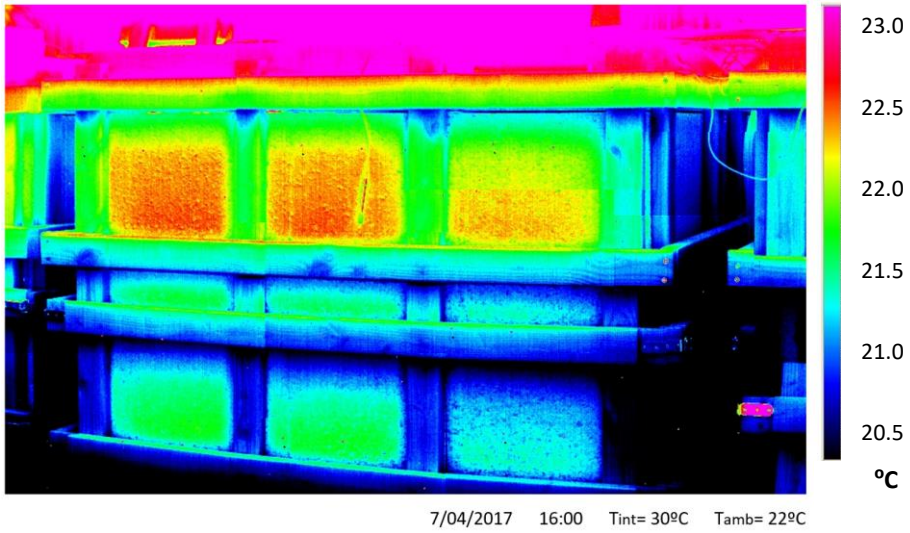

Figure 4.2 - Infrared thermography

Through this test, it was seen that the heating inside the chamber was located only in the top half of the chamber (red area ~ 22,7ºC) in comparison with the low half (green area ~ 22.0ºC). Therefore, three computer fans (each fan with voltage:12v and amperage: 0.20A) were installed in order to homogenise the T of the air inside the chamber.

After installing the ventilation, the infrared capture was repeated in order to check if it had succeeded as well as to understand where the biggest heat losses through the cork happened. The result is shown in Figure 4.3(a).

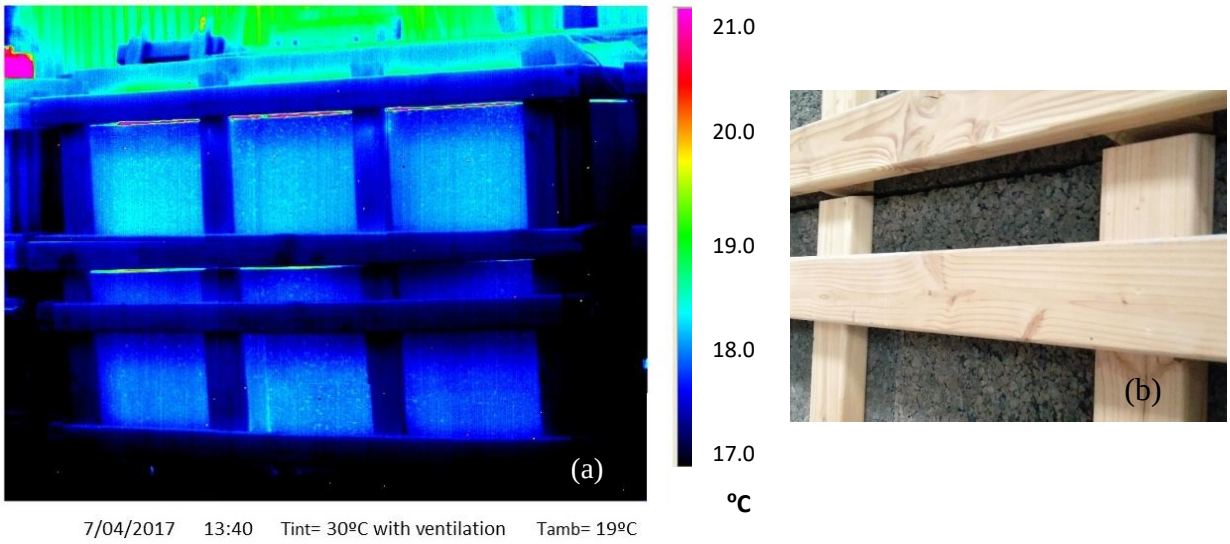

Figure 4.3 - Infrared thermograpy with ventilation (a), junctions between cork boards (b)

After ensuring the homogenization of T inside the chamber, the losses in junctions between cork boards were analysed. However, the losses are greater on the top of the chamber (~20.5ºC versus ~18ºC on chamber sides), as can be observed Figure 4.4 and in Figure 4.3 (a).

The heat energy is lost through the junctions between the cork boards and through the holes done to connect the cables from the sensors to data acquisition (pink area ~21.0ºC). The joints and holes on the cork are vindicated in Figure 4.3 (b).

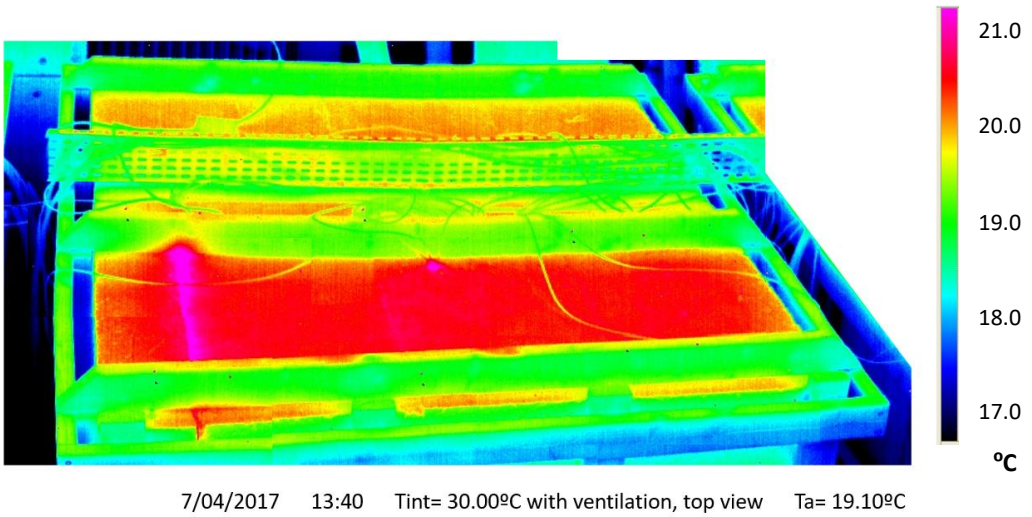

Figure 4.4 - Infrared thermography with ventilation - Upper view

The results obtained suggested the necessity to insulate the cork chamber due to its significant heat losses.

Finally, a test was recorded by the sensors with T set to 30ºC for 5 days, the obtained results are depicted in Figure 4.5.

If the 10 cm of cork chamber was enough to insulate the interior of the chamber, then Ta_int would be constant. It is evidenced that the variation of T_ref_air has an influence on Ta_int being noticed a variation of 0.2 ºC from the average value. As such, an improved insulation must be applied to the chamber walls. Comparing the thermography results (Figure 4.3 and Figure 4.4) to the sensors data (Figure 4.5), the latter are more conservative as the minimum and the maximum values vary less than 1ºC. That mean that the heat loss are not as significant as it seemed in infrared thermography, where 1ºC differential from wood structure to cork and 2ºC differential from side to top of the cork region of the chamber are measured.

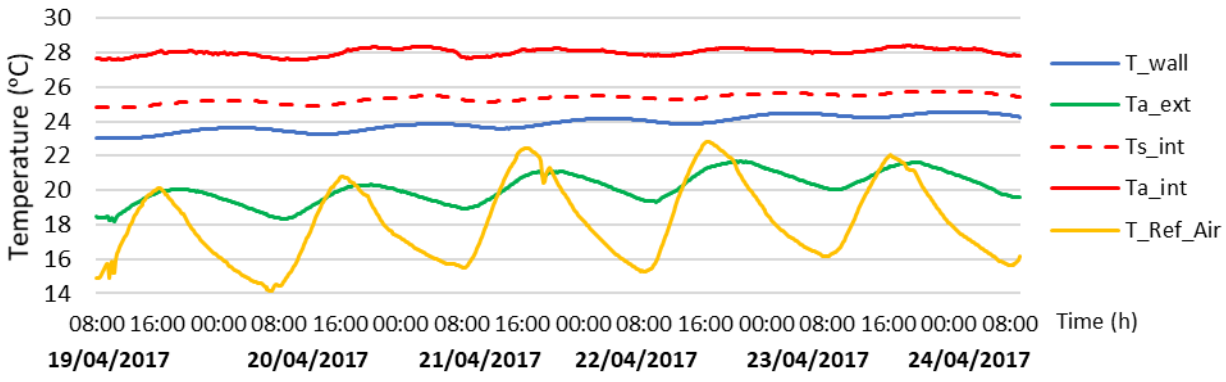

Figure 4.5 – T constant in constructive solution 1

4.2.3. Theoretical Formulas and Sensor's Data

During constructive solution 1, the interior T was kept constant at 30ºC. The exterior side has not a constant T, but its dairy variation was less than 2ºC. So, the average value was obtained, and a quasi-steady state were assumed. During this test, the heat flux that crosses the interior boundary of the rammed earth wall was measured using heat flux plate. The discrepancy between theoretical formulas and sensor's data was computed.

The heat flux measured was compared with Fourier's Law (equation (2)), for steady-state unidirectional heat conduction, which for the unidimensional case can be written as equation (26).

$$q_x = \lambda \frac{\Delta T}{d} = -\frac{1}{0{,}15}(T_{wall} - Ts_{int}) \tag{26}$$

Besides, Newton's Law of cooling which describes the heat transfer coefficient by convection, was compared as well. This equation was introduced in equation (4) in chapter 2 and now it is applied to this case study (equation (27)).

$$q_{conv} = h_c(Ts_{int} - Ta_{int}) \tag{27}$$

In equation (26), h_c is the inverse of value of internal resistance, R_{si}. Although the R_{si} has a known value of 0,13 (m².ºC)/W (presented before in chapter 2.3.1) it was recalculated for the existing conditions using the average values obtained from the data showed in Figure 4.6.

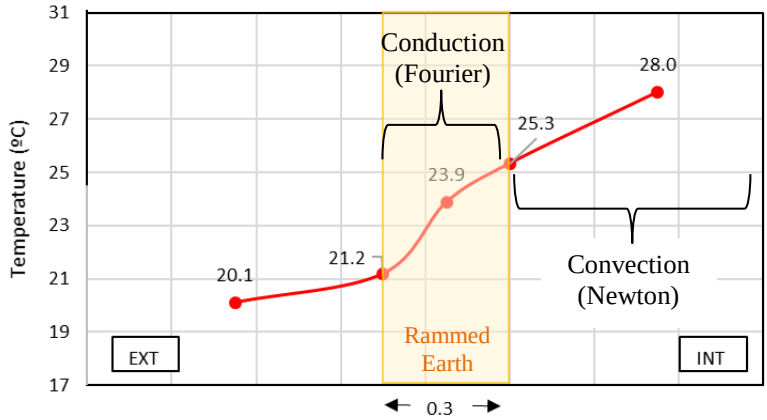

Figure 4.6 – Average temperature profile assuming quasi-steady state conditions

Considering the surface and interior ambient temperatures given by Figure 4.6 and the average heat flux value as 15,5 W/m², Rsi value is determined by equation (28).

$$R_{si} = \frac{Ta_{int} - Ts_{int}}{HF_{int}} = 0.17\ (m^2.°C)/W \tag{28}$$

Despite the error included in the sensors results and assuming the quasi-steady state, the value obtained was very close to the standardized (Rsi= 0.13 (m².ºC)/W).

The heat flux measured with the sensor for five cycles and the expected one through the equations of Fourier's law, Newton's law and Newton's using the Rsi calculated value, discussed above, were obtained and are showed in Figure 4.2.

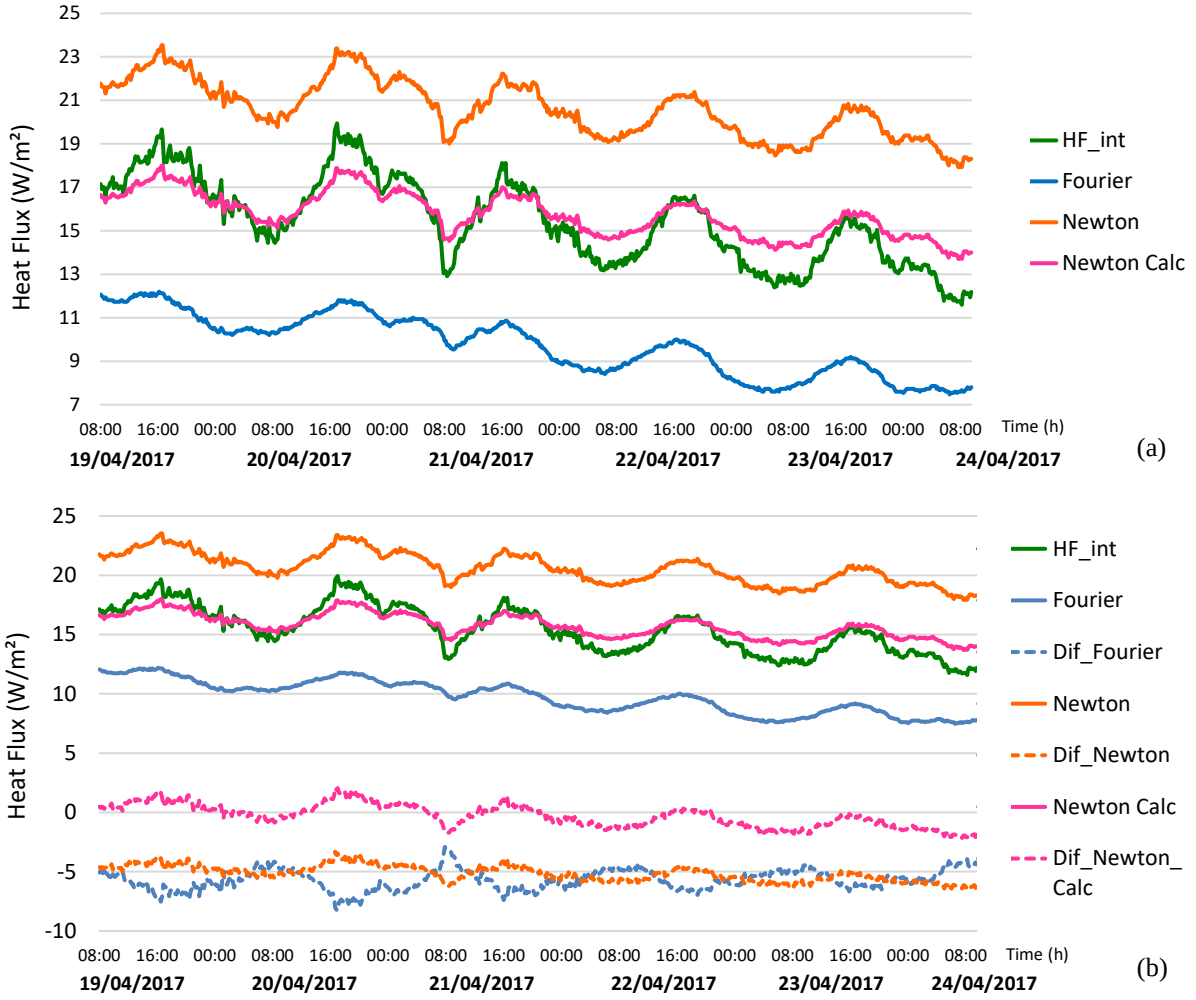

Figure 4.7 - Comparison between theoretical formulas and sensor's data (CS1 – T cte)

The heat flux plate allows to know the heat flux that crosses the wall even in situations that temperature is changing every minute. It considers the convection of the chamber and the conduction inside the wall.

For conduction in steady-state, Fourier equation presents the blue line in Figure 4.7 that give a lower heat flux than the values reading by the sensor. In turn, Newton presents an equation for convection that gives a higher heat flux than the sensor reading. However, when the convective coefficient is calculated with the values given by sensors data (with R_{si}=0.17 (m².ºC)/W) instead of using the standard value, "Newton Calc" presents results similar to data results (HF_int).

The Fourier's values should be closer to the heat flux given by the sensor since it measures the flux that passes through the wall. Fourier law is based on the calculation of the heat conductivity between the interior wall surface and the middle of the wall, in contrast with convection that measures the heat transfer between the ambient T and the surface T. The reason of such discrepancies may be due to fact that the tests

have not been made at steady-state or at dynamic conditions; thus, there were not in condition to apply the Fourier's law.

4.3. Constructive Solution 2 - Chamber with Insulation

4.3.1. RH Cycles

The RH was set to 80% on the interior side of the chamber from 9:30 to 17:30 (grey-shadowed area in Figure 4.8) and turned off in the remaining time while T was kept constant at 30ºC during the whole test. The same test was repeated one week after and the results obtained for both weeks, for the T, RH and HF measurements, are shown in Figure 4.8.

One may notice that the start of the RH cycle (RH_int) has an impact on Ta_int, that has a slightly decrease and are then counterbalanced with the heater that increase its power leading T back to 30ºC.

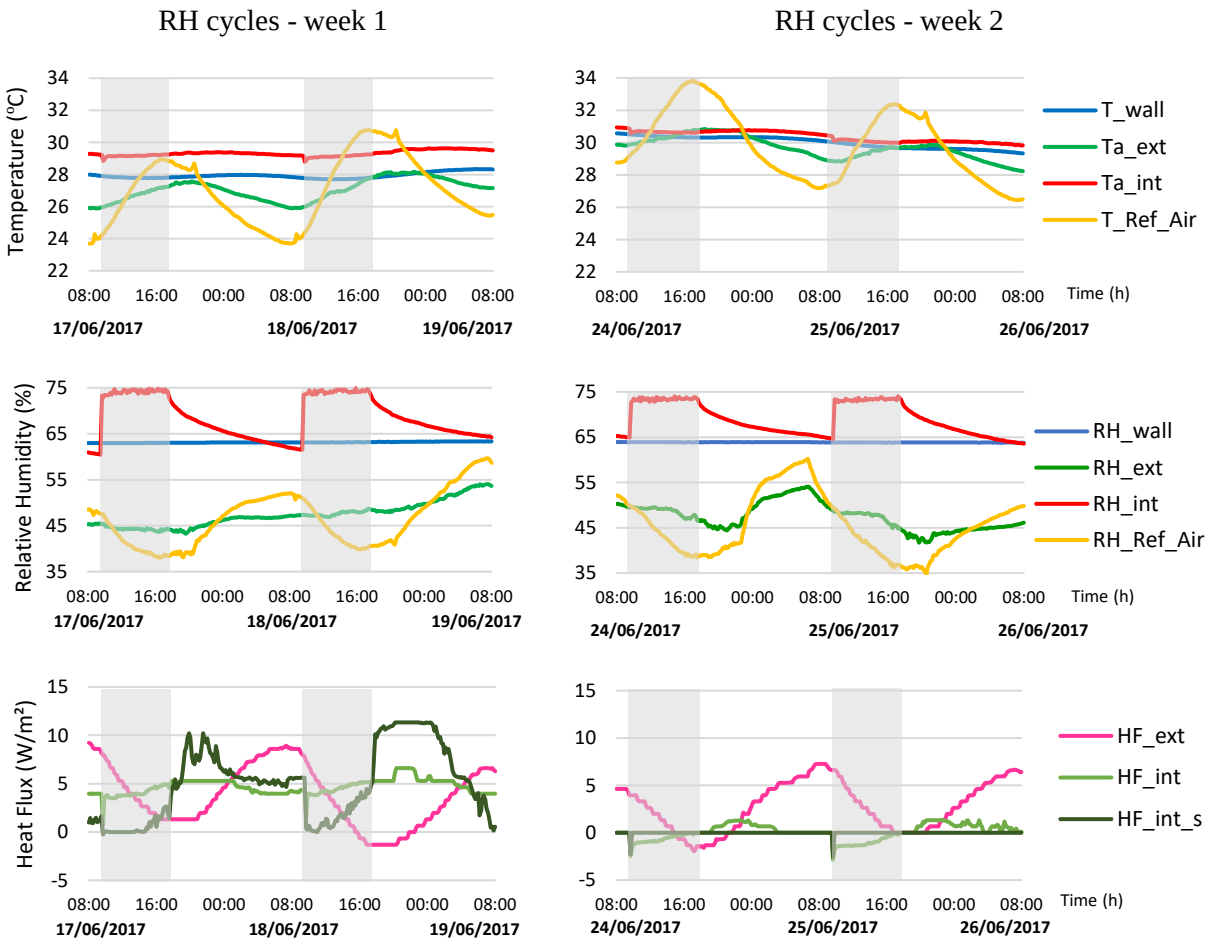

Figure 4.8 – RH cycles in constructive solution 2

In the first week (left side) great variations of HF_int_s can be observed. High T lead the values up until 11 W/m^2 and the increase of RH, due to the begging of the new cycle has an immediate impact reducing the heat flux in 5 W/m^2.

In contrast, in the second week (right side) the activity of the HF_int_s is almost null. However, is still visible a negative peak due to effect of RH_int increasing in Ta_int, in the begging of the cycle. HF_int barely varies in the second week because the T values obtained for T_wall and Ta_int are so close that the wall is almost in equilibrium. These values are closer in the second week because the wall was warmed in the week before and during this cycle, T_ref_air is not sufficiently low to decrease T_wall (Ta_ext are close to Ta_int).

When a cycle of 80% of RH is imposed to the chamber, it can be seen in most of the results that the RH never reaches such value; e.g. in Figure 4.8 it only reaches 75%.

Despite the sensors have been submitted to calibration, during the results analyses some inconsistences between them were found. Considering that RH_int and RH_control_int were placed together inside the chamber, the sensor RH_int should provide the same values of RH_control_int, the sensor that control the RH of the cycles. As it can be seen in Figure 4.9, it did not happened.

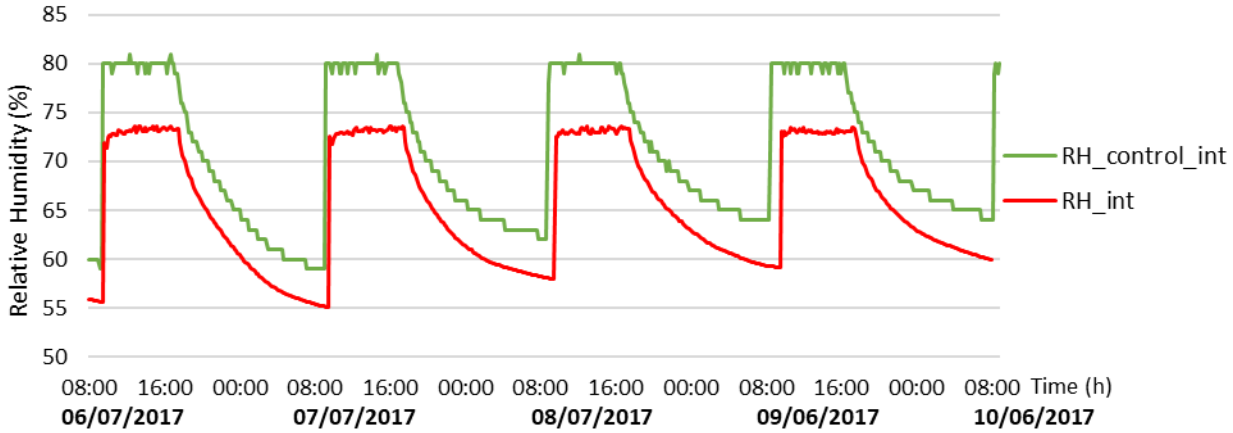

Figure 4.9 – Inconsistence between RH_int and RH_control_int

When RH reaches 80% (its maximum defined value), it should remain constant until 17:30, when the cycle ends. However, it is visible in Figure 4.9 that during the period that RH should remain constant, it has slight variations of 1%. This happens because the LabView program was set to compare if the RH value were correct from 10 to 10 min (the same period that is recording the data). When LabView detects that RH are lower (or higher) than it supposed to be, it immediately adapts the potency of the humidifier in order to lead the value back to 80%.

Similarly, the majority of tests presented in chapter II, in Appendix, show that T_int never reaches 30ºC as previously set, but stop between 28 - 29ºC.

4.3.2. T Cycles Against RH Cycles

When the influence of T and RH in heat flux were studied separately, it was seen that heat flux is much more affected by T, because minor variations of 6ºC affect the heat flux in 11 W/m^2, presented in Figure 4.10 (left side). The same cannot be affirmed to RH; variations of 10% barely had an effect in heat flux

variation (1 W/m^2), presented in Figure 4.10 (right side). However, the little effect matches perfectly with the cycles of RH, putting in evidence that the rammed earth wall is a hygroscopic material and if RH variations were more evident, it will be reflected in bigger heat flux variations. This information also gives an indication on the ability of the heat flux meters to measure the latent heat effect. During the RH cycles the small heat flux meter recorded greater heat flux variation directly due to the RH variation. This is may suggest that the larger size of the other heat flux meter is blocking the vapour diffusion behind the heat flux meter and therefore is limiting the effect.

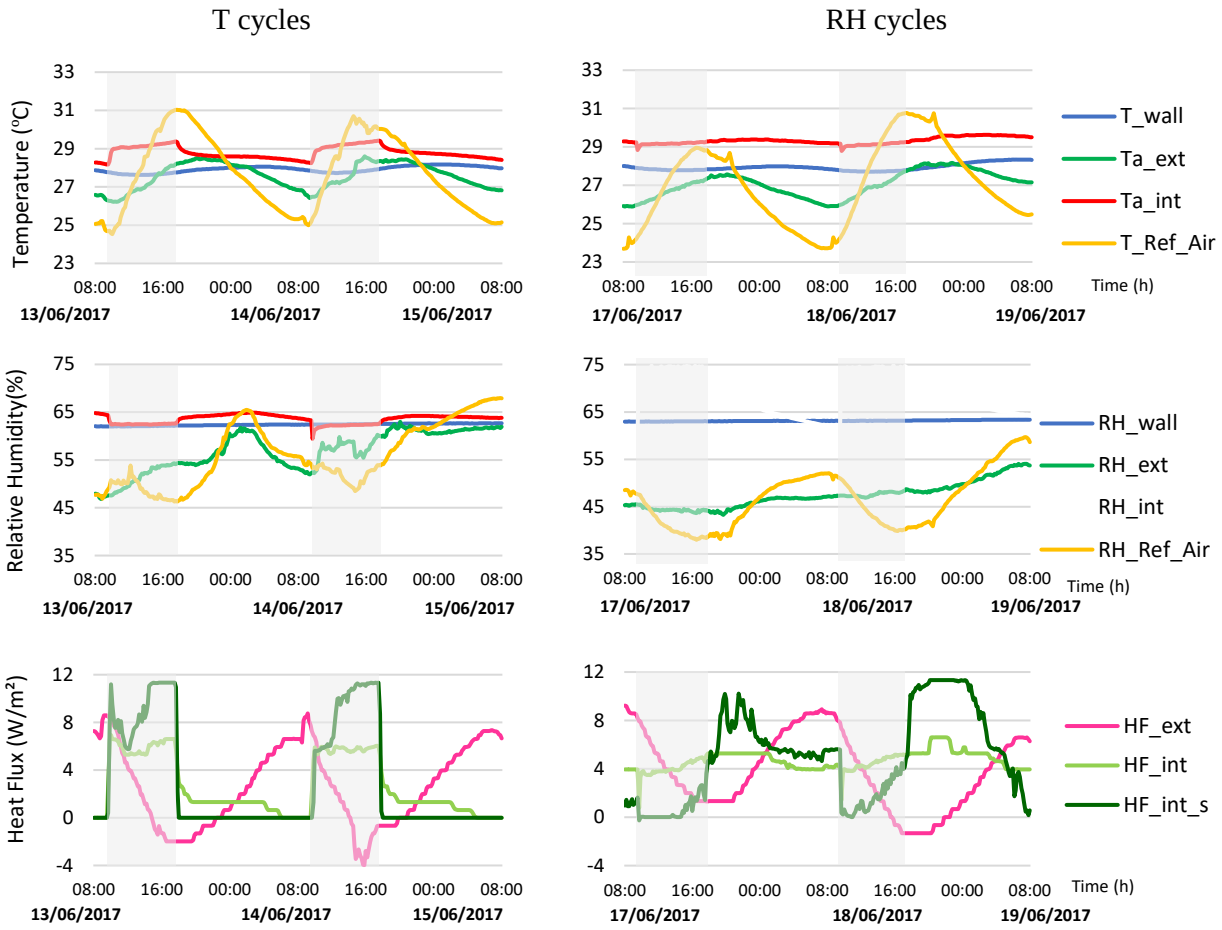

Figure 4.10 – T and RH cycles in constructive solution 2

4.4. Constructive Solution 3 - Rammed Earth with Polystyrene Insulation

The last improvement made on the chamber was the introduction of polystyrene which corresponds to constructive solution 2, 3 and 4 earlier presented in Figure 3.3 (b).

In Figure 4.11 is evidenced that red colour (~41.02ºC) is constant in all polystyrene extension; hence, all the weak spots of the chamber previously identified were enhanced.

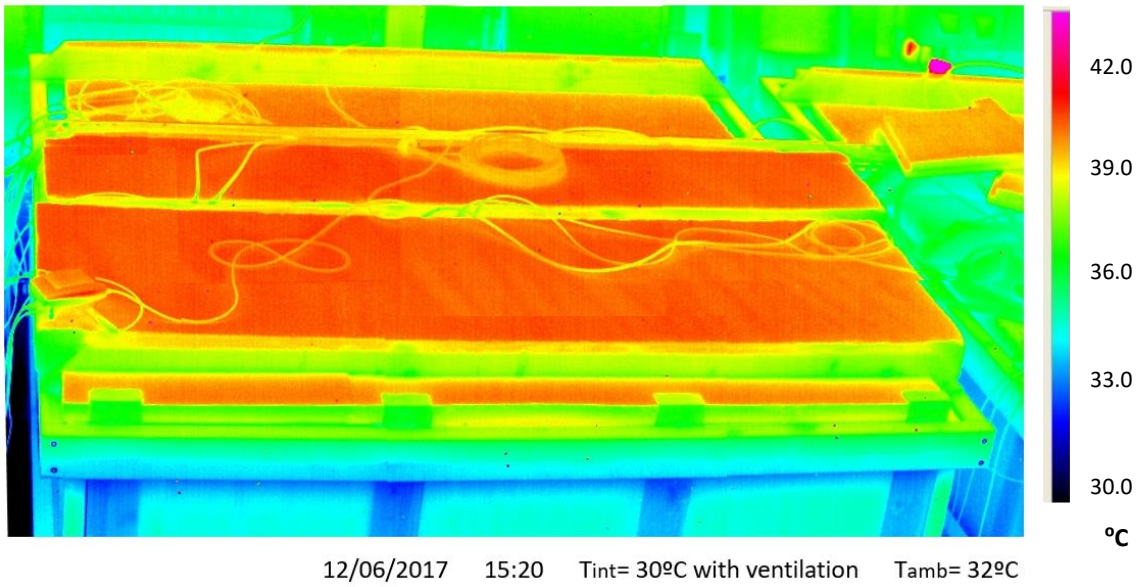

Figure 4.11 - Infrared thermography with polystyrene - Upper view

After the insulation of the chamber with the EPS, Ta_int should have remained constant to 30ºC. Moreover, in Figure 4.12 is visible that Ta_int has been slightly influenced, in less than 0.1ºC, by T variation from outside the chamber, instead of the 0.2ºC previously identified in chapter 4.2.2, for the situation of chamber without insulation. In conclusion, polystyrene insulation in the chamber was indeed an improvement. Nevertheless, the chamber is influenced by the external conditions.

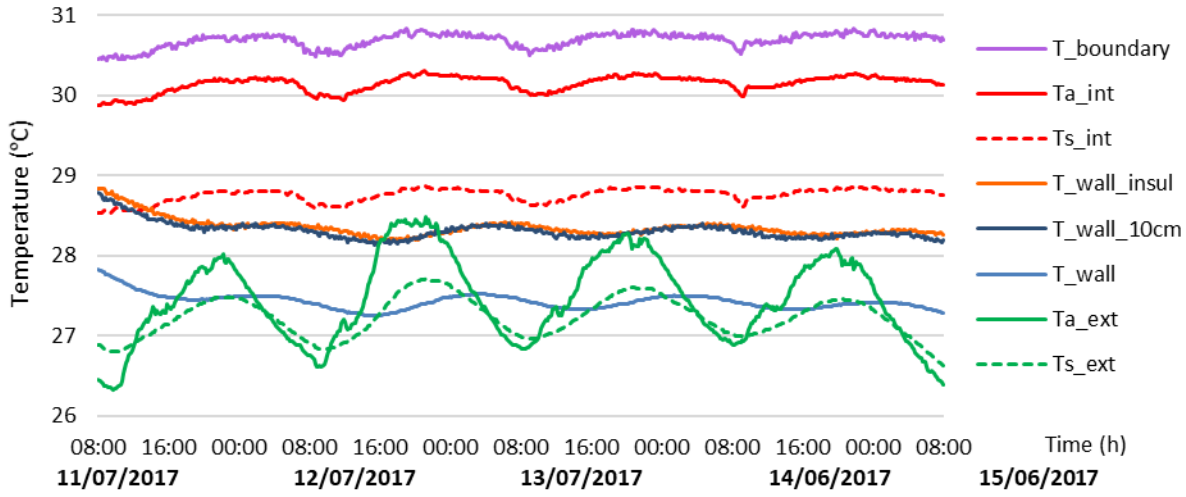

Figure 4.12 – T along the insulated wall

In Figure 4.12, T increases from the interior to the exterior side of the wall, as expected, since the T ambient on the interior side is higher than on the exterior side. The only exception is the T_boundary (placed in the internal surface of insulation) that should have a lower T than Ta_int. However, its localization is near to the heater which may give higher values.

The lower value belongs to T_wall. As it can be seen, although the T was set to 30ºC there are slight variations due to environment variations. It is expected that T_Wall_10cm has a closer value to T_wall because they both are inside the wall and have 5 cm of distance between them. The same sequence was verified for other tests.

In addition, T_wall_insul, T_wall_10 cm and T_wall have a periodical variation with a buffering from Ta_ext, visible in Figure 4.12. For the 12th of July 2017, the minor values for T lines was collected, presented in Table 4.1. Followed by Ta_ext variation, Ts_ext has its minimum peak 2:00h after external ambient T, with a decrease in amplitude variation. In the middle of the wall, T_wall, has its minimum peak 2:20h after, with a visible buffering in amplitude variation. Only 5 cm distant from T_wall, T_wall_10cm has a 1:10h delay. Finally, the minimal peak arrives on the internal surface of the wall (before insulation) with an 1:20h delay. In conclusion, the rammed earth wall induces an average T buffering of 1h for every 7 cm of rammed earth that T has to penetrate, and due to insulation barrier, T_int seem not to have any influence on the conduction of heat through the wall.

Table 4.1 – Time lag of temperature buffering

Ta_ext	Ts_ext	T_wall	T_wall_10cm	T_wall_ins
08:50	11:50	14:10	15:20	16:40

By placing the EPS board on the interior side of the rammed earth wall, the thermal inertia of the wall is lost. The wall is no longer able to warm the interior side when the heat is needed due to the EPS insulation barrier. The interior side will remain hot as long as there is a heat source.

4.5. Constructive Solution 4 - Rammed Earth with Hemp Insulation

The last constructive solution consists the application of in hemp-lime plastering mortar by manual projection on the interior surface of the rammed earth wall. As stated earlier, four months were not sufficient to dry the plaster. Thus, the performance tests of this insulation were not accomplished. Nevertheless, the rammed earth wetting, and drying cycle with the hemp-lime plaster were analysed in Figure 4.13.

Based on Figure 4.13, the first layer of hemp-lime plaster was applied to the rammed earth wall on 19/07/2017, and its visible an impact on all the surrounding areas. Two days after the plaster application, the centre of the rammed earth wall (RH_wall) was affected and started to gradually increase the RH value until reaching its maximum value, 94.5%, on 14/9/2017, almost one month after the first layer was applied. Before the RH increase, it slightly decreases. This behaviour might be due to the exothermic reaction of lime with water that heats up the mortar and consequently decreases RH.

Is also evidenced that the ambient RH (RH_int) is influenced by the drying of hemp insulation. Before the insulation have been applied (represented as B.I in the graphic) the RH was around 50% and then increased up to 70%.

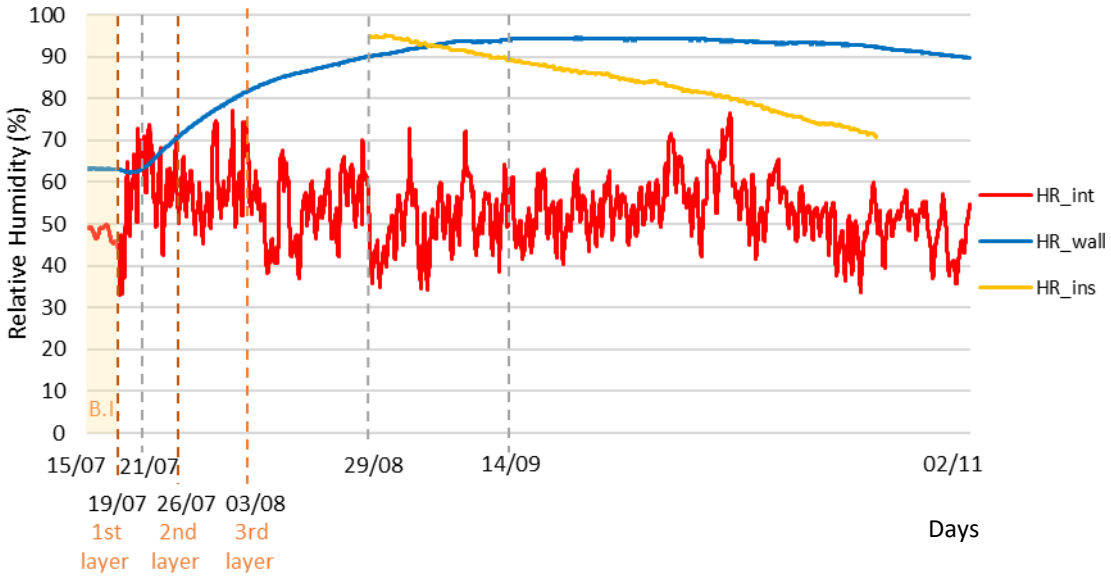

Figure 4.13 – Drying cycle of hemp-lime plaster

In addition, the second and the third layer were added on 26/07/2017 and 03/08/2017 respectively.

Water content in the centre of the wall, presented in Figure 4.14, started to increase 8 days after the hemp insulation was applied on the surface (instead of two days in Figure 4.13). Two levels were also evidenced before it reaches the maximum water content value, 8.3%, on 28/08/2017, two weeks before the RH peak.

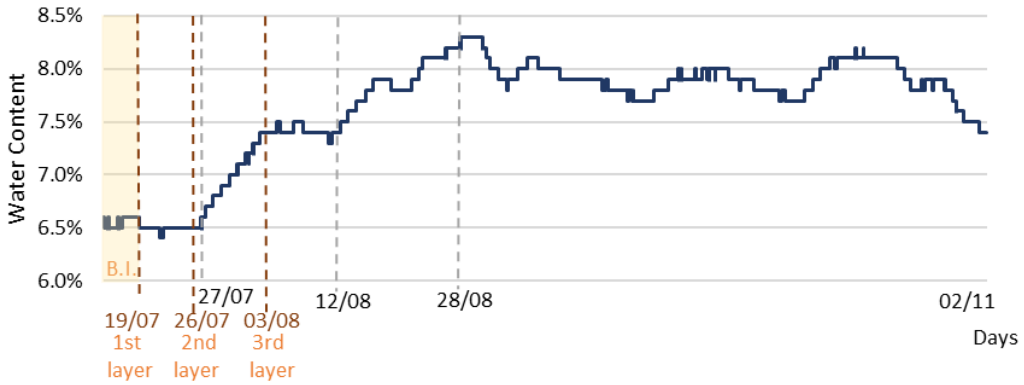

Figure 4.14 – Water content in the middle of the rammed earth wall

Rather than the gradually increasing curve of RH, water content offers well defined levels, that shows the three situations of mortar application, and consequently, water adding. However, after the second layer was applied, it took 16 days (double time) to water content be affected once again. This delay might be due to the longer thickness that the water needs to go through until the centre of rammed earth and the additional resistance that the first layer offers.

After it reaches its maximum value, hemp-lime plaster starts to dry, along with the rammed earth wall. It is shown in Figure 4.13 and highlighted in Figure 4.15, apart from associated errors, the drying data can be well described by linear trend line over the measured period.

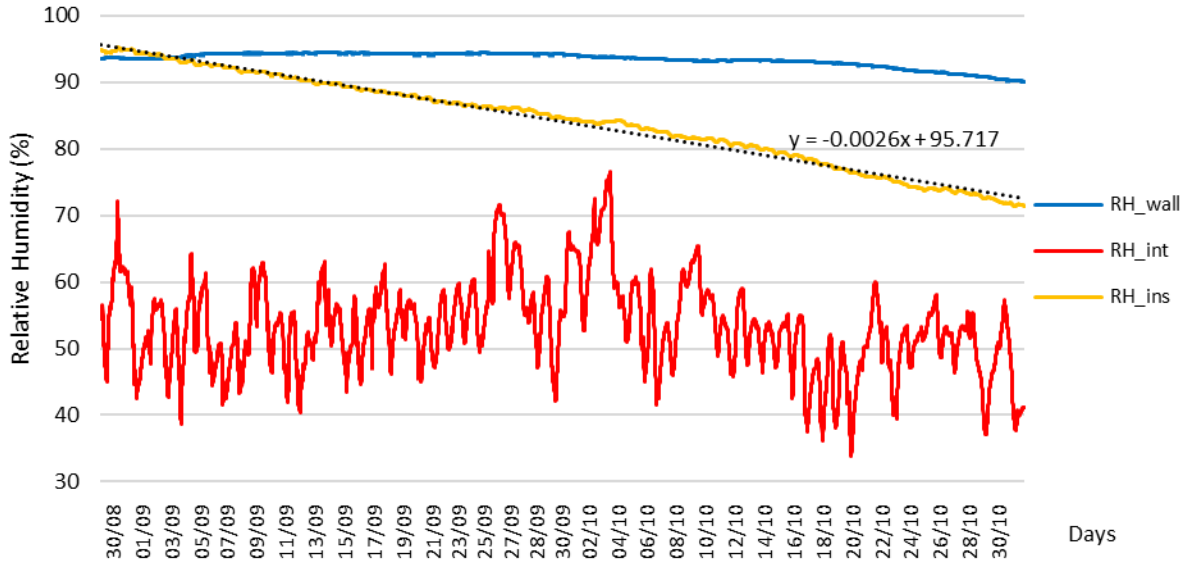

Figure 4.15 – Drying cycle of hemp-lime plaster

Considering that data values are recorded every ten minutes, the obtained slope for the insulation drying is 0.0026 %/10 min. This corresponds to 0.37%/day and 11.23%/month. This means that, on average, the RH is decreasing 11% every month.

The slow drying process of the hemp plaster combined with the rammed earth might be due to the excessive rate of water used in the hemp-lime mortar, its hygroscopicity and also due to moisture adsorption and storage power of rammed earth which decreased less than 5% of RH for 2 months.

4.6. Comparison Between Constructive Solutions

4.6.1. Heat Storage Capacity

The data from the sensors along the wall, as well as the outside and inside temperatures are represented in Figure 4.16, at different times during an entire day. The heater placed in the interior side have been programmed with a 30ºC cycle from 9:30 to 17:30 hours, while the exterior side is open to the laboratory and therefore the T variation follows the T of the laboratory.

In Figure 4.16 (a), the interior T is always higher than exterior T, which means the heat flux always goes from interior to exterior. Considering that the tests are performed inside the laboratory, the exterior T is not representative of the real outdoors T when compared to real values obtained from the weather station (AccuWeather) in the same day in Lyon, with the average of maximum T of 16°C and minimum T of 7°C. It is not either realistic to think about 30ºC of T inside a room in the beginning of May.

(a) Const. Solution 1

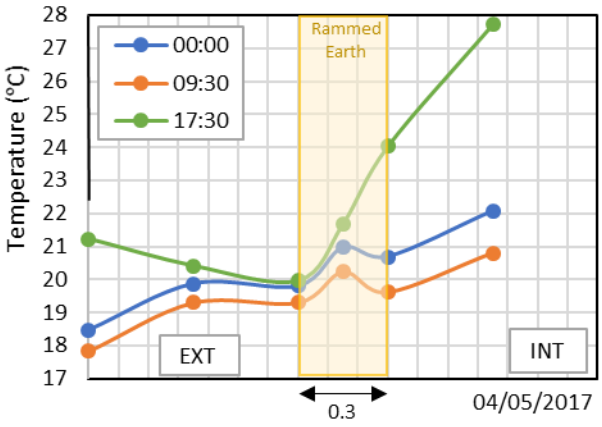

(b) Const. Solution 2

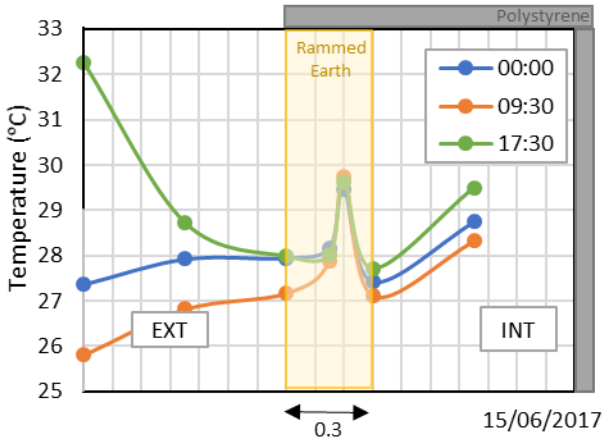

(c) Const. Solution 3

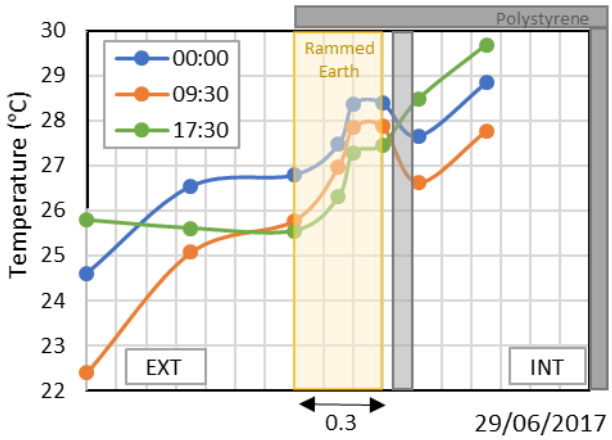

Figure 4.16 – T profile for each constructive solution

On the interior of the chamber, being the cycle activated from 9:30 (orange line) to 17:30 (green line), an increase of T can be noticed from 21ºC to 28ºC. At 17:30 the cycle is turned off and the T starts to decrease until the next day cycle is activated.

Inside the rammed earth wall of every Figure 4.16 graphics, the T buffering can be noticed with the delay related to thermal inertia and it an accumulation of heat can be evidenced. However, in the case of Figure 4.16 (b), the T values inside the wall are higher than the T values on the interior side. It is not possible for the wall to be hotter than the only energy generation of the chamber, unless it has stored energy from previous cycles. That is also confirmed by the fact that T was kept quite stable through the different times of the day and it is not being influenced neither by exterior nor by interior T.

In Figure 4.16 (c), by introducing the EPS board on the interior side, a barrier has been created, and the thermal inertia of the wall has been neglected. Previously, the flux went from the interior to exterior, which means the HF_ins is always positive or in the limit the value is zero, when the system is in equilibrium. In Figure 4.17 is evidenced that on the interior side the wall is receiving heat from the generator but just before the beginning and end of the cycle the wall released heat for the interior side. On the exterior

side the wall is releasing heat during the entire day. HF_ext presents a positive value while it is losing heat because the heat flux plate is set up in order to provide an "positive flux" if the heat transfer goes from interior to exterior side.

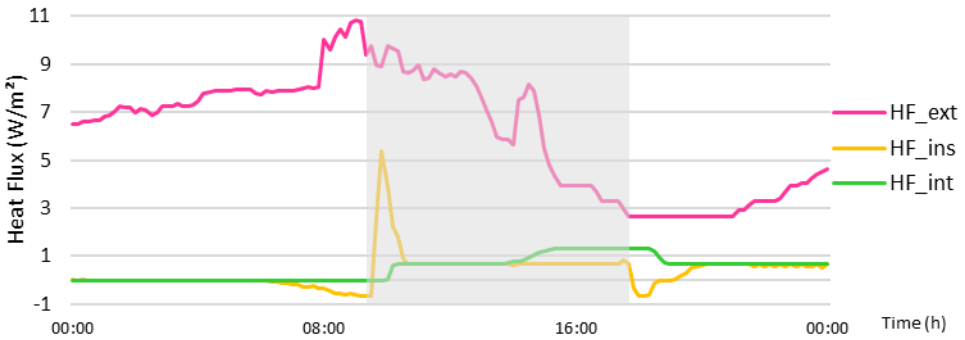

Figure 4.17 - Heat flux in constructive solution 3

4.6.2. Thermal Inertia

Getting closer to dynamic situations, T and RH were submitted to a variation through time. The rammed earth has a predictable behaviour as when the T starts to increase, the heat immediately starts to pass through the wall, being evidenced by the HF_int and in HF_int_s evolution with time (see Figure 4.18). The T in the middle of the wall (T_wall) slightly increases when the heating and humidifying cycle begins (shaded area) and slightly decreases 7 hours after the end of the cycle. This delay in T_wall proves that the rammed earth can retain heat and release it hours after.

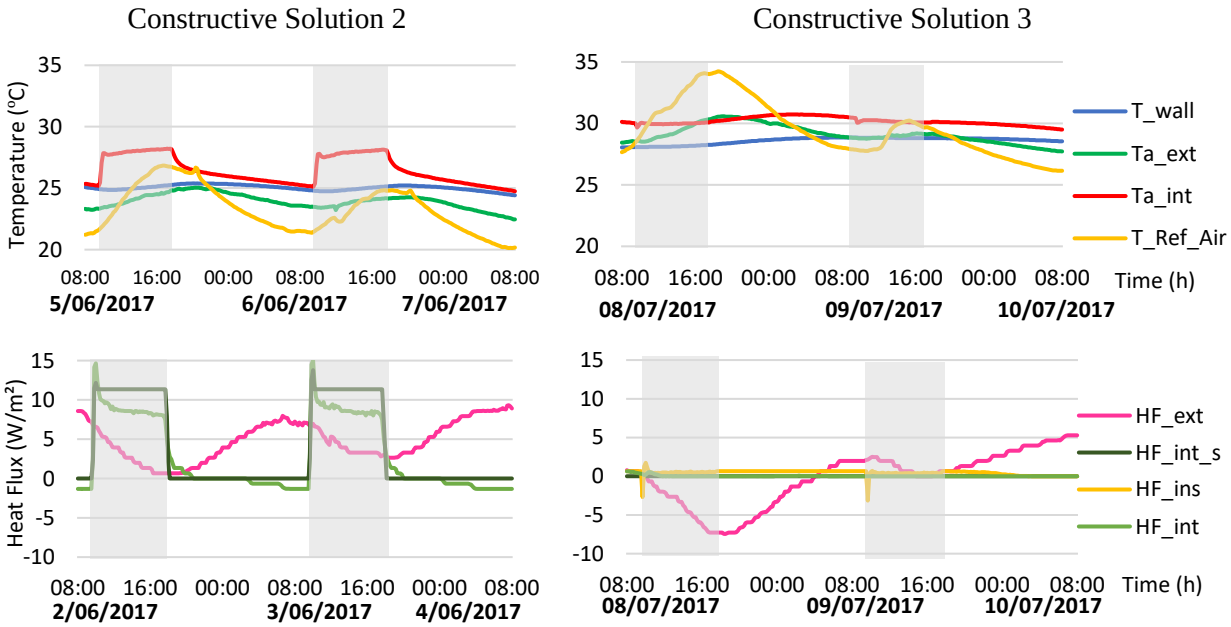

Figure 4.18 – Thermal inertia of the wall without and with polystyrene

On the other hand, in constructive solution 3, there is almost no heat passing through the polystyrene (HF_ins ~1.3 W/m^2) and through the surface of the wall (HF_int ~1.0 W/m^2). However, in the surface of

polystyrene, a peak at the beginning of the cycle (HF_ins ~ -2.7 W/m^2) is measured. HF_int_s is always null due to its lower sensibility comparing with HF_int. It is visible that the polystyrene heat barrier is blocking the heat to reach the wall. Still, the T inside the wall (T_wall) is increasing through the week due to external variation, that is higher than T_wall. When Ta_ext gets lower than T_wall, its value starts to decrease immediately. This proves that polystyrene applied on the interior surface is not an appropriate solution. The presence of this kind of insulation promotes the lack of efficiency on the rammed earth's release of heat through the interior surfaces, thus wasting its thermal inertia properties.

Every result obtained for T and RH cycle are presented in Figure A. 7 for constructive solution 2, and in Figure A. 11 for constructive solution 3, in Appendix. This effect is also visible when only T performed with an 8h cycle, presented in Figure A. 6 for constructive solution 2 and in Figure A. 9 for constructive solution 3, in Appendix.

4.6.3. Time Lag

Time lags and decrement factors are used to evaluate the thermal performance of a wall. To study the influence of the time lag, the same procedure was repeated through the different constructive solutions. In Figure 4.19, an 8h cycle was set where the T reaches 30ºC and, then, is turned off in the remaining time. The cycle is highlighted by the grey-shaded area.

The first construction solution test was run in early May. Therefore, the weather was colder than for the other two tests. For this reason, the T cycle (performed in the interior side of the chamber and, consequently, shown by the Ta_int sensor represented in red) is more evident than it is in the others. It also has a bigger initial peak due to the sun radiation that hit the dark cork at that period. The same cannot be seen in the other two solutions because the cork chamber was insulated and covered with polystyrene.

The peaks of Ta_ext are due to T_Ref_Air, and they have a time lag because although the entrance door was kept open, the Ta_ext was covered inside the cork chamber and it has been influenced from the T of the wall.

In Table 4.2 are presented the maximum and minimum values of Ts_ext and Ts_int from Figure 4.19. Time lag was determined based on equation (20) presented in chapter 2.3.2. Analogously, it was also determined for Ts_int and T_wall. Decrement factor was determined based on equation (19) presented in the same chapter.

As presented in section 2.3.2, given that for most of cases Ts_int is higher than Ts_ext, the time it takes for the heat wave to propagate from the interior surface to the exterior surface is appointed as 'time lag'. In turn, 'decrement factor' is the decreasing ratio of its amplitude during this process.

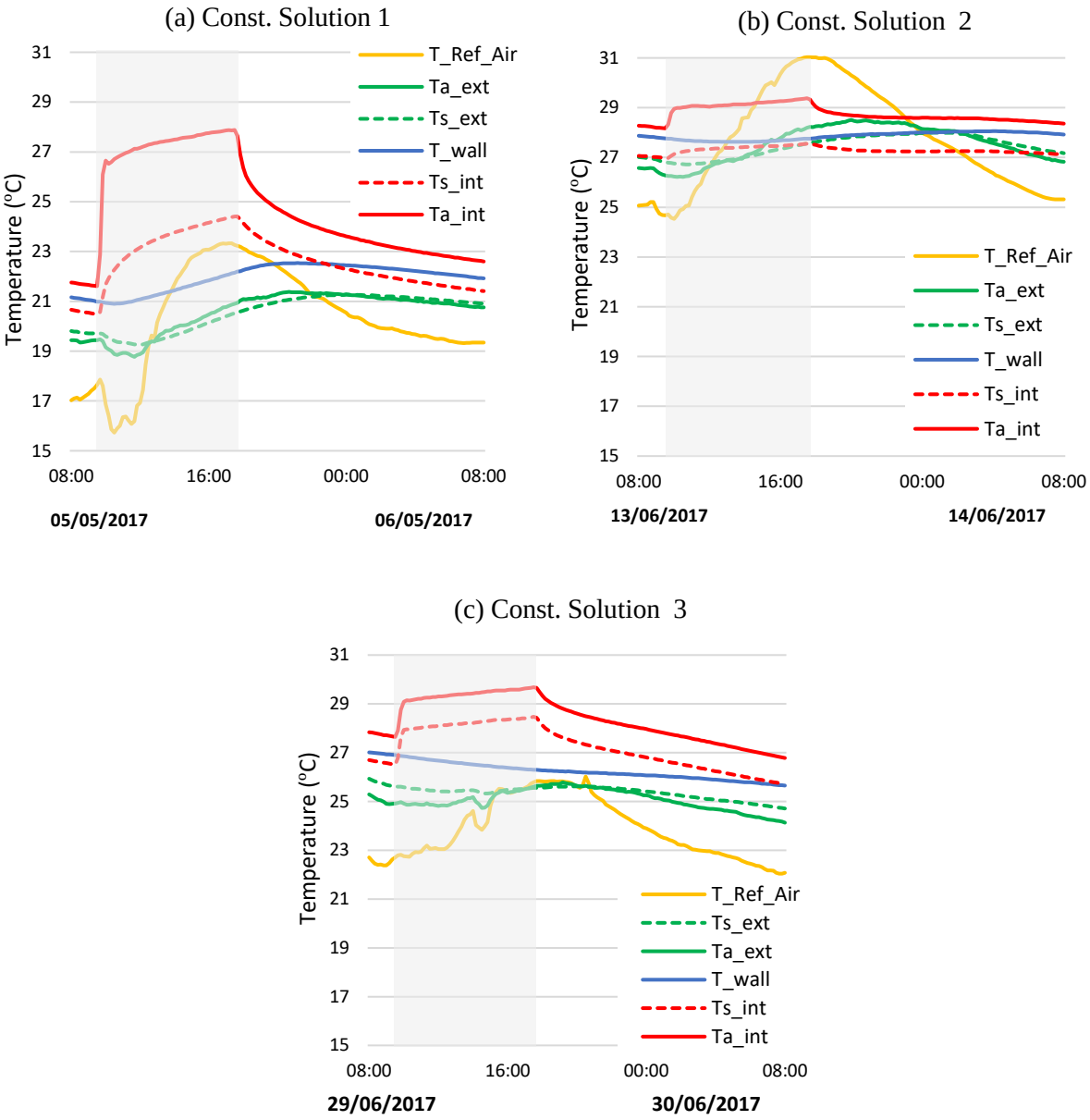

Figure 4.19 – Time lag in every constructive solutions

By increasing the thermal resistance, by adding an insulation of polystyrene (constructive solution 3), the time lag increases. This may be an indicator that the insulation is hampering the heat access to the wall.

Moreover, the lower decrement factor match with constructive solution 2. Figure 4.19 (b) shows that constructive solution 2 has the lowest amplitude between exterior T and interior T, since Ta_ext reaches values even higher than T_wall.

Walls with high time lags and low decrement factors provides almost constant interior T, resulting in a good comfort level (Soudani et al., 2017).

Table 4.2 – Time lag and decrement factor

C.S.	Date	Ts_int				Ts_ext				T_wall			
		Max		Min		Max		Min		Max		Min	
		Time	Value	Time	Value	Time	Value	Time	Value	Time	Value	Time	Value
CS1	05/05/2017	17:40	24.4	09:30	20.5	00:00	21.3	11:40	19.3	21:10	22.5	10:30	20.9
CS2	13/06/2017	17:40	27.6	09:30	27.0	00:40	28.0	10:40	26.7	04:00	28.1	12:40	27.6
CS3	29/06/2017	17:30	28.5	08:00	25.7	08:00	25.9	08:00	24.7	08:00	27.01	08:00	26.78

Constructive Solution	Time Lag	Decrement Factor
1	06:20	14.2
2	07:00	6.8
3	14:30	7.1

4.6.4. Water Content

The liquid water content is a key parameter to understand the behaviour, including the strength, of a rammed earth wall. In constructive solution 1, during the test that T inside the chamber diverges with outside variation, presented in Figure 4.20, it was confirmed that the water content inside the wall (Vw_wall) increases with the increasing T inside the wall (T_wall), and vice versa. That tendency was verified for all performed tests during this work.

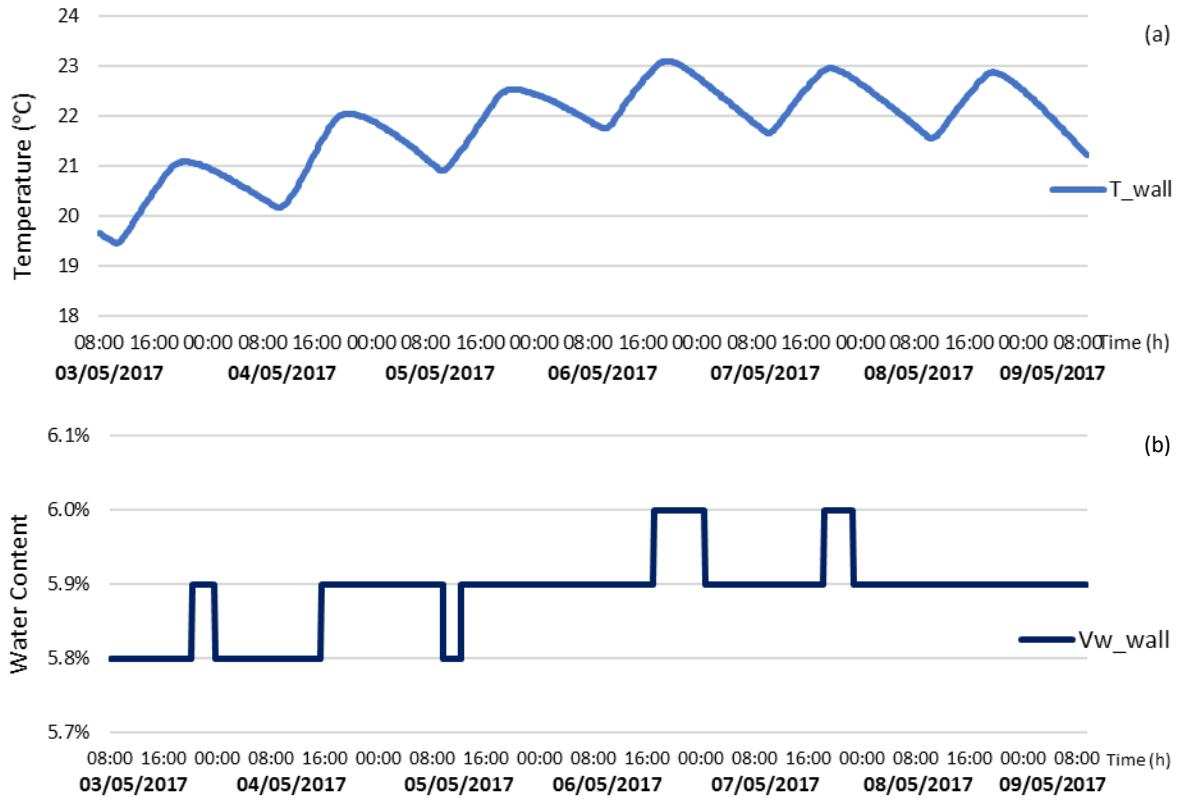

Figure 4.20 – Relation between T inside the wall (a) and water content (b)

In all tests performed in this work, the water content varied from 5.6% to 6.8% to a range of temperatures between 14ºC and 31ºC. The obtained values are excessively high compared to the water content of an earth wall with the same material from previous studies, that present values ranging between 0.5% and 3% in normal conditions (Chabriac et al., 2014), (Soudani, 2016). However, the water content of a rammed earth wall can drastically increase when the walls are submitted to pathology like capillarity or to construction moisture, for instance from the application of a new plaster.

In this specific case, the capillarity can be laid aside as these measurements are conducted in laboratory and the rammed earth is not in contact with soil. Therefore, the water content variation is due to phase change and water transport on the boundary of the rammed earth wall.

The only explanation for these high values is the possibility that the sensors are not properly calibrated since they have been calibrated by Chabriac some years ago (Chabriac et al., 2014) and it was impossible to recalibrate them because they were already placed inside the wall.

4.6.5. Moisture Buffering

When T cycles are imposed on a rammed earth wall with and without polystyrene insulation, the moisture behaviour of the wall is not identical.

The T variation in both constructive solutions was very similar with T_wall variation between 26ºC and 28ºC, Ta_ext variation between 24ºC and 29ºC and Ta_int between 26ºC and 30ºC, presented in Figure A. 7 and Figure A. 11, in Appendix. Comparing both cases, the T never had a discrepancy between them more than 2ºC. Thus, the moisture behaviour presented is due to the influence of the lack of vapour permeability of the chosen insulation, the EPS.

It is visible, in Figure 4.21 (b), the moisture accumulation inside the wall when the polystyrene was applied. The rammed earth wall increased the RH (RH_wall) until 63% due to the existent higher RH values on the interior side of the wall. However, the RH values on the interior of the wall were kept constant and equal to 63% during the whole month of June, even when the interior and exterior HR values were lower than 60%. That means the rammed earth is keeping the moisture and will release it when the environment presents low RH values and there is no vapour barrier.

Between the insulation and the wall there was a 2 cm gap that created a micro environment with a higher RH than the existent RH on the interior, predominantly influenced by the rammed earth. It is possible that this level of RH is less well supported by the polystyrene insulation and that accumulation of moisture at the interface occurs. On the long term this may lead to moisture related pathologies, such as decreasing the polystyrene insulation properties and the mechanical strength of the rammed earth.

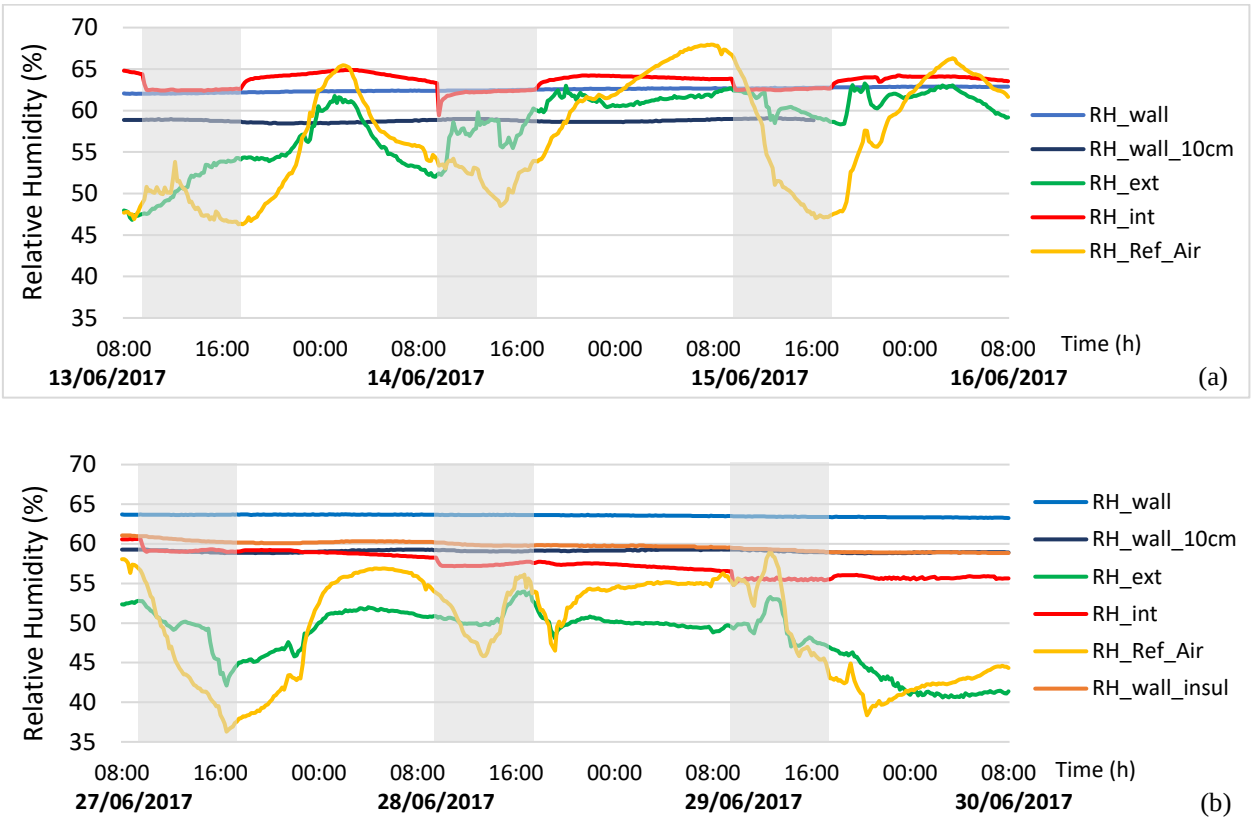

Figure 4.21 – Moisture behaviour of the wall without (a) and with (b) polystyrene insulation

4.6.6. Water Vapour Penetration

When a simulation was calculated in COMSOL Multiphysics, results show in Figure 4.22 that, for a constant HR on the interior of 50%, the penetration depth of the water vapour was up to 0.04m from the surface of the wall, for the first day (86400 sec) and until 0.07m for a week (6.048e5 sec).

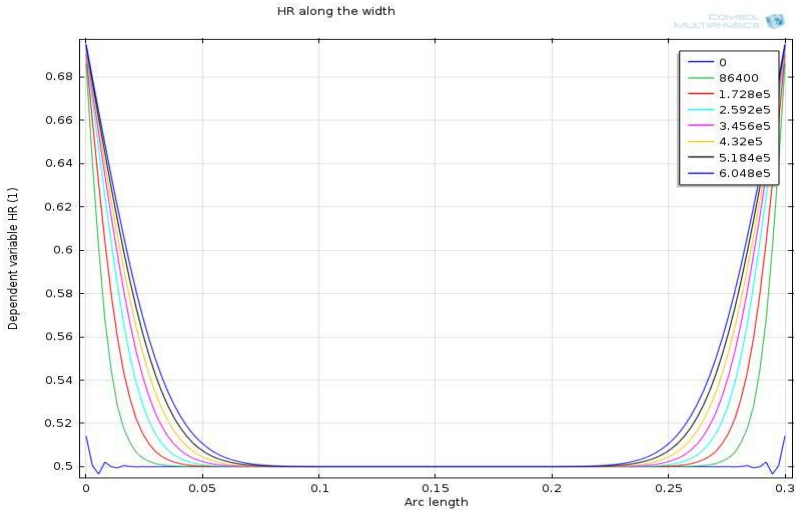

Figure 4.22 – Water vapour penetration in rammed earth

The acquired data from the sensors confirmed that RH_wall_10cm is not affected by RH variations during all week test. Furthermore, RH in the middle of the wall (RH_wall) is not affected as well (see chapter II, in Appendix).

5. Conclusion

5.1. Final Conclusions

There is a growing interest in passive climate control provided by the microstructure of earth materials. Scientific community needs more material characterisation of earth-based materials both from laboratory experiments, as is the case of this dissertation, and case studies of *in situ* monitored earth buildings, since only a few case studies of earth buildings can be found in the literature. Experimental data is of extreme importance as it allows improvement of the current models as well as improving the knowledge on the construction of buildings with lower embodied energy and indoor air quality.

With the development of research on rammed earth walls, it is assumed that rammed earth has not an R-value as competitive as other currently used constructive solutions. That seems to disable the possibility of constructing new buildings with rammed earth walls without very thick walls without including thermal insulation materials in the walls, in some regions of the world, as the case of France and Portugal. The same for rehabilitation works where the application of complementary insulation materials seem to be needed to respect national and European thermal regulations, when a non-dynamic analysis is made. Therefore, the study of the performance of rammed earth walls combined with insulations were the aim of this work.

A rammed earth wall was tested by itself and combined with two insulations: a polystyrene and a hemp-lime plaster, both applied on the internal surface of the wall. Each improvement corresponds to one constructive solution, submitted to several tests to study their hygrothermal behaviour. These tests consisted in 8h cycles of T and RH separately and combined.

It must be taken in consideration that the obtained values for T are not realistic comparing to *in situ* measurements, because these values are measured inside the laboratory. The T outside the chamber is the T in the interior of the laboratory, where high values up to 31ºC were reached in May.

To achieve the aimed objectives, it was necessary to acquire knowledge to optimise an experimental set up and monitor sensors along a rammed earth wall, preparation of a plaster insulation and application technique.

When the wall started to be monitored, it become apparent that the cork chamber was not efficient keeping the generated heat on the interior, since when T=30ºC was set in the interior of the chamber for a week, T_int had variations of 0.2 ºC from the average value, instead of remaining constant and equal to 30ºC. Therefore, a polystyrene insulation was applied to the chamber, leading to an improvement of 0.08ºC variation from the average value.

T and RH are the variables of this work and they are influenced by each other. Higher values of T induce lower values of RH (while water vapour concentration is kept constant) and vice versa. By increasing T values, higher T gradient is created between T_wall and Ta_int, and consequently, heat flux will reach

higher values, negative or positive, according to its direction. On the other hand, if there is no gradient, the wall will be in equilibrium with the environment and the heat flux will be close to zero.

When rammed earth was tested alone, it was always detected a delay in T_wall from Ta_ext evidencing that rammed earth is capable of retaining the heat and releases it hours after. It also induces an average T buffering of 1h for every 7 cm of rammed earth that the T has to penetrate. Therefore, it is clearly demonstrated that the rammed earth walls have the potential to buffer T and RH.

By placing 10 cm of polystyrene on the interior side of the rammed earth wall, with a 2 cm gap, the thermal inertia of the wall is lost. The wall is no longer able to capture heat and afterwards slowly release it, warming the indoor environment when the T indoor is lower than the T of the wall, due to the polystyrene barrier. Since the wall is mainly influenced by the exterior environment, it seems not to store more heat than the rammed earth by itself. Therefore, adding the polystyrene clearly worsen the performance of the rammed earth.

If the rammed earth is exposed to an extended period with the vapour barrier provided by the EPS insulation, the gap existing between the interior surface of the wall and the EPS the wall surface will reach values above 80% RH. Consequently, it might originate the growing of moulds, creating a problem that originally did not happen to the wall.

Finally, the hemp-lime plaster has proven to have a really slow drying process (only 11% of RH drying every month) when in contact to the rammed earth wall which absorbed its moisture and kept humid for long time. Not having the influence of fundamental factors as wind and sun to help drying the plaster, the process has a very slow drying. Thus, when used in construction or renovation the building methods have to adapt to this long drying stage. This is already the case for hemp-lime, builders are aware of the drying process and have adapted their building habits to it (not covering the insulation before the end of the drying to avoid any appearing of mould).

Due to the slow drying process of the hemp-lime plaster and to time limitations of this work, it was not possible to analyse the hygrothermal behaviour of the hemp-lime plaster combined with the rammed earth wall.

The water content varied from 5.6% to 6.8% in a range of temperatures between 14ºC and 31ºC. The obtained values are excessively high since previous works determined that the percentage of water content of an earth wall is between 0.5% and 3% in normal conditions. Since this wall has been constructed three years ago and does not have contact with rain and capillarity issues, the only explanation is that sensors have lost calibration during time.

Although the various experimental constrains that happened and that are common on this type of campaigns, it is considered that valuable informative data were obtained in this dissertation, that might be used for numerical validation of heat air and moisture models, therefore contributing for following research and more eco-efficient practices, particularly in the eco-friendly construction industry.

5.2. Proposals for Future Work

As it always happens in research work, there were topics initially proposed that could not be accomplished due to a limited period of six months internship at ENTPE in Lyon. Nevertheless, some interesting ideas appeared during the work progress. To further develop the work already done in this dissertation, the proposals for future work are as follows:

Laboratory measurements:

- As soon as the **hemp-lime plaster is dry, start to test** its combination with the rammed earth to assess if it works as a good insulation, without the limitations of the tested EPS;
- For future investigations, **apply the hemp-lime insulation in a (already dried) board** instead of plastering, due to its slow drying process;
- **Apply both insulations in the exterior surface of the wall** and assess results. Nevertheless, in real conditions, particularly in the case of EPS, an appropriate finishing coating system would need to be applied and the buildings aesthetics would completely change;
- The RH values on tests performed inside the chamber had very limited range because the equipment used did not enable to decrease the RH values, just to increase. It is proposed for future works to **increase the range variation of RH from 30% to 80%** to facilitate observation of a bigger influence of RH in heat flux;
- **Analyse the heat flux plate size**: during this work, it became impossible to study the heat flux plate size due to the little range of RH variation that caused a minimal variation of heat flux on the bigger plate and therefore, any variation on the small plate (because this one has a lower sensitivity).

Viability of the achieved results:

Must be noted that the obtained values have limitations - *in situ* conditions have been neglected (ex: wind and sun) - as well as presents an error associated (calibration of sensors, etc), as previously referred.

- **Comparison between measured and simulated data:** use of the data obtained with a compute software model, like COMSOL Multiphysics, to validate theoretical models;
- **Comparison between *in situ* and laboratory measurements:** check the viability of the data obtained because real houses walls are influenced for many factors that are not affected when in laboratory such as solar radiation, capillarity from soil, wind and rain.

References

Allinson, D., & Hall, M. (2010). Hygrothermal analysis of a stabilised rammed earth test building in the UK. Energy and Buildings, 42(6), 845–852. https://doi.org/10.1016/j.enbuild.2009.12.005

Arnaud, L., & Gourlay, E. (2012). Experimental study of parameters influencing mechanical properties of hemp concretes. Construction and Building Materials, 28(1), 50–56. https://doi.org/10.1016/j.conbuildmat.2011.07.052

Arundel, A. V., Sterling, E. M., Biggin, J. H., & Sterling, T. D. (1986). Indirect health effects of relative humidity in indoor environments. Environmental Health Perspectives, 65(3), 351–361. https://doi.org/10.1289/ehp.8665351

Bornehag, C.-G., Blomquist, G., Gyntelberg, F., et al. (2001). Dampness in Buildings and Health Nordic Interdisciplinary Review of the Scientific Evidence on Associations between Exposure to "Dampness'' in Buildings and Health Effects (NORDDAMP). Indoor Air, 11, 72–86. https://doi.org/10.1034/j.1600-0668.2001.110202.x

Bui, Q. B., Morel, J. C., Venkatarama Reddy, B. V., & Ghayad, W. (2009). Durability of rammed earth walls exposed for 20 years to natural weathering. Building and Environment, 44(5), 912–919. https://doi.org/10.1016/j.buildenv.2008.07.001

Campbell Scientific, Inc. (2013). Instruction Manual: CR1000 Measurment and Control System. https://s.campbellsci.com/documents/br/manuals/cr1000.pdf

Campbell Scientific, Inc. (2016a). Instruction Manual: CS215 Temperature and Relative Humidity Probe. https://s.campbellsci.com/documents/us/manuals/cs215.pdf

Campbell Scientific, Inc. (2016b). Instruction Manual: Model 107 Temperature Probe. https://s.campbellsci.com/documents/us/manuals/107.pdf

Campbell Scientific, Inc. (2016c). Instruction Manual: CS215 - Temperature and Relative Humidity measurement probe. https://s.campbellsci.com/documents/us/manuals/cs215.pdf

Chabriac, P. A., Fabbri, A., Morel, J. C., Laurent, J. P., & Blanc-Gonnet, J. (2014). A procedure to measure the in-situ hygrothermal behavior of earth walls. Materials, 7(4), 3002–3020. https://doi.org/10.3390/ma7043002

Chabriac, P. A. (2014). Mesure du comportement hygrothermique du pisé. PhD thesis, ENTPE; CNRS-LTDS (UMR 5513)

Champiré, F., Fabbri, A., Morel, J., Wong, H., & Mcgregor, F. (2016). Impact of relative humidity on the mechanical behavior of compacted earth as a building material. Construction and Building Materials, 110, 70–78. https://doi.org/10.1016/j.conbuildmat.2016.01.027

Collet, F., Chamoin, J., Pretot, S., & Lanos, C. (2013). Comparison of the hygric behaviour of three hemp concretes. Energy and Buildings, 62, 294-303. https://doi.org/10.1016/j.enbuild.2013.03.010

Fabbri, A. (2017). Physics and Mechanics of porous media for civil engineering applications. Habilitation à diriger les recherches, ENTPE; LGCB-LTDS (CNU 60).

Fokaides, P. A., & Kalogirou, S. A. (2011). Application of infrared thermography for the determination of the overall heat transfer coefficient (U-Value) in building envelopes. Applied Energy, 88(12), 4358-4365. https://doi.org/10.1016/j.apenergy.2011.05.014

Habert, G., Castillo, E., Vincens, E., & Morel, J. C. (2012). Power: A new paradigm for energy use in sustainable construction. Ecological Indicators, 23, 109-115. https://doi.org/10.1016/j.ecolind.2012.03.016

Hall, M. R. (2007). Assessing the environmental performance of stabilised rammed earth walls using a climatic simulation chamber. Building and Environment, 42(1), 139–145. https://doi.org/10.1016/j.buildenv.2005.08.017

Hall, M., & Allinson, D. (2009). Analysis of the hygrothermal functional properties of stabilised rammed earth materials. Building and Environment, 44(9), 1935–1942. https://doi.org/10.1016/j.buildenv.2009.01.007

Hall, M., & Djerbib, Y. (2004). Rammed earth sample production: Context, recommendations and consistency. Construction and Building Materials, 18(4), 281–286. https://doi.org/10.1016/j.conbuildmat.2003.11.001

Henriques, F. (2011). Comportamento higrotérmico de edifícios. Faculdade de Ciências e Tecnologia.

Hens, H. (2012). Building physics-heat, air and moisture: fundamentals and engineering methods with examples and exercises. John Wiley & Sons. 2nd edition. ISBN: 9783433030271

Hill, R. (1952). The elastic behaviour of a crystalline aggregate. Proceedings of the Physical Society. Section A, 65(5), 349. https://doi.org/10.1088/0370-1298/65/5/307

Holcroft, N., & Shea, A. (2013). Moisture buffering and latent heat effects in natural fibre insulation materials. Portugal SB13 - Contribution of sustainable building to meet the EU, 20-20. https://doi.org/10.13140/2.1.4503.6162

Hukseflux Thermal Sensors B.V. (2016) HFP01 & HFP03: User Manual. http://www.hukseflux.com/sites/default/files/product_manual/HFP01_HFP03_manual_v1620.pdf

Hukseflux Thermal Sensors B.V. (2016) HFP01SC: User Manual. http://www.hukseflux.com/sites/default/files/product_manual/HFP01SC_manual_v1624.pdf

Janssen, H., & Roels, S. (2009). Qualitative and quantitative assessment of interior moisture buffering by enclosures. Energy and Buildings, 41(4), 382–394. https://doi.org/10.1016/j.enbuild.2008.11.007

Jaquin, P. (2012). History of earth building techniques. Modern Earth Buildings, 307–323. https://doi.org/10.1533/9780857096166.3.307

Morel, J. C., Pkla, A., & Walker, P. (2007). Compressive strength testing of compressed earth blocks. Construction and Building Materials, 21(2), 303-309. https://doi.org/10.1016/j.conbuildmat.2005.08.021

Künzel, H (1995). Simultaneous heat and moisture transport in building components, Tech. rep., Fraunhofer Institute of Building Physics, Fraunhofer IRB Verlag Stutgart, ISBN 3-8167-4103-7.

Lourenço, T., Matias, L., Faria, P. (2017). Anomalies detection in adhesive wall tiling systems by infrared thermography. Construction and Building Materials, 148, 419-428. https://doi.org/10.1016/j.conbuildmat.2017.05.052

McGregor, F., Heath, A., Maskell, D., Fabbri, A., & Morel, J.-C. (2016). A review on the buffering capacity of earth building materials. Proceedings of the Institution of Civil Engineers - Construction Materials, 169(5), 241–251. https://doi.org/10.1680/jcoma.15.00035

McGregor F., Fabbri A., Ferreira J., Simões T., Faria P., Morel J.-C.(2017). Procedure to determine the impact of the surface film resistance on the hygric properties of composite clay/fibre plasters, Materials and Structures, 50 (4), 193. https://doi.org/10.1617/s11527-017-1061-3

Miccoli, L., Mueller, U., & Fontana, P. (2014). Mechanical behaviour of earthen materials: A comparison between earth block masonry, rammed earth and cob. Construction and Building Materials, 61, 327–339. https://doi.org/10.1016/j.conbuildmat.2014.03.009

Mizoue, T., Andersson, K., Reijula, K., & Fedeli, C. (2004). Seasonal variation in perceived indoor environment and nonspecific symptoms in a temperate climate. Journal of Occupational Health, 46(4), 303–309. https://doi.org/10.1539/joh.46.303

Morel, J. C., Mesbah, A., Oggero, M., & Walker, P. (2001). Building houses with local materials: means to drastically reduce the environmental impact of construction. Building and Environment, 36(10), 1119-1126. https://doi.org/10.1016/S0360-1323(00)00054-8

Morel, J. C., Pkla, A., & Walker, P. (2007). Compressive strength testing of compressed earth blocks. Construction and Building Materials, 21(2), 303-309. https://doi.org/10.1016/j.conbuildmat.2005.08.021

Rahim, M., Douzane, O., Tran Le, A. D., Promis, G., & Langlet, T. (2017). Experimental investigation of hygrothermal behavior of two bio-based building envelopes. Energy and Buildings, 139, 608–615. https://doi.org/10.1016/j.enbuild.2017.01.058

Naveros, I., Ghiaus, C., & Ruíz, D. P. (2017). Frequency response limitation of heat flux meters. Building and Environment, 114, 233–245. https://doi.org/10.1016/j.buildenv.2016.12.025

Ramos, N. (2007). A importância de inércia higroscópica no comportamento higrotérmico dos edifícios. PhD thesis, Faculdade de Engenharia da Universidade do Porto

Santos, P., & Matias, L. (2006). ITE 50–Coeficientes de transmissão Térmica de elementos da envolvente dos Edifícios. Laboratório Nacional de Engenharia Civil. Versão Actualizada. ISBN: 9789724920658

Serrano, S., de Gracia, A., & Cabeza, L. F. (2016). Adaptation of rammed earth to modern construction systems: Comparative study of thermal behavior under summer conditions. Applied Energy, 175, 180–188. https://doi.org/10.1016/j.apenergy.2016.05.010

Shea, A., Lawrence, M., & Walker, P. (2012). Hygrothermal performance of an experimental hemp-lime building. Construction and Building Materials, 36, 270–275. https://doi.org/10.1016/j.conbuildmat.2012.04.123

Soudani, L. (2016). Modelling and experimental validation of the hygrothermal performances of earth as a building material. PhD thesis, ENTPE; LGCB-LTDS (UMR 5513)

Soudani, L., Fabbri, A., Morel, J. C., Woloszyn, M., Chabriac, P. A., Wong, H., & Grillet, A. C. (2016). Assessment of the validity of some common assumptions in hygrothermal modeling of earth based materials. Energy and Buildings, 116, 498–511. https://doi.org/10.1016/j.enbuild.2016.01.025

Soudani, L., Woloszyn, M., Fabbri, A., Morel, J.-C., & Grillet, A.-C. (2017). Energy evaluation of rammed earth walls using long term in-situ measurements. Solar Energy, 141, 70–80. https://doi.org/10.1016/j.solener.2016.11.002

Sun, C., Shu, S., Ding, G., Zhang, X., & Hu, X. (2013). Investigation of time lags and decrement factors for different building outside temperatures. Energy and Buildings, 61, 1–7. https://doi.org/10.1016/j.enbuild.2013.02.003

Taylor, P., Fuller, R. J., & Luther, M. B. (2008). Energy use and thermal comfort in a rammed earth office building. Energy and Buildings, 40(5), 793–800. https://doi.org/10.1016/j.enbuild.2007.05.013

Taylor, P., & Luther, M. B. (2004). Evaluating rammed earth walls: A case study. Solar Energy, 76(1–3), 79–84. https://doi.org/10.1016/j.solener.2003.08.026

Tran Le, A. D., Maalouf, C., Douzane, O., Promis, G., Mai, T. H., & Langlet, T. (2016). Impact of combined moisture buffering capacity of a hemp concrete building envelope and interior objects on the hygrothermal performance in a room. Journal of Building Performance Simulation, 9(6), 589–605. https://doi.org/10.1080/19401493.2016.1160434

Zhang, H., & Yoshino, H. (2010). Analysis of indoor humidity environment in Chinese residential buildings. Building and Environment, 45(10), 2132–2140. https://doi.org/10.1016/j.buildenv.2010.03.01

Websites

AccuWeather, website visited on November 2017, retrieved from: https://www.accuweather.com/en/fr/lyon/171210/month/171210?monyr=5/01/2017

EPS technical report, website visited on November 2017, retrieved from: http://iwi-gmbh.com/iwi/pdf/IWI_EPS_en.pdf

Appendix

I – Sensors Location – Side View

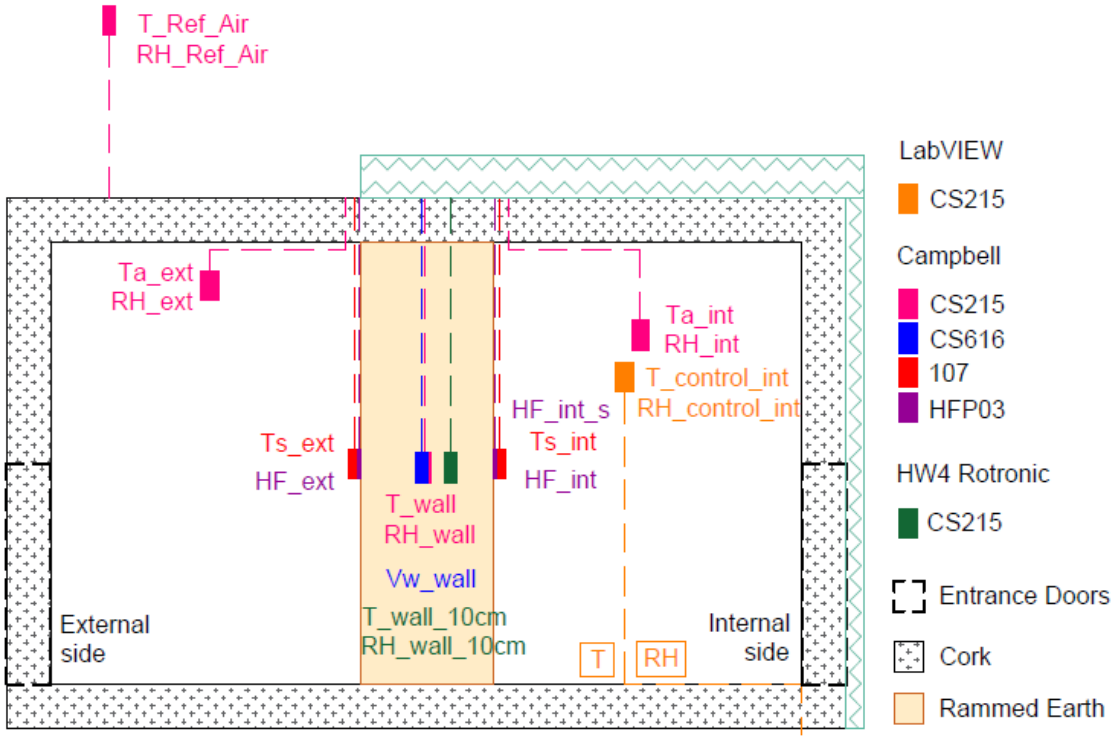

Figure A. 1 - Sensors location in constructive solution 2 - side view

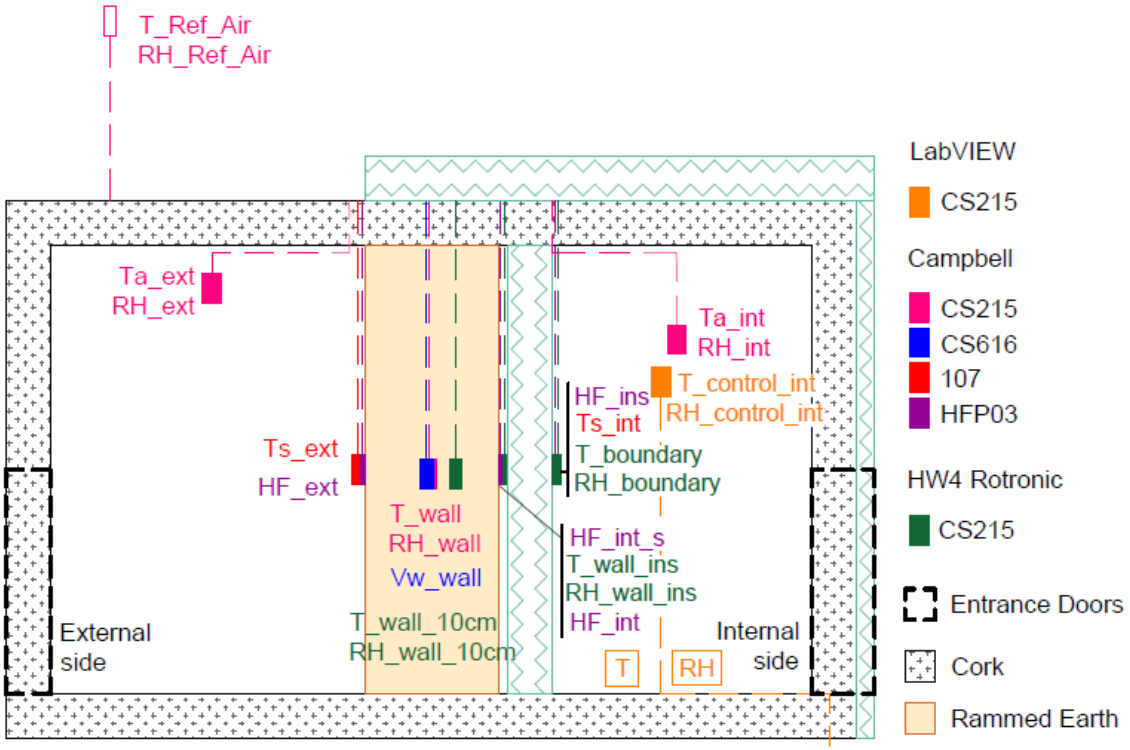

Figure A. 2 - Sensors location in constructive solution 3 - side view

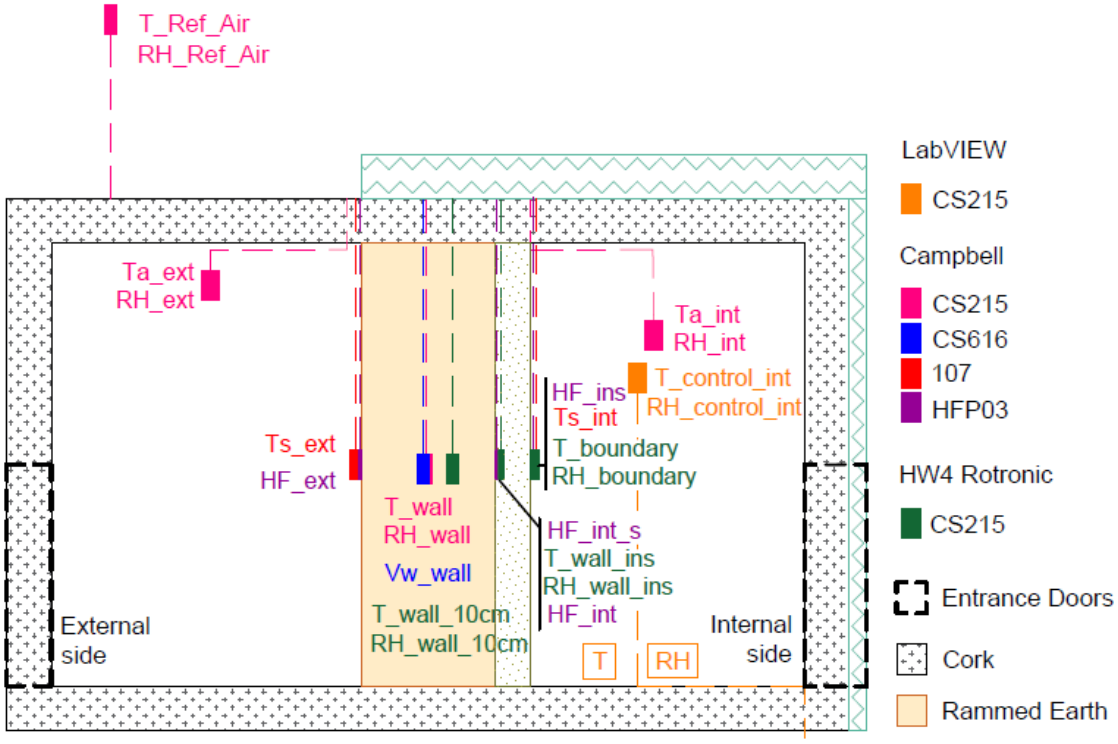

Figure A. 3 - Sensors location in constructive solution 4 - side view

II – Constructive solutions results

A.1. Constructive Solution 1 – Outside Variation

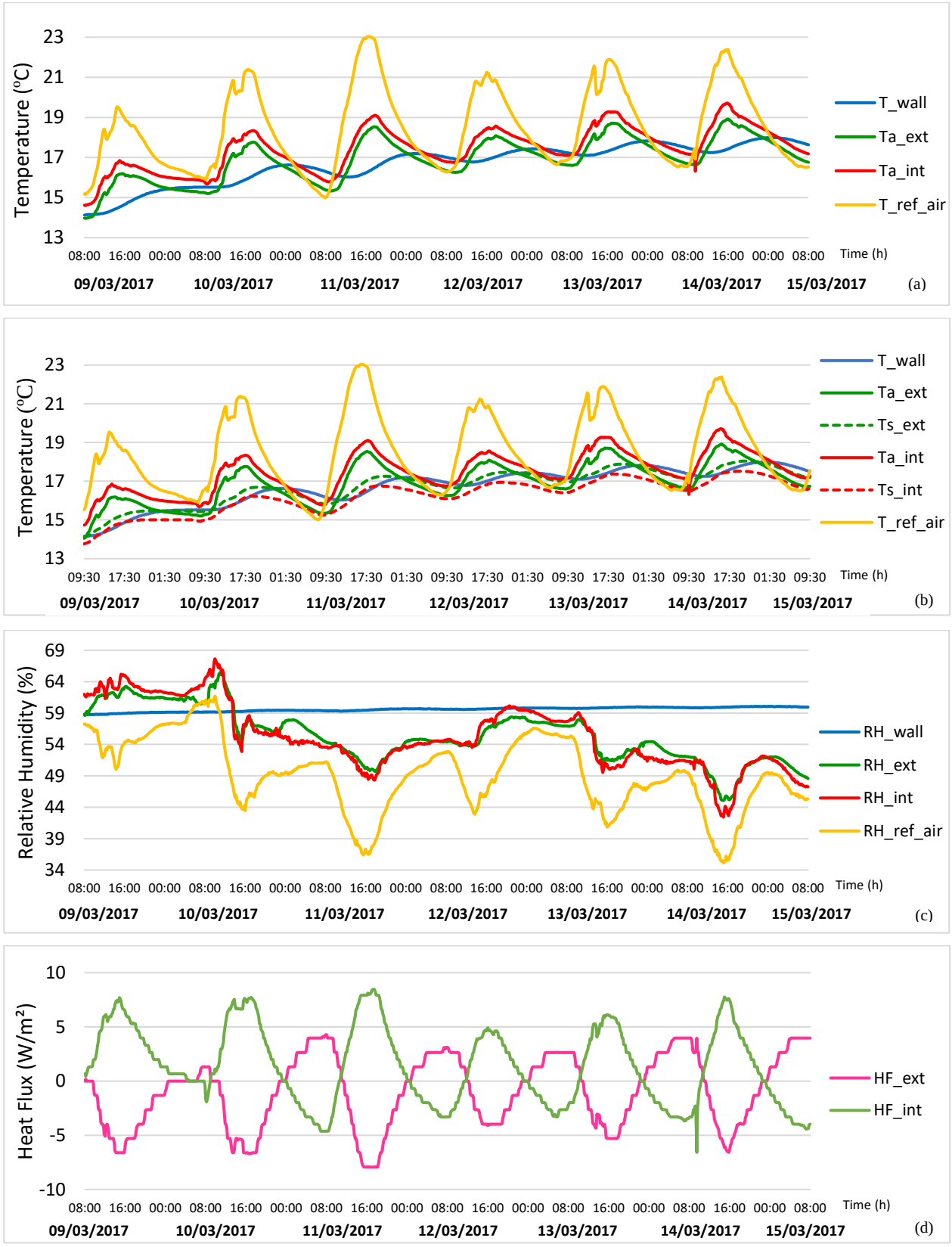

Figure A. 4 – Constructive Solution 1 – Outside variation: (a) Temperature variation; (b) Surface temperature variation (c) Relative humidity variation; (d) Heat Flux variation; from 09/03 to 15/03

A.2. Constructive Solution 1 – T constant

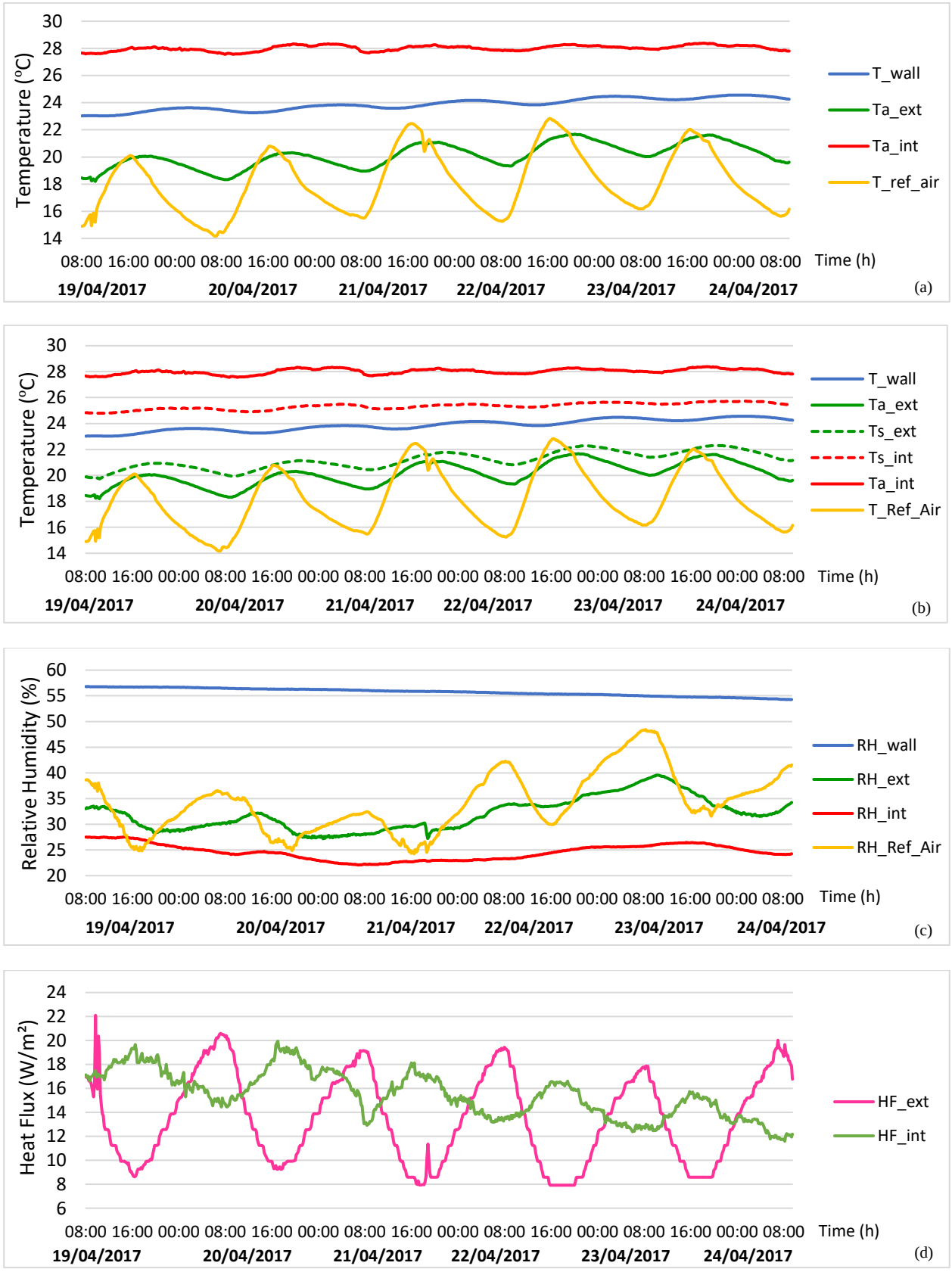

Figure A. 5 – Constructive Solution 1 – T constant: (a) Temperature variation; (b) Surface temperature variation (c) Relative humidity variation; (d) Heat Flux variation; from 19/04 to 24/04

A.3. Constructive Solution 1 – T cycle

Figure A. 6 - Constructive Solution 1 – T cycle: (a) Temperature variation; (b) Surface temperature variation (c) Relative humidity variation; (d) Heat Flux variation; from 03/05 to 09/05

B.1. Constructive Solution 2 – T cycle

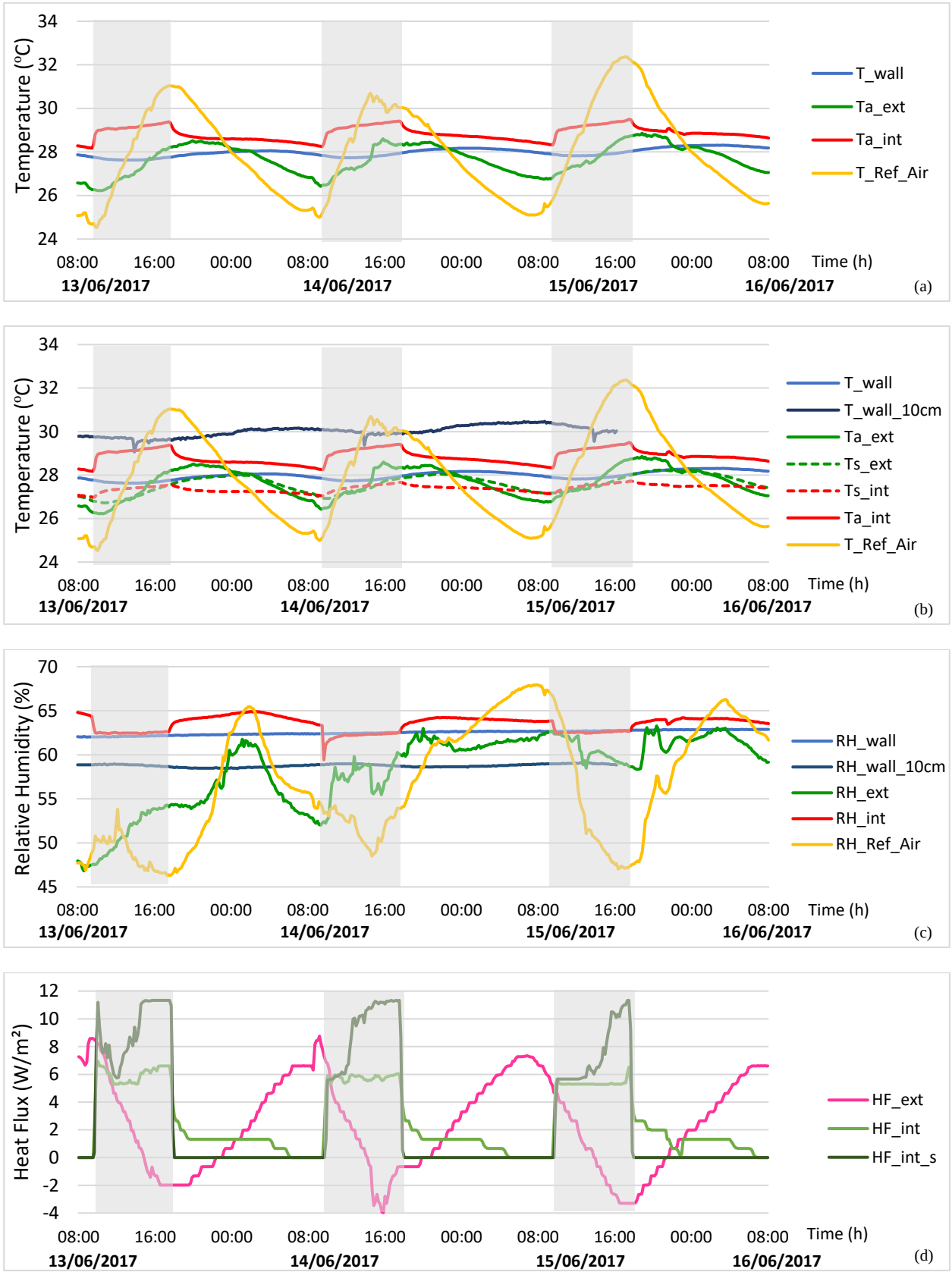

Figure A. 7 – Constructive Solution 2 – T cycle: (a) Temperature variation; (b) Surface temperature variation (c) Relative humidity variation; (d) Heat Flux variation; from 13/06 to 16/06

B.2. Constructive Solution 2 – RH cycle

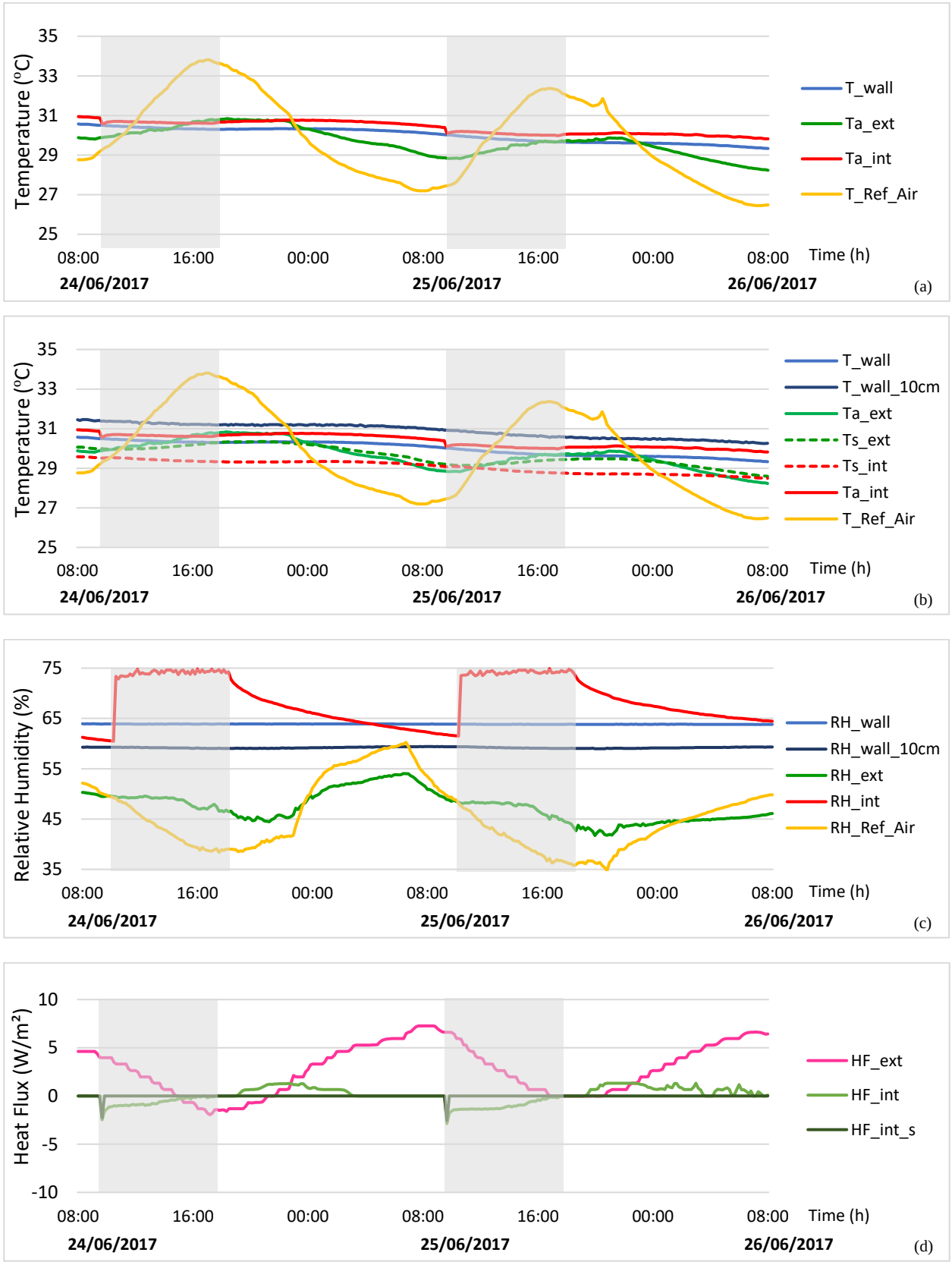

Figure A. 8 – Constructive Solution 2 – RH cycle: (a) Temperature variation; (b) Surface temperature variation (c) Relative humidity variation; (d) Heat Flux variation; from 24/06 to 26/06

B.3. Constructive Solution 2 – T & RH cycle

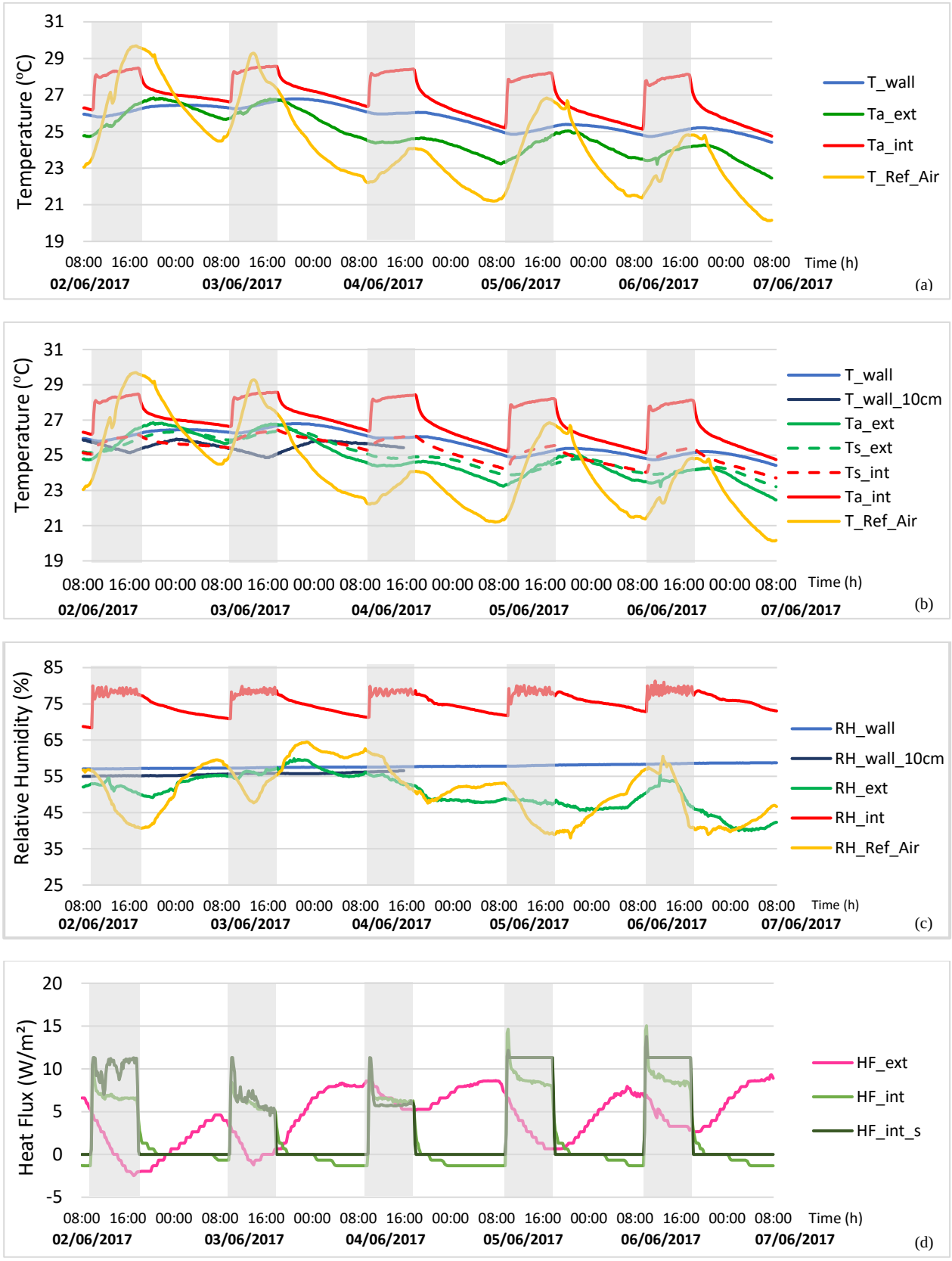

Figure A. 9 – Constructive Solution 2 – T & RH cycle: (a) Temperature variation; (b) Surface temperature variation (c) Relative humidity variation; (d) Heat flux variation; from 02/06 to 07/06

C.1. Constructive Solution 3 – T constant

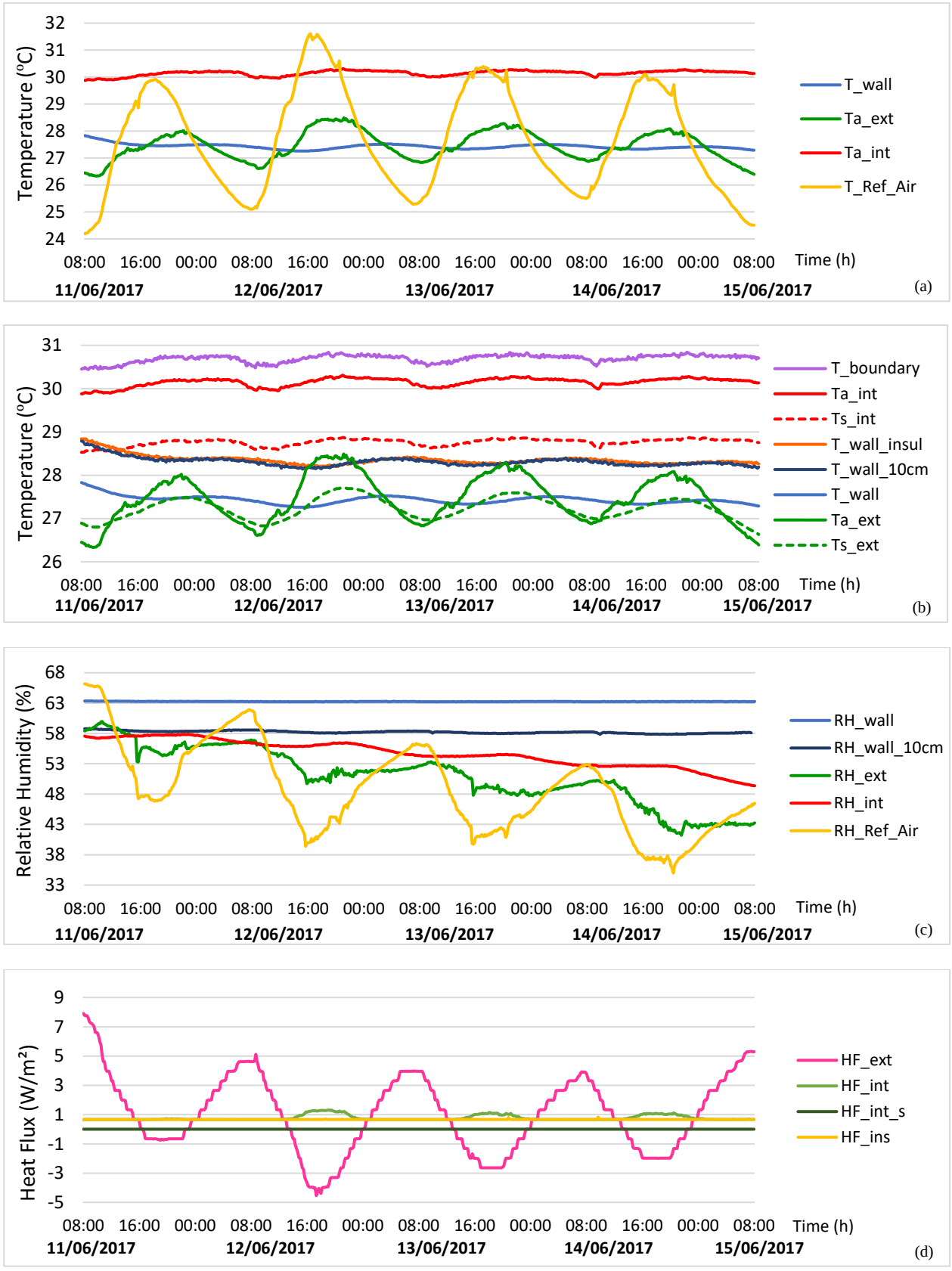

Figure A. 10 – Constructive Solution 3 – T constant: (a) Temperature variation; (b) Surface temperature variation (c) Relative humidity variation; (d) Heat Flux variation; from 11/06 to 15/06

C.2. Constructive Solution 3 – T cycle

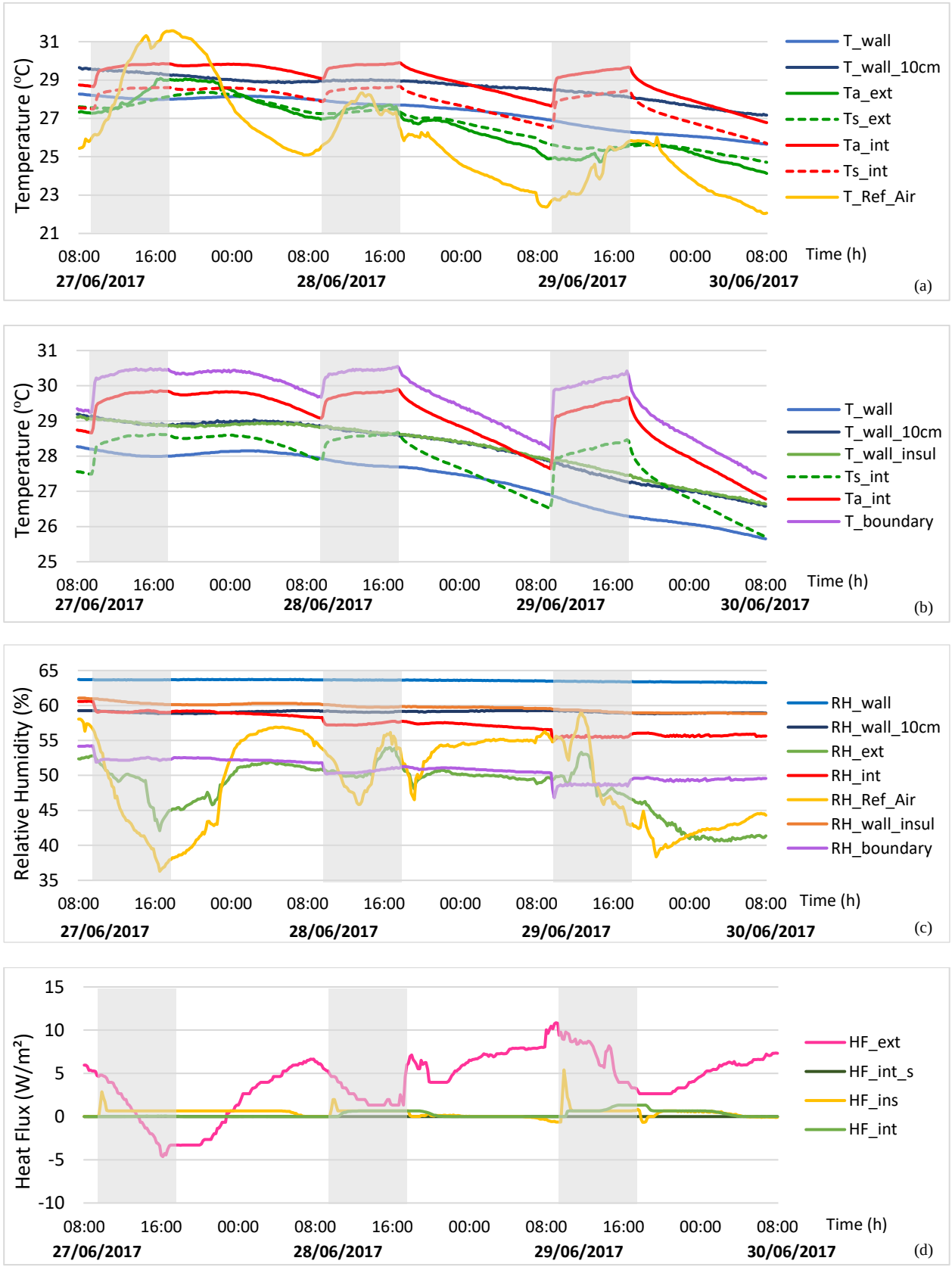

Figure A. 11 – Constructive Solution 3 – T cycle: (a) Temperature variation; (b) Along wall temperature variation (c) Relative humidity variation; (d) Heat Flux variation; from 27/06 to 30/06

C.3. Constructive Solution 3 – RH cycle

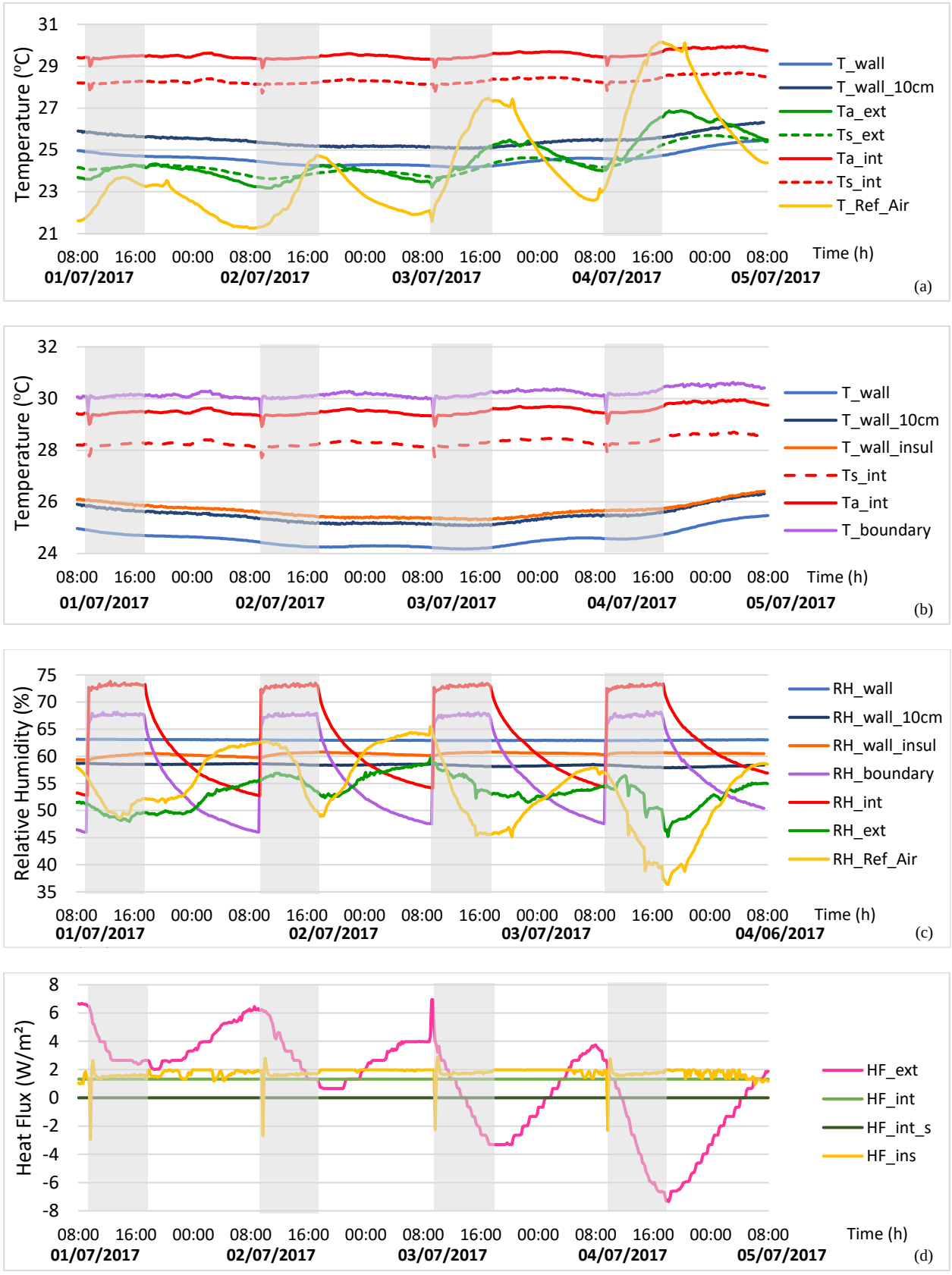

Figure A. 12– Constructive Solution 3 – RH cycle: (a) Temperature variation; (b) Surface temperature variation (c) Relative humidity variation; (d) Heat Flux variation; from 01/07 to 05/07

C.4. Constructive Solution 3 – T & RH cycle

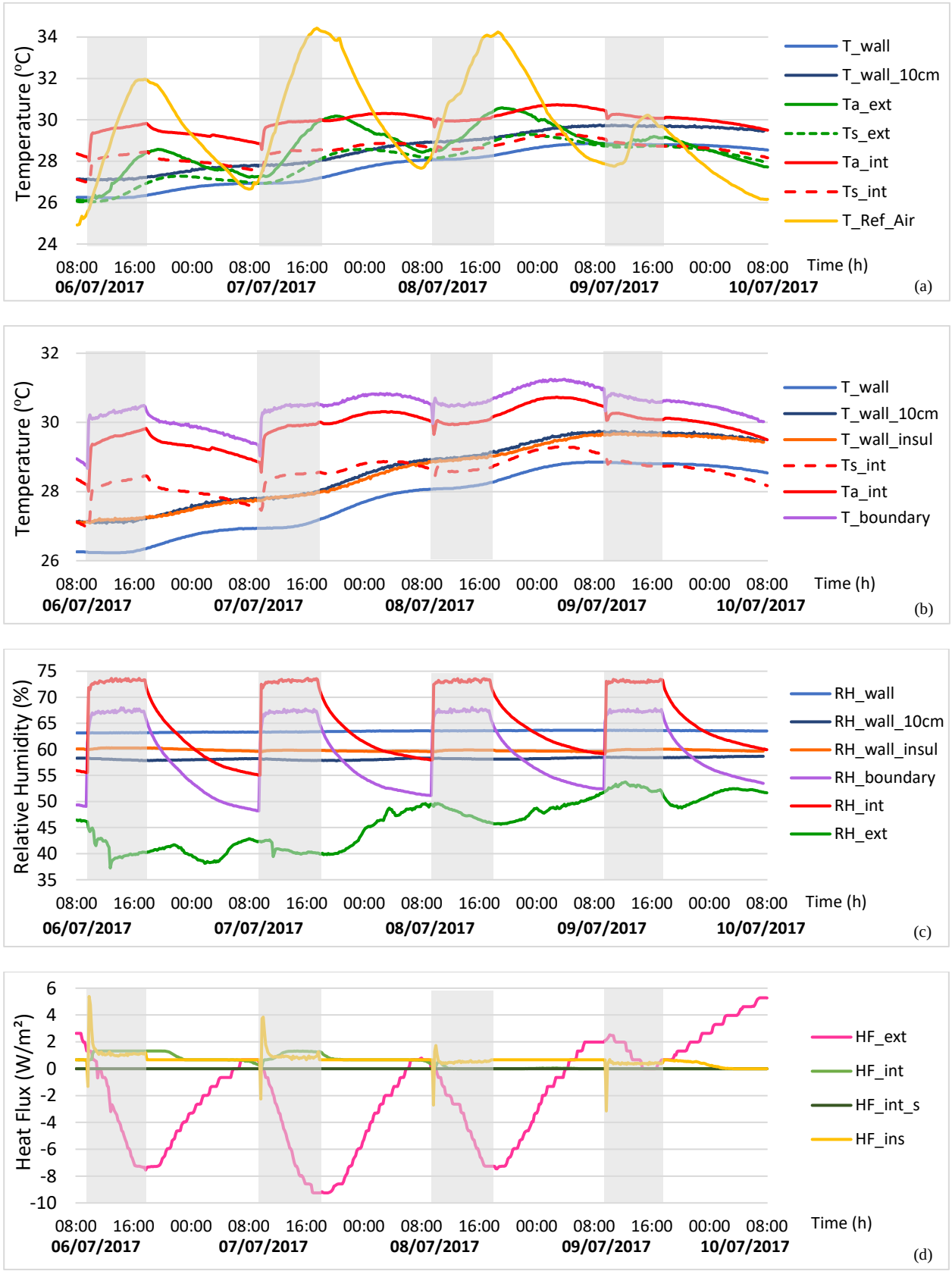

Figure A. 13 – Constructive Solution 3 – T & RH cycle: (a) Temperature variation; (b) Surface temperature variation (c) Relative humidity variation; (d) Heat Flux variation; from 06/07 to 10/07